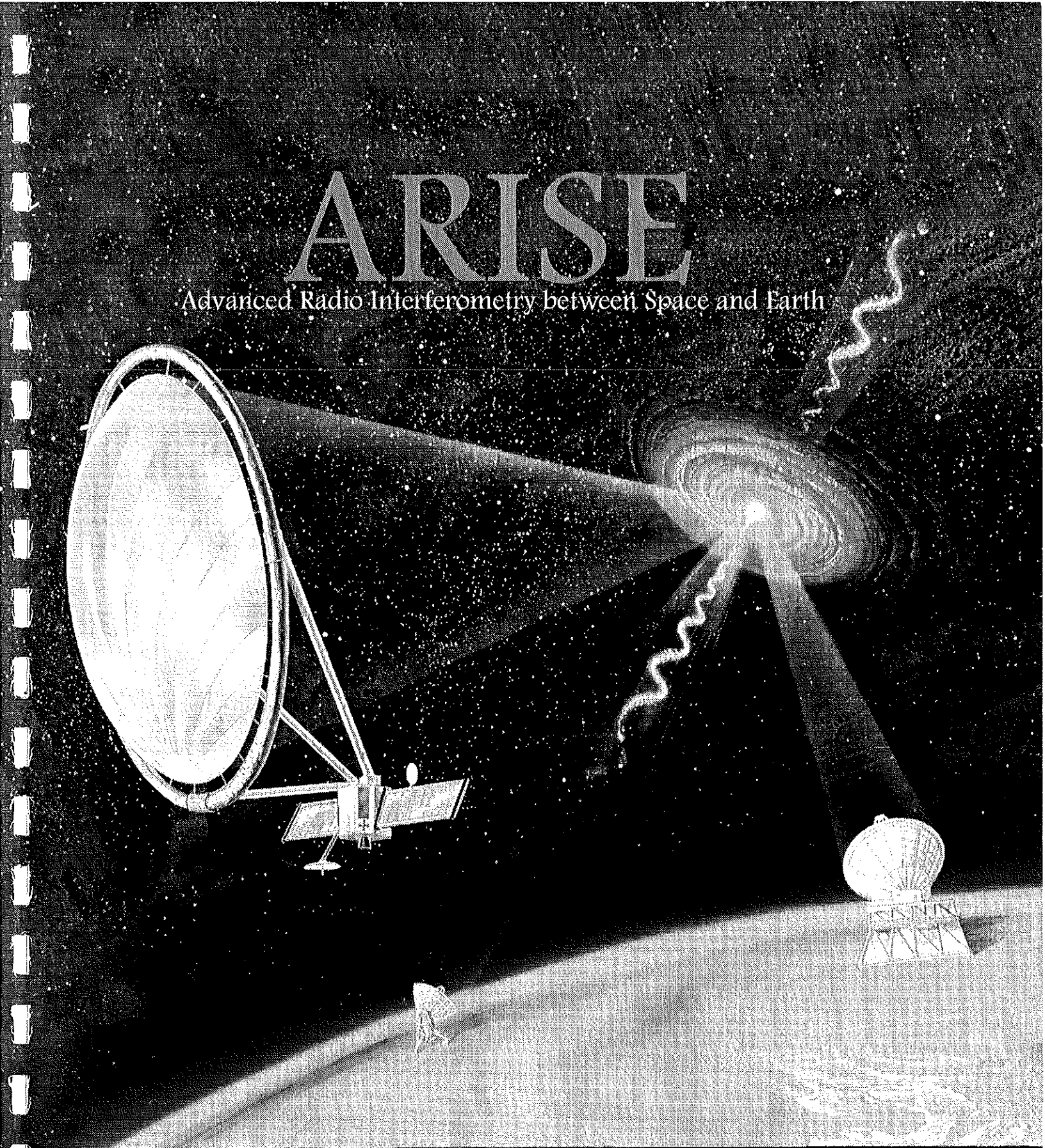

Mission and Spacecraft Description

First Edition
Jet Propulsion Laboratory
December 1998

National Aeronautics and
Space Administration

Document prepared by the ARISE Team:

Art B. Chmielewski - Preproject Manager
Jim Ulvestad (NRAO) - Preproject Scientist

Pradeep Bhandari - Cryocoolers
Robert Chave - Subreflector design
Bob Freeland, Paul Willis - Antenna materials
Todd Gaier - Science instruments
Henry Garrett - Space environments
Rick Helms - Structures, inflatable antenna cognizant engineer
Mike Jones - Ground systems
Carol Lewis, Sal DiStefano, Gene Wester - Power
Leo Lichodziejewski (L'Garde) - Inflatable structure
Roger Linfield, Rick Wietfeldt - VLBI and VLBI processing
Bob Miyake - Spacecraft thermal design
David Murphy - Orbits and coverage
Muriel Noca - Systems
Yahya Rahmat-Samii, Robert Hoferer (UCLA) - Antenna design and RF compensation
Vincent Randolph - Avionics
Larry Roe (Univ. of Arkansas) - Inflation system
Sam Sirlin, Marco Quadrelli - Antenna dynamics, Attitude control
Dan Thunnissen - Propulsion
Charles Wang - Telecom

Space VLBI consultants:

Robert Preston
Joel Smith

The purpose of this document is to summarize the technical work performed by the ARISE Team in FY'98. The work focused on the space segment of ARISE. Ground segment will be studied in more detail in FY'99 and will be available in the next edition of this document. Roadmaps for all the technologies involved in the ARISE mission can be found in separate documents.

TABLE OF CONTENTS

1. ARISE Mission Description

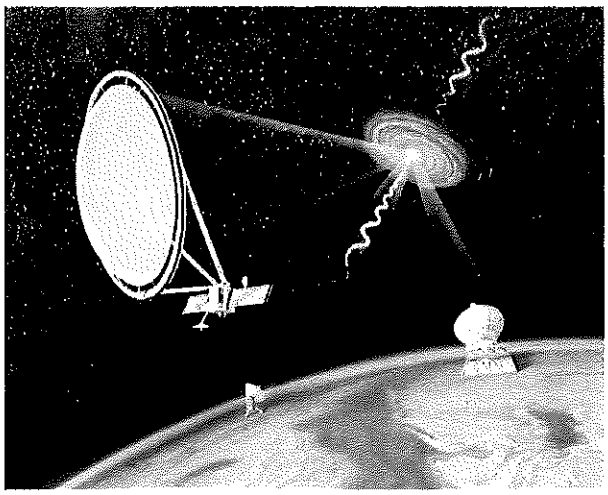

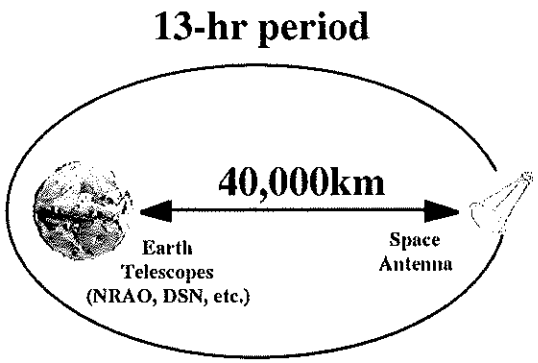

ARISE (Advanced Radio Interferometry between Space and Earth) is a space Very Long Baseline Interferometry (VLBI) mission consisting of one (or possibly two) 25-meter radio telescope(s) in a high elliptic Earth orbit. In conjunction with arrays of ground telescopes, ARISE will image the most energetic astronomical phenomena in the universe, namely supermassive black holes. The mission objectives are to image radio sources with a resolution of 10-20 microarcseconds, which corresponds to an improvement in resolution over today's Space VLBI mission by two orders of magnitude. ARISE's observing bands will be 8, 22, 43, (60), and 86 GHz, and system noise temperatures down to 10-20 K. Science data will be downlinked at a rate of 1-8 Gbps

The ARISE spacecraft is placed in a high elliptical Earth orbit in order to synthesize the largest possible imaging aperture. The nominal orbit has a perigee altitude of 5000 km and an apogee altitude of 40000 km. The mission lifetime is approximately 3 years, with a potential start in 2005 and launch in 2008. The spacecraft launch mass is about 1700 kg, allowing for a launch to the desired orbit with a Delta II class launch vehicle.

The ARISE spacecraft is designed with two primary goals: 1) to make the mission as low cost as possible, 2) to maximize the antenna performance. Several innovative ideas were used to make the mass and volume a minimum. An inflatable antenna is baselined with a mechanical antenna as secondary option. An inflatable antenna can be packed into a volume that is about 100 times less than an equivalent mechanical structure; the inflatable also is about 5 times lighter and 6 times less expensive to manufacture. The inflation system was combined with the attitude control and propulsion system for additional mass savings. All the structural elements of the antenna will be rigidized after the deployment, to nullify the need for any supplemental gas. The reflector structure also will be operated at a pressure of 1/10,000 atmospheres to lower the requirement for make-up gas, which will be needed to replace the gas lost by leakage due to micrometeoroid penetrations. The inflatable antenna peformance is enhanced by using mechanically shaped secondary reflector and an adaptive feed.

To further lower the cost of the mission, ARISE will take advantage of technology development by other missions and programs. It will use the coolers and low noise amplifiers which are being developed for the Europe-led Planck mission, scheduled for launch in 2007. The data systems will take advantage of the developments by the ground VLBI and DOD programs. The inflatable antenna technology development will be greatly aided by the Space Inflatables Program.

2. ARISE Science

The primary goal of ARISE is the study of the environment of black holes and other compact objects, as well as the disks of matter surrounding these objects. Secondary goals are the studies of gravitational lenses throughout the universe, and of coronae in active stellar systems.

Massive black holes are believed to be the power sources for active galactic nuclei, including the gamma-ray "blazars" first detected by the Compton Gamma Ray Observatory. Among the questions of scientific interest are the method of feeding these black holes, and how they use the fuel to generate the light-speed jets seen in blazars. ARISE will image the region of primary energy deposition and delivery in these objects with a resolution of light days to light months, depending on the blazar distances. Observations at 43 and 86 GHz are required to image these regions in optically thin emission, so that our view is not restricted to an opaque surface. Imaging of these regions in polarized radiation will map out the inner magnetic field structures, required for understanding the energy-generation processes. The combination of the ARISE imaging with gamma-ray observations and X-ray spectroscopy is particularly important to provide a complete picture of the highly energetic phenomena near massive black holes.

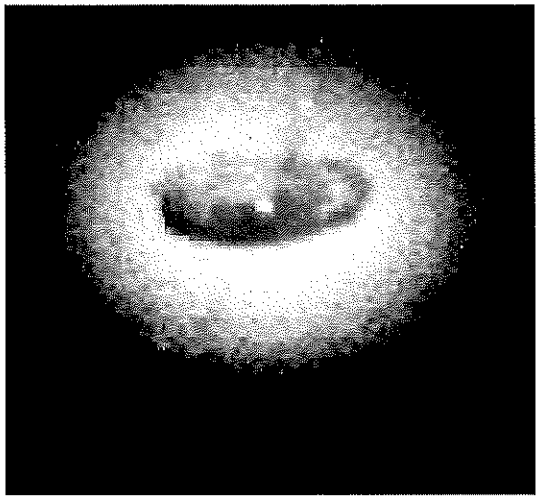

This image from Hubble shows a disk of dust fueling a massive black hole in the center of the galaxy NGC 4261.

Fig. 1.1

An important corollary to the study of black holes is the study of accretion disks on a variety of spatial scales (Fig. 1.1). Such disks are the reservoirs of fuel for black holes, other compact objects, and star-forming regions. Understanding the physics of these disks, and the relation among disks of various sizes, is critical to understanding the complete life cycle of matter near massive objects. ARISE will image the 22-GHz water megamaser emission at the centers of active galaxies, providing direct measurements of black hole masses and of the physics of the accretion process (Fig. 1.2). Weaker maser emission from disks in galactic star-formation regions will also be imaged to help show how the accretion phenomenon scales with mass and power of the accreting objects. Finally, continuum radio imaging of superluminal jets associated with energetic x-ray binary stars in our galaxy will probe the accretion processes on much smaller scales than is possible in extragalactic objects.

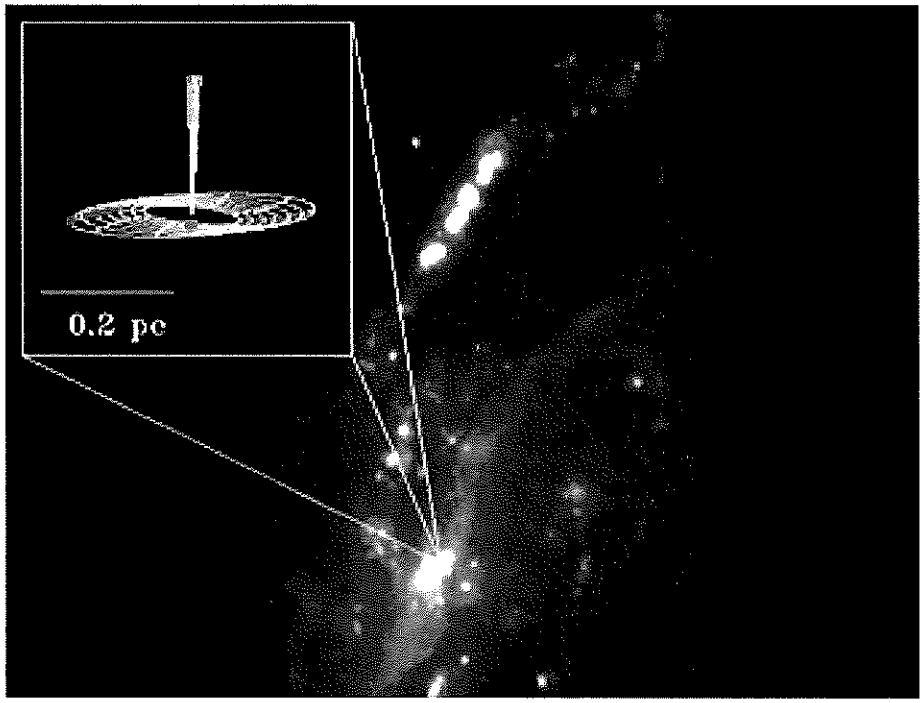

Fig. 1.2

A key secondary science goal for ARISE is the study of gravitational lenses throughout the universe. The accessible resolution of tens of microarcseconds (Fig. 1.3) provides sensitivity to compact objects in the mass range of 10^4 to 10^6 solar masses; no other astronomical technique has access to such objects, which are among the candidates for the "missing" dark matter in the universe. These lenses also can be used as "cosmic telescopes", since their magnification provides enhanced linear and angular resolution of distant objects. Thus, it may be possible for ARISE to have an effective resolution even better than that indicated just by the size of its orbit and its observing frequencies.

Another important secondary goal for ARISE is the study of the coronae of active star systems. Very sensitive imaging at 5 GHz or 8 GHz will allow mapping of these coronae with an effective linear resolution much smaller than a stellar radius. In addition, motions in coronal mass ejection events more powerful than those on our Sun can be followed in time scales of hours. Of particular interest is the capability of imaging stellar flares to search for brightness temperatures that indicate coherent emission processes in the coronal plasma; such high brightness temperatures can only be accessed using VLBI baselines much larger than an Earth diameter.

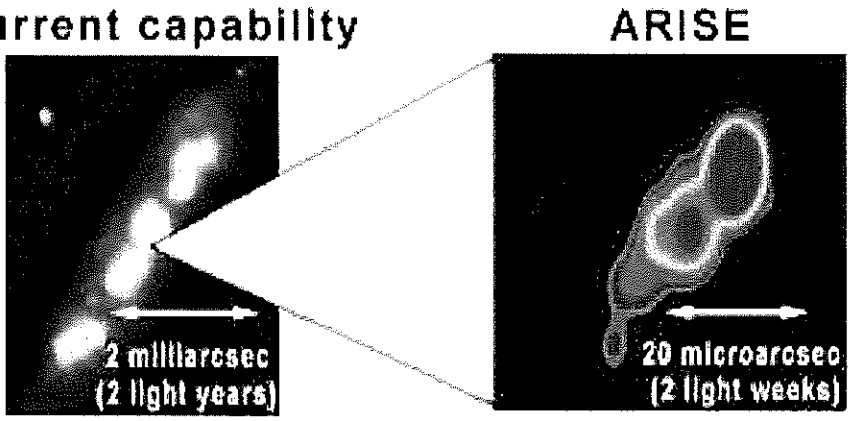

Simulated comparison of the improvement in imaging resolution from ground VLBI to ARISE.

Fig. 1.3

ARISE Science Advisory Team

Members from U.S. Institutions:

Prof. Moshe Elitzur, University of Kentucky
Dr. Lincoln Greenhill, Harvard-Smithsonian Astrophysical Observatory
Prof. Jacqueline Hewitt, Massachusetts Institute of Technology
Dr. Arieh Konigl, University of Chicago
Dr. Julian Krolik, Johns Hopkins University
Dr. Roger Linfield, Jet Propulsion Laboratory
Prof. Alan Marsher (Chairman), Boston University
Prof. Robert Mutel, University of Iowa
Dr. Susan Neff, NASA Goddard Space Flight Center
Dr. Robert Preston, Jet Propulsion Laboratory
Dr. Jonathan Romney, National Radio Astronomy Observatory
Dr. Ann Wehrle, California Institute of Technology

Members from Foreign Institutions:

Dr. Denise Gabuzda, Lebedev Physical Institute, Russia
Dr. Michael Garrett, Joint Institute for VLBI in Europe
Dr. Leonid Gurvits, Joint Institute for VLBI in Europe
Prof. Hisashi Hirabayashi, Institute for Space and Astronautical Science, Japan
Prof. Russell Taylor, University of Calgary, Canada
Prof. Esko Valtaoja, Tuorla Observatory, Finland

3. Mission design, coverage and constraints

3.1 Nominal orbit and sensitivity

The ARISE orbit is one of the major factors in determining the science return from the ARISE mission. The final orbit selection will be made after a detailed trade-off between scientific goals and spacecraft design, and after the VSOP and RadioAstron results. In the meantime, a nominal orbit for ARISE has been specified by the science requirements, along with a range of possible values for each parameter. Table 3.1 summarizes these parameters.

Quantity	Nominal	Possible Range
Semi-major axis	29,000 km	15,000 - 50,000 km
Eccentricity	0.6	0.25 - 0.75
Apogee Altitude	40,000 km	40,000 - 100,000 km
Perigee Altitude	5,000 km	1,000 - 6,000 km
Inclination	60 deg	30 - 63.4 deg
Orbital Period	13.5 hr	5 - 30+ hr
Perigee Precession	6 deg/yr	0 - 280 deg/yr
Node Precession	21 deg/yr	5 - 180 deg/yr
Orbit Knowledge	10 cm	3 - 20 cm

Table 3.1: Orbit parameters for ARISE

The selection of the perigee altitude should allow for overlap between ground-ground and ground space telescope baselines for calibration purposes. Low perigee (near 1000 km) will cause more rapid precession of the orbit plane. The apogee altitude should be high enough to provide information at the desired resolution, and will result from a trade between high angular resolution and high dynamic range imaging.

There are several different approaches to examining the ARISE sensitivity. The approach we adopt here is a quasi-physical approach. Given the 7-σ sensitivities from ARISE to a single VLBA antenna of 1.7, 4.3, 13.8, and 110 mJy at 8, 22, 43, and 86 GHz respectively, we may ask the question on a given ARISE baseline, what type of sources are we able to detect. In this analysis, a source is represented as a single Gaussian component of total flux density, S_o, and brightness temperature, T_o. In Figure 3.1, the detection limits for the 4 ARISE observing bands for 3 different values of baseline length (20,000, 40,000, and 80,000 km) are shown. The straight line corresponds to when the visibility function reaches a value of 0.9. Thus, to the right of this line even though a source might be detected, we would be unable to determine its size. With this simple Gaussian source model, the minimum brightness temperature that can be detected on a baseline of length D with a detection limit of S_d is given by:

$$T_{bmin} = 3.1 \times 10^8 \, (D/10^4 \text{ km})^2 \, (S_d/\text{mJy}) \text{ K}$$

This minimum detectable brightness temperature is for a source with a flux density of $2.7S_d$. From Figure 3.1, we can see which sources can be detected as a function of observing frequency and baseline length. As an alternative to representing a Gaussian source by its total flux density and brightness temperature, we can represent it by its total flux density and FWHM size. In Figure 3.2, we show what sources can be detected as a function of these two source parameters and baseline length. From this figure we can see the size scales that will be probed by the different ARISE observing bands. In this figure the 0.9 visibility straight line is different for each observing band.

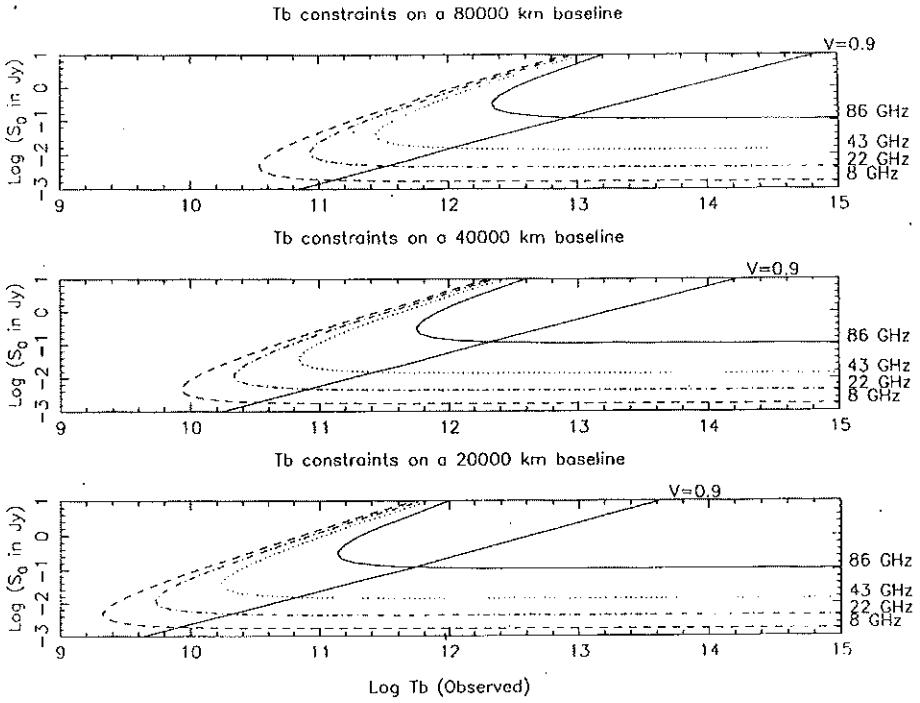

Fig. 3.1: Detection limits for the 4 ARISE observing bands as a function of source flux density (*So*) and maximum brightness temperature (*Tb*) for 3 different values of baseline length. Sources at the right of the curved lines are detectable, while sources to the left of the diagonal lines are resolvable.

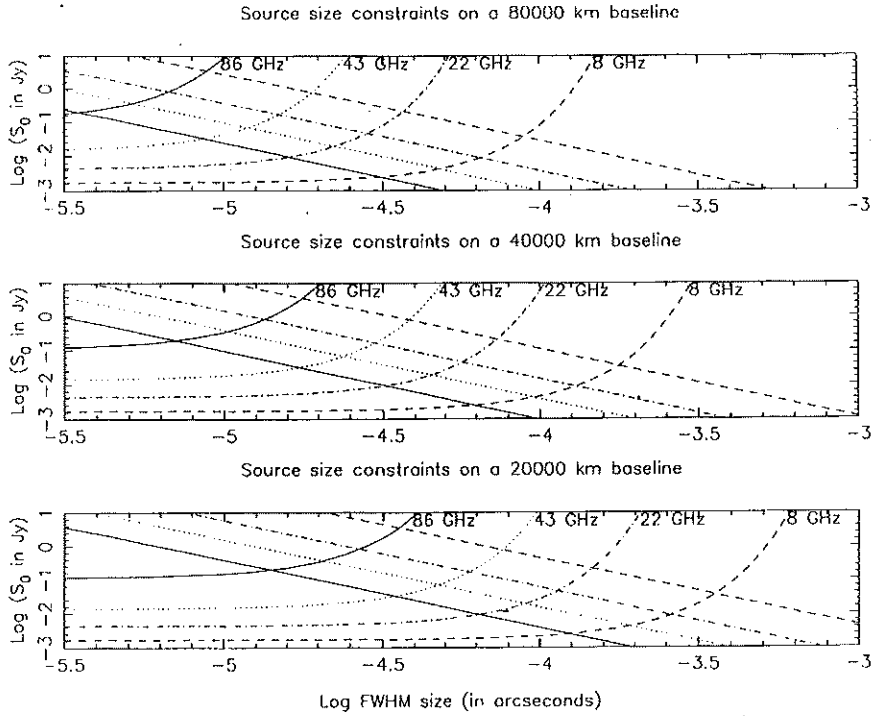

Fig. 3.2: Detection limits for the 4 ARISE observing bands as a function of source flux density (*So*) and FWHM size for 3 different values of baseline length. Sources above the curved lines are detectable, while sources below the diagonal lines are resolvable.

3.2 Orbit normal and (u,v)-coverage

One of the prime goals of the ARISE mission is to image sources with unprecedented angular resolution. The highest angular resolution (u,v)-coverage is obtained for sources that lie along the orbit normal and anti-normal directions. In equatorial coordinates (α, δ) these directions are given by (Ω - 6h, 90° -i) and (Ω + 6h, i-90°). In Figure 3.3, we show the (u, v)-coverage obtained for a one orbit observation with ARISE in its nominal orbit and the VLBA as a functional of the equatorial co-ordinates of the source. Note, that the (u,v)-coverage is essentially linear when the source lies in the orbit plane, shown as a sinusoidal curve in Figure 3.3. Due to the nodal precession ($d\Omega/dt$) the position in the sky of the orbit normal and anti-normal directions precess with time. In the nominal orbit for ARISE, this precession period is 15.7 years compared to 1.61 years for the current Japanese space VLBI satellite, HALCA. For the nominal mission lifetime of 3 years, Ω only precesses by 70°, implying that some directions of the sky would never have outstanding (u,v) coverage. The science tradeoffs involved in such a situation are under discussion (also, see sec

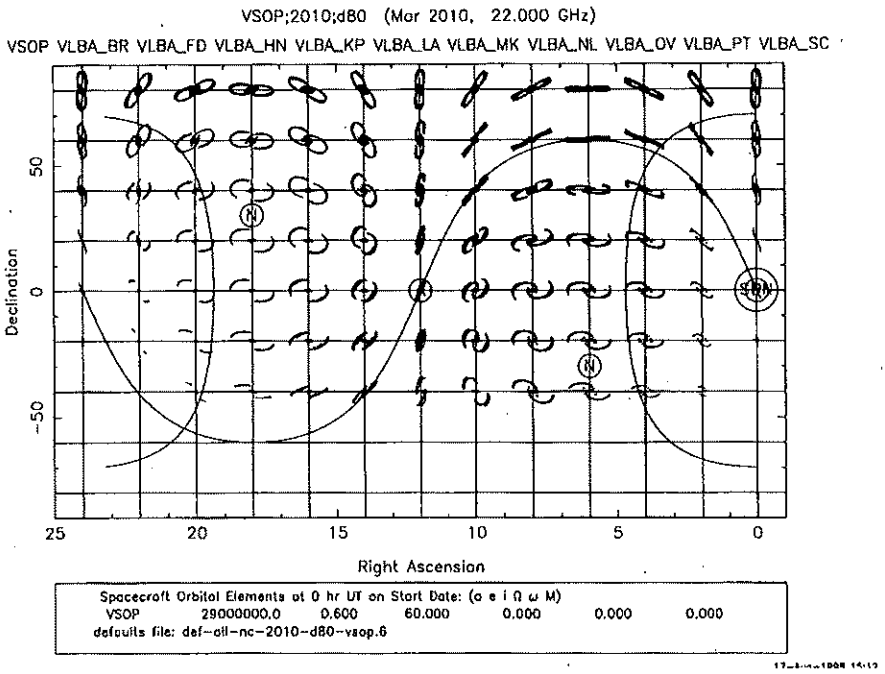

Fig. 3.3: All-sky (u,v)-coverages for a one orbit observation with ARISE in its nominal orbit and the VLBA.

3.3 Precession of the orbital elements

At the moment, both the injection argument of perigee ω_0 and the right ascension of the ascending node Ω_0 are free parameters. However, for the assessment of the ARISE orbit environment, a value of $\omega_0 = 0°$ has been assumed. The nominal orbit has an orbital period (T) of 13.56 hours and the precession rates of ω_0 and Ω_0 are +6°/yr and -23°/yr respectively for 60° inclination (and +63°/yr and -40°/yr respectively for 30° inclination). These nominal ARISE orbit precession rates can be compared to the HALCA precession rates for both ω and Ω which are +353°/yr and -228°/yr respectively. The relatively low precession rate for ω may not be a problem provided that there are no spacecraft link constraints except for the requirement that ARISE must be above the elevation limit of a tracking station. However, the injection value of ω, ω_0 needs to be further studied as the optimum value depends on the geographical distribution of tracking stations. If we assume DSN

tracking (with 2 tracking stations in the northern hemisphere and one in the southern hemisphere) then $\omega_o = 180$ is to be preferred over $\omega_o = 0$ for orbits with $i < 63.4°$ and hence $d\omega/dt > 0$. The low precession rate of Ω is of some concern and will be further addressed in Section 3.4.

3.4 Orbit trade-offs

It is instructive to examine how the derived orbital parameters P, $d\Omega/dt$, and $d\omega/dt$ depend on h_p, h_a, and i. In Figure 3.4, we show how the orbital period (P) depends on h_p and h_a. The nominal orbit has a period of 13.56 hours, which coincides quite nicely with the typical ground-based VLBI observation length. Increasing the orbital period much beyond this value has some disadvantages, since the typical imaging observation must last at least one orbit, and radio source structures may vary on time scales appreciably shorter than 24 hours. In Figures 3.5 and 3.6 we show the nodal precession rate $d\Omega/dt$ for orbit inclinations of 60° and 30° respectively. By lowering the inclination from the nominal 60° to 30° we increase the nodal precession rate, for a given h_p and h_a, by a factor of sqrt (3) (Ωdot is proportional to cos i). However, this in itself, only reduces the nodal precession period from 15.7 years to 9.06 years. Reducing h_p from 5,000 km to 1,000 km (while keeping h_a at 40,000 km) and reducing i from 60° to 30° reduces the nodal precession period to 3.95 years, which is comparable to the mission lifetime.

One consequence of lowering both the perigee height and the inclination is to increase the perigee precession rate (since $d\omega/dt$ is proportional to $5\cos^2 i - 1$). At an inclination of 60°, $d\omega/dt$ is very low since this inclination is close to $i = 63.4°$, where $d\omega/dt = 0$. For h_p = 1,000 km, h_a = 40,000 km, and i = 30°, ωdot = 145°/yr. With these orbital parameters over the 3 year ARISE mission lifetime there are 2.48 ω precession periods. With DSN tracking, ARISE will be able to be tracked longer when $\omega = 270°$ compared to $\omega = 90°$. Thus, in this case, an injection value of $\omega_o = 180°$ would to be preferred over a value of $\omega_o = 0°$.

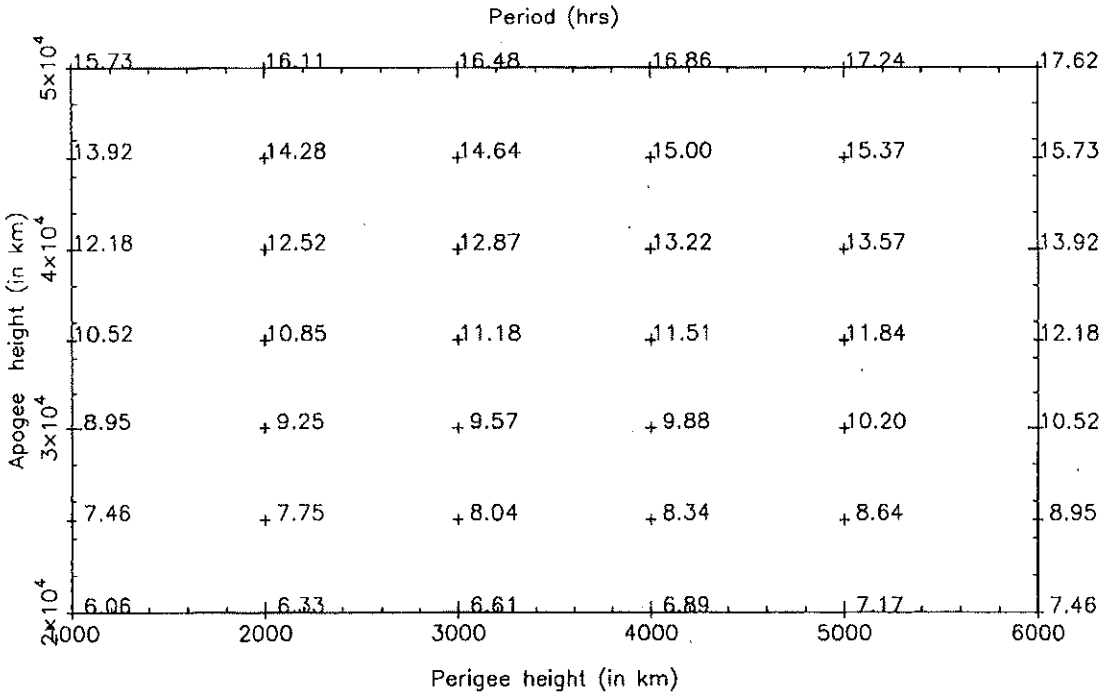

Fig. 3.4: Orbital period as a function of perigee and apogee heights.

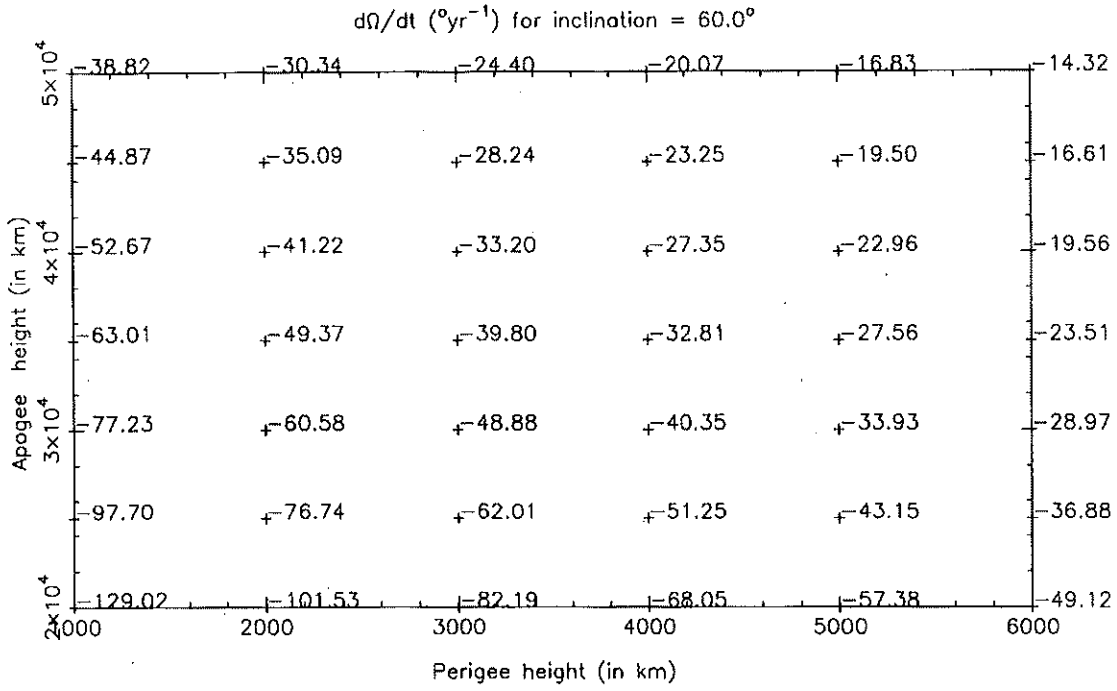

Fig. 3.5: Nodal precession rate dΩ/dt as a function of perigee and apogee heights for i=60°.

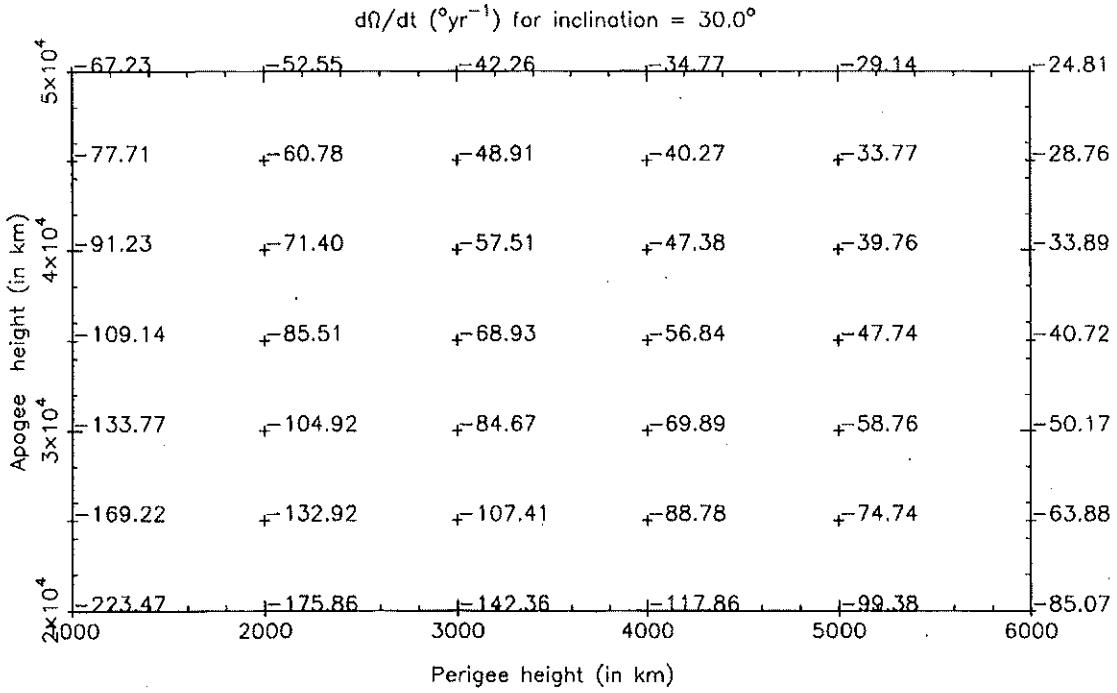

Fig. 3.6: Nodal precession rate dΩ/dt as a function of perigee and apogee heights for i=30°.

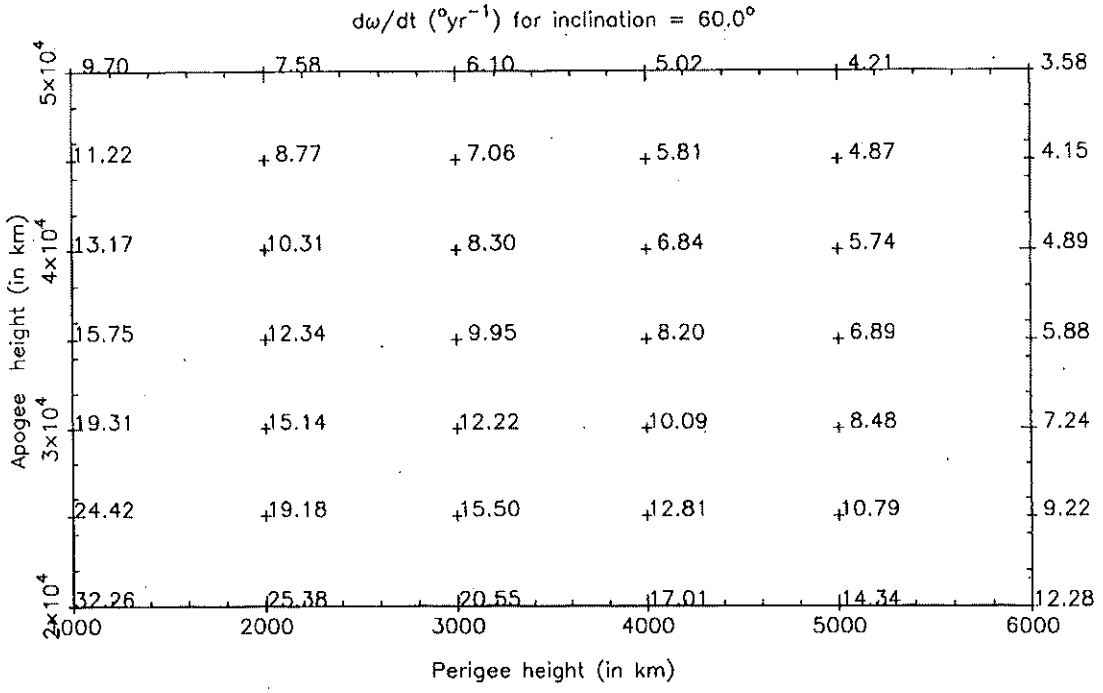

Fig. 3.7: Perigee precession rate dω/dt as a function of perigee and apogee heights for i=60°.

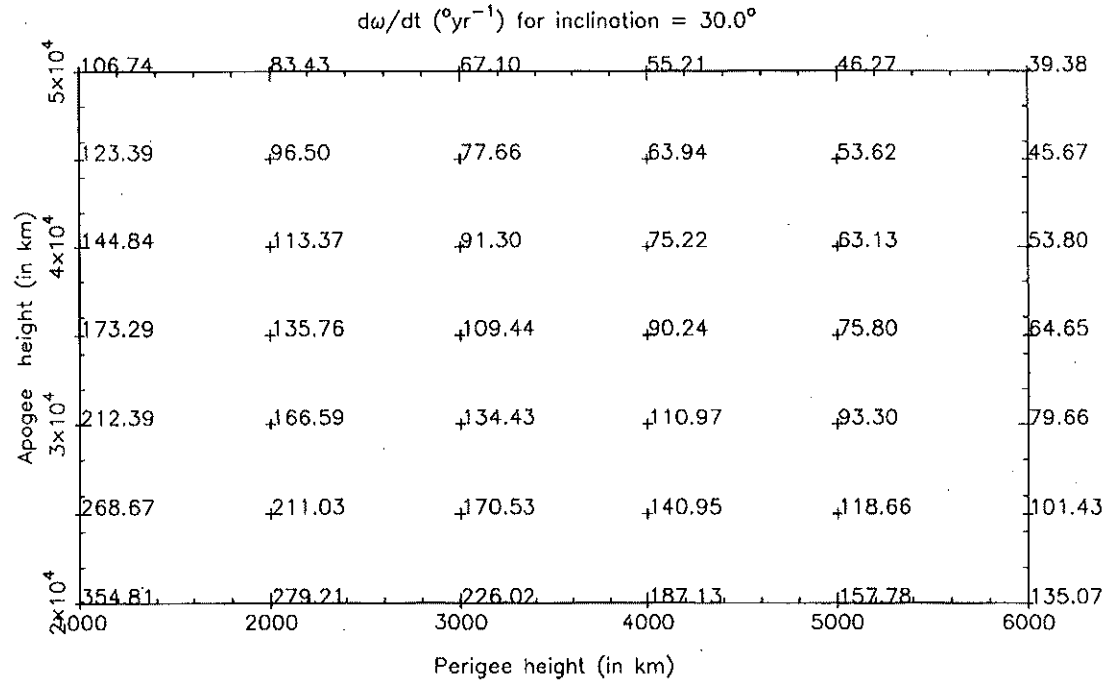

Fig. 3.8: Perigee precession rate dω/dt as a function of perigee and apogee heights for i=30°.

In conclusion, nodal precession rate can be increased significantly by lowering the perigee height from 5,000 to 1,000 km and lowering the inclination from 60 to 30°.

3.5 Launch capability and sequence

The launch vehicle selected for the ARISE mission is the McDonnell Douglas Delta 7925. The 7925 version features 9 solid rocket motors, and a Star 48B spinning third stage. Its delivery capability can be summarized as:

- 1720 kg on a 185 x 40000 km altitude orbit, i=28.7 deg., 3-m dia. fairing
- 1330 kg on a 185 x 40000 km altitude, i=90 deg., 3-m dia. fairing
- 1220 kg on a Molniya orbit (370 x 40000 km), i=63.4 deg., 2.9-m dia. fairing
- 1170 kg on a Molniya orbit (370 x 40000 km), i=63.4 deg., 3-m dia. fairing.

Figure 3.9 shows the injected mass as a function of apogee altitude and fairing type for the 3-stage 7925 vehicle. For ARISE, the 2.9-m diameter (9.5-ft) fairing was selected since it allowed enough space for the stowed spacecraft and since the injected mass was larger than the 3-m, leaving more margin for spacecraft mass growth. Figure 3.10 shows the performance capability of the 2-m dia. fairing as a function of inclination. Ultimately, the choice of the inclination for the ARISE orbit will depend on the spacecraft mass.

Once launched, the spacecraft will go through a de-spin and stabilization mode. A perigee raise maneuver will then occur at the GTO (Geo Transfer Orbit) apogee. Then several sequences of deployment will happen: deployment of the inflatable antenna and solar arrays; deployment of a rigid astro-mast type arm to carry the sub-reflector to about 3.6 m from the spacecraft; and finally deployment of the telecom antenna.

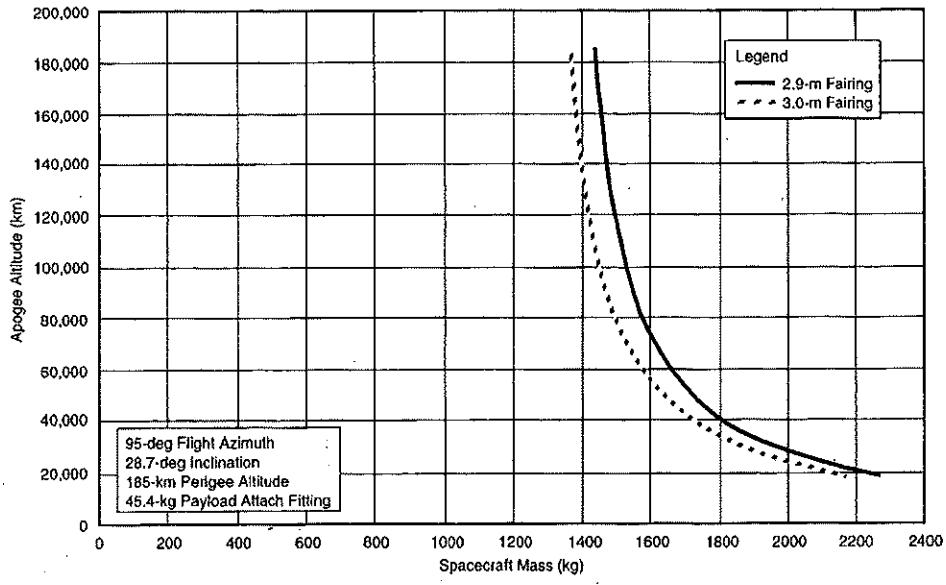

Fig. 3.9: Delta 7925 three stage launch vehicle capability

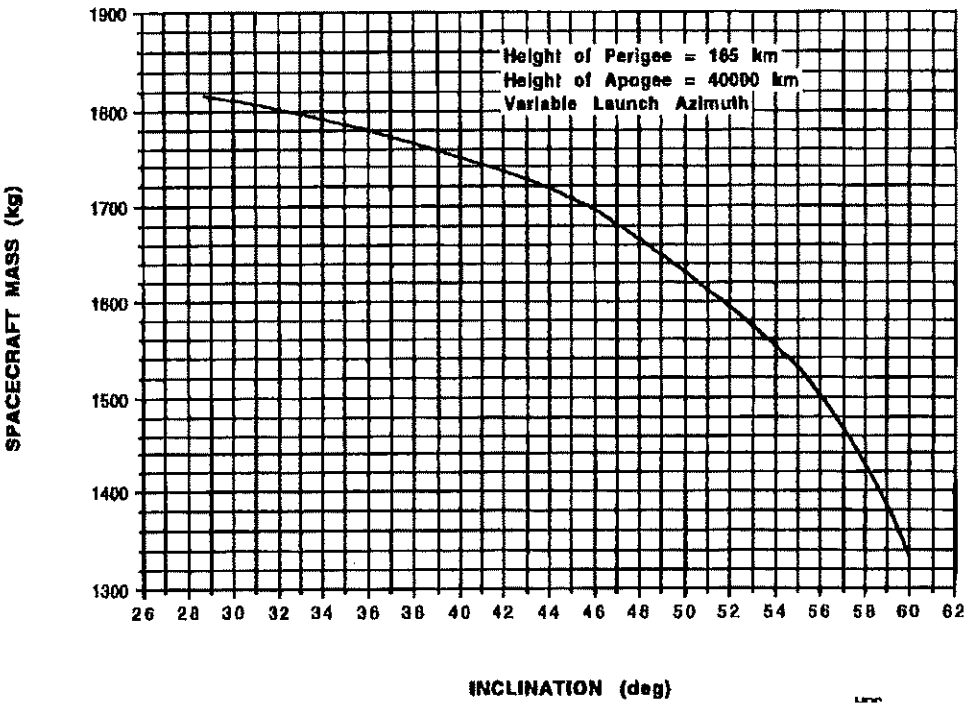

Fig. 3.10: Injected mass as a function of inclination. Delta 7925 2.9-m fairing.

3.6 Space environment

The radiation environment for two different inclinations and two different arguments of perigee was assessed. In summary, the trapped magnetospheric charged particles (electrons and protons) dose behind 100-mils of aluminum was:

- 105 krad[Si]/year @ i = 30 deg., $\omega = 0°$.
- 40 krad[Si]/year @ i = 60 deg., $\omega = 0°$.
- 102 krad[Si]/year @ i = 30 deg., $\omega = 90°$.
- 60 krad[Si]/year @ i = 60 deg., $\omega = 90°$.

The solar flares proton dose have been calculated to be on average about 10 krad[Si] for 3 years, which is small compared to the trapped magnetospheric particles. The requirement for the reflector radiation material resistance was assessed. Surface dose on the reflector was estimated at about 130 Mrad/year, while bulk dose adds up to about 40 Mrad/year. More details on the radiation environment can be found in Appendix E.

The electrical surface charging (ESD) of the ARISE main reflector was also investigated. In summary, differential static potential between the two thin Kapton sheets (one Al coated) forming the main reflector could reach about 20 kV under worst conditions, which could lead to self-sustained arcs. Although the use of an ITO coated Kapton sheet for the canopy might be satisfactory, electrostatic discharge still remains a materials issue until appropriate tests are done. Details on the ESD environment can be found in Appendix F.

4. ARISE Inflatable Antenna

An inflatable antenna was chosen for the ARISE main reflector because of mass, cost and low storage volume considerations. However, a lower risk approach is currently being evaluated using mesh antenna types. Results of this investigation will be reported in the second edition of this document.

4.1 Antenna General Description

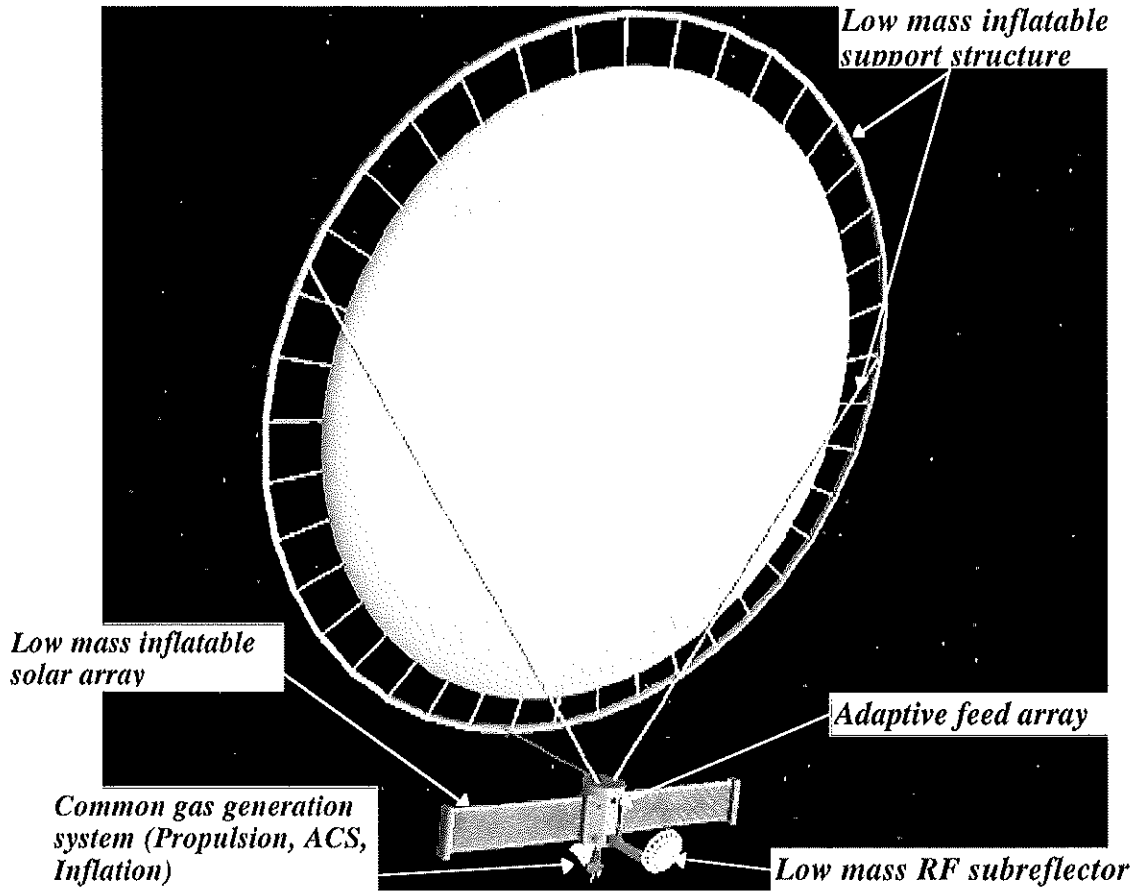

Fig 4.1: ARISE antenna depicting innovative technologies

The ARISE primary reflector is comprised of a reflective membrane with an RF transparent front canopy to complete the inflated lenticular envelope. The lenticular is combined with a tubular peripheral support torus forming a large, lightweight, yet relatively stiff space structure. To minimize membrane stress, the lenticular structure is pressurized with $< 4 \times 10^{-4}$ psi of N_2 and attached to the torus ring with constant force springs in a "trampoline" fashion.

Figure 4.1 shows the configuration of deployable/inflatable/rigidizable technologies used by the ARISE antenna to meet the large structure, low cost, low mass, low storage volume performance requirements.

The antenna assembly is aligned and attached to the spacecraft using three tubular support struts that are inflation deployed from a stowage canister located at the top of the S/C bus. At the torus the antenna support struts are kinematically attached at 120° intervals. They are designed with

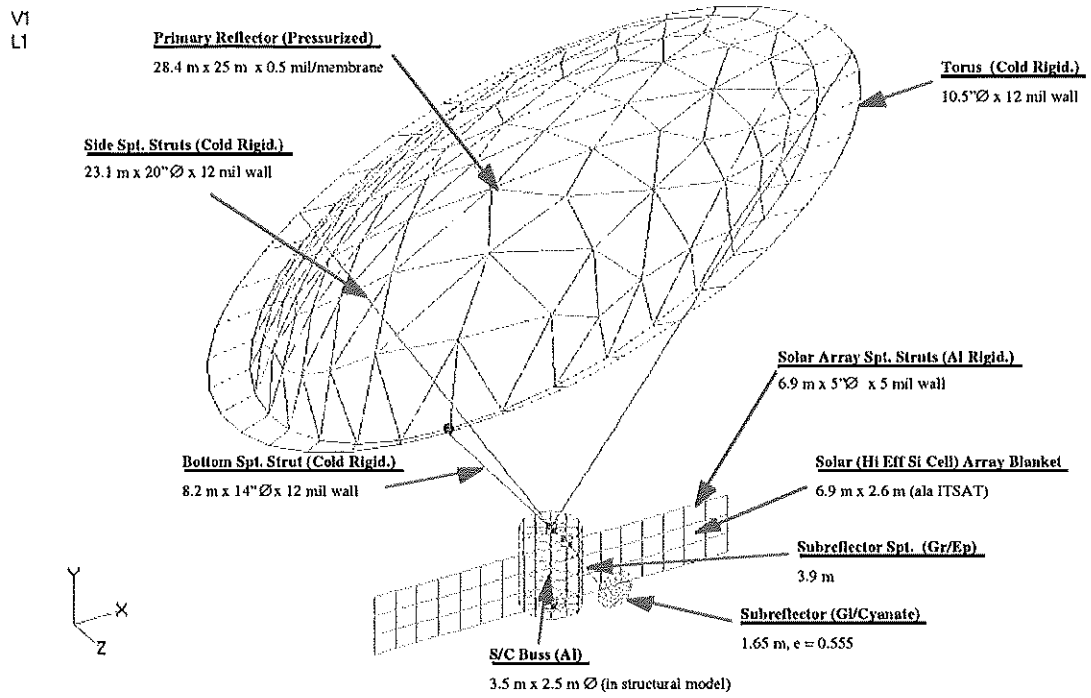

Fig. 4.2: ARISE structural configuration diagram

optimum diameters, wall thickness, and lengths to give mechanical rigidity (bending, torsion) yet minimal obscuration and shadowing of the primary (see Fig. 4.2).

Recent advances in thin film photo-voltaics and the demonstration of the L'Garde ITSAT Inflatable Solar Array have been incorporated into the ARISE design. To meet its power needs, ARISE requires a large solar array, but at the same time needs low array mass and stowed volume to meet launch vehicle constraints. The ITSAT Solar Array with its high packaging efficiency, low areal density, and solar blanket/inflatable frame design is the best available technology to meet the ARISE requirements.

Rigidizable support structure technologies are used wherever possible on ARISE in order to minimize the need for "make-up" inflation gas. The primary reflector torus and antenna support struts maintain their mechanical stiffness and shape by using cold rigidizable rubber and/or polymer materials that solidify (phase change) in cold space environments. To maintain low temperatures and minimize thermal gradients these support members will be wrapped in MLI blankets. Because of high temperature conditions, the ARISE solar array blankets will be supported by thin walled polymer struts laminated with aluminum foil. The strut tubes are initially over-inflated past the aluminum foil's yield point. Once the pressure is removed, the stressed aluminum maintains much of the strut's rigidity and shape.

4.2 Reflector Configuration

The current reflector configuration was selected after extensive evaluation of various reflector antenna geometries, and resulted from some early trade-offs between on-axis and off-axis configurations. Figure 4.3 pictures the two different configurations and Table 4.1 summarizes the pros and cons. Upon thorough examination, it was determined that an off-axis configuration offered better science performance (less obscuration) and fewer constraints for the rest of the spacecraft design.

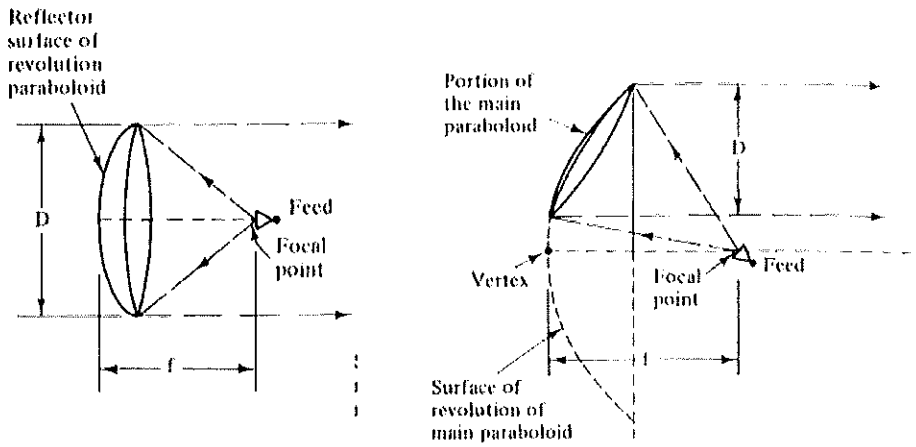

Fig. 4.3: On-axis versus off-axis configurations

	On-axis Pros	Off-axis pros
FOV		No Obscuration
Structures	Symmetry	
ACS	Ease of control	
RF		Un-Obscured Pointing
Fabricability	Same complexity and reflector **RMS**	Same complexity and reflector **RMS**

Table 4.1: On-axis versus Off-axis trade-off

Four different off-axis configurations were then evaluated (Prime Focus, Gregorian, Cassegrain, and Schmidt Cassegrain (see Figure 4.4)) using the following criteria: dynamics/structural stiffness, thermal stiffness, RF performance, mass, complexity, deployment reliability and alignment. It was determined that the Gregorian off-axis design uses a smaller and less complex structure and secondary reflector than Cassegrain types. Furthermore, the Gregorian off-axis system offers the possibility of a mechanically shaped secondary that is reasonably sized and controlled.

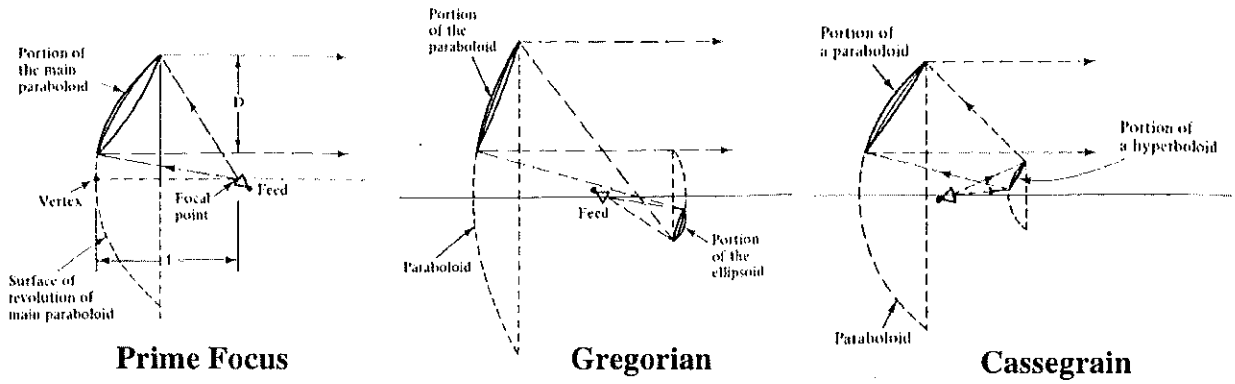

Fig. 4.4: Various off-axis configurations

Based on these arguments, a Gregorian dual-reflector antenna system was selected for ARISE. Figure 4.5 displays a vertical cross-section through the reflector configuration. All the dimensions

shown in this figure are in meters. The geometrical parameters, which fully define the reflector configuration as shown in Figure 4.5, are given below:

On-axis "mother" reflector diameter	D = 50 m
On-axis "mother" focal length	F = 11.55 m
Off-axis sub-aperture diameter	D = 25 m
Tilt angle between main reflector and subreflector axis	β = 5.67 deg.
Inter foci distance	L = 2.4 m
Subreflector eccentricity	ε = 0.555

Figure 4.6 shows a three-dimensional representation of the reflector configuration. A ray, coming in from the antenna bore-sight direction, reflected off the center of the main reflector and the subreflector and received by the antenna feed at focus, is also sketched.

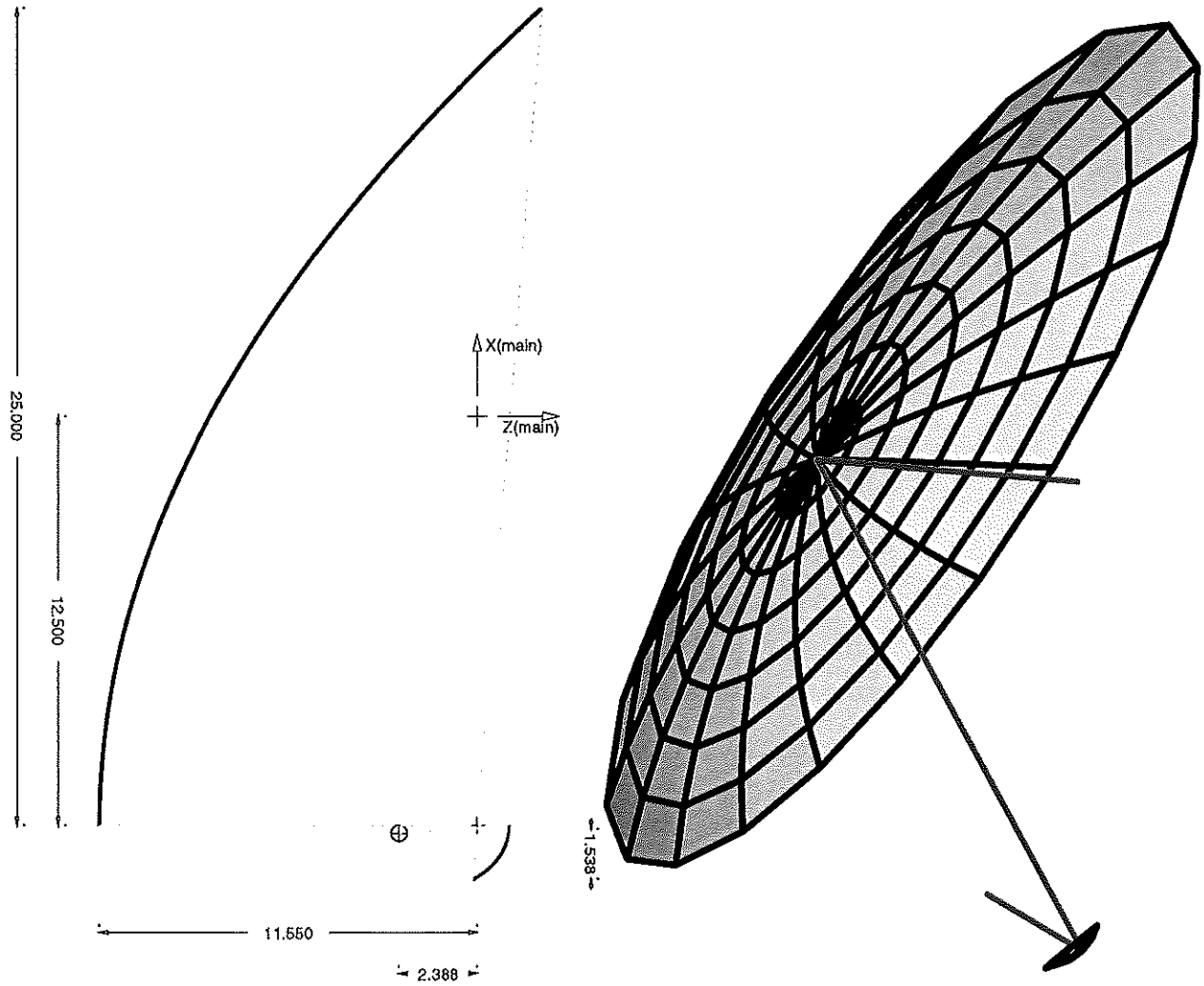

Figure 4.5 (left): Vertical cross-section through the dual reflector geometry as proposed for ARISE. Figure 4.6 (right): Three-dimensional representation of the ARISE dual reflector geometry. Additionally a ray incoming from the bore-sight direction, reflected off the main and subreflector and received at the focus is sketched.

4.3 ARISE Structures and Thermal Analyses

A major consideration in the determination of the relative merits of the off-axis Prime Focus and the Gregorian configurations was structural and thermal behavior. Of special concern were dynamic response, inertial static loading, and thermal distortion effects on antenna shape and alignment. Because of the "soft" nature of inflatable structures, and the temperature sensitivity of polymeric membranes, Structural and Thermal analytical models were created that had more resolution than simple static diagrams and lumped masses. The structure model consisted of over 700 elements (Appendix C) that closely approximated off-axis parabolic curvatures, strut orientation, subreflector alignment, solar array geometry, and S/C mass distribution. Special attention was given to membrane elements, polymer properties, and tubular geometries; all critical to inflatable structural behavior. The thermal model was based on the same nodal geometry and properties allowing a direct one-to-one correspondence between temperature profiles and structural elements.

Analytical Results: When the Prime Focus and Gregorian performance predictions were compared, there was very little difference across the board. The Gregorian antenna dynamic performance fared slightly better than the Prime Focus since its center-of-mass was closer to the S/C bus and its antenna support struts were shorter. Inertial response (static thrust) and thermal distortions were virtually the same between the two configurations. Consequently, the Gregorian was selected over the Prime Focus for other reasons than structural and thermal performance (obscuration, corrective optics, ...).

ARISE's dynamic response was analyzed using normal modes analysis (force driven vibration stimuli have not yet been specified). Table 4.2 lists the first six non-rigid body normal modes for the off-axis Gregorian. In general, the modal frequencies were shown to be representative of large space structures, and are within acceptable bounds given ARISE's operating scenarios. The resultant modal shapes are classic with tip displacements that are non-critical. (Refer to Appendix C for coordinate references.)

Mode #	Modal frequency (Hz)	Modal Shape	Max. *Tip* Displacement (cm)
1	0.3	Primary & S/C bus "nodding" to each other	12.5
2	0.5	Primary Y tilt	13.5
3	0.8	Subreflector Y cantilever	5.5
4	0.9	Subreflector Y tilt	5.8
5	1.0	Primary "trampoline" motion	6.1
6	1.2	Subreflector X tilt	2.5

Table 4.2: ARISE Normal Modes Analysis

Figure 4.7 shows the resulting structural displacements due to a conventional, static (without transients) thrust maneuver loading. A thrust vector of 0.015g at 2° off-axis was applied at the base of the S/C bus in order to study worst case asymmetric inertial loading. A maximum of 4 mm displacement was predicted. Since thrust maneuvers will not be performed during science observations, it was felt, based on these preliminary results, that thrust/slewing maneuvers would not create critical/castastrophic stress or strain conditions.

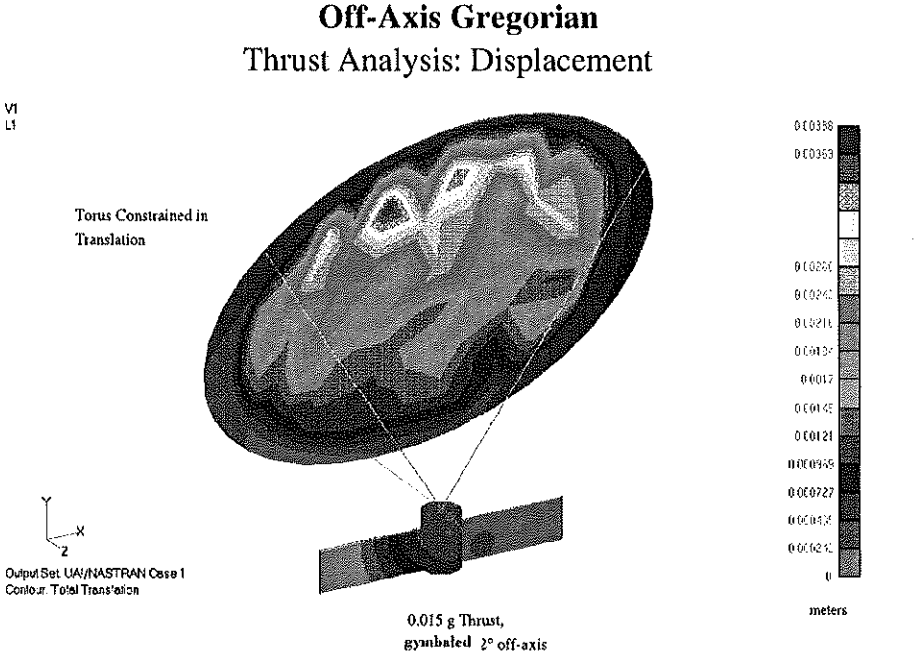

Fig. 4.7: Structural displacements due to a static thrust maneuver loading

After the initial nominal thermal analysis showed no difference between the Gregorian and Prime Focus configurations, a more detailed worse case orbital thermal analysis of the off-axis Gregorian structure was performed. One of the sub-solar points of the ARISE elliptical orbit was chosen for this test case. It was felt that the combination of solar heating at the bottom edge of the lenticular antenna structure with the Earth's albedo/IR would generate large gradients across the reflector membrane. The results shown in Appendix C, Frame 5 indicate a large gradient of approximately 115 C°. The resultant thermal distortions from this thermal profile are currently being analyzed.

4.4 Antenna surface precision

An essential element of the ARISE design is the reflector precision. L'Garde has built a 7 meter reflector with a 1.7 mm RMS accuracy but is predicting 1mm RMS accuracy on reflectors of 25m or more with appropriate development effort. To generate a credible estimate of the magnitude and shape of the 25m ARISE antenna error, ground measurements from the 14m Inflatable Antenna Experiment (IAE) reflector were utilized. The IAE reflector shape is shown in the top right of Figure 4.8. It was measured during a ground test in preparation for flight. During the test, one of the torus supports slipped and was not discovered until after the measurements were taken. Nonetheless it is considered representative of the types of errors seen in this class of reflector albeit somewhat exaggerated. As a projection of the type of errors that will be seen in future reflectors which are expected to be more systematic, a FAIM software model prediction of the reflector shape was utilized. FAIM predicts the shape of the inflated reflector analytically, but includes no random errors as seen in material properties and manufacturing errors. The two reflectors were interpolated together resulting in the reflector shape representing the convolution of the theoretical global error generated by FAIM and the manufacturing errors scaled from the as-measured IAE.

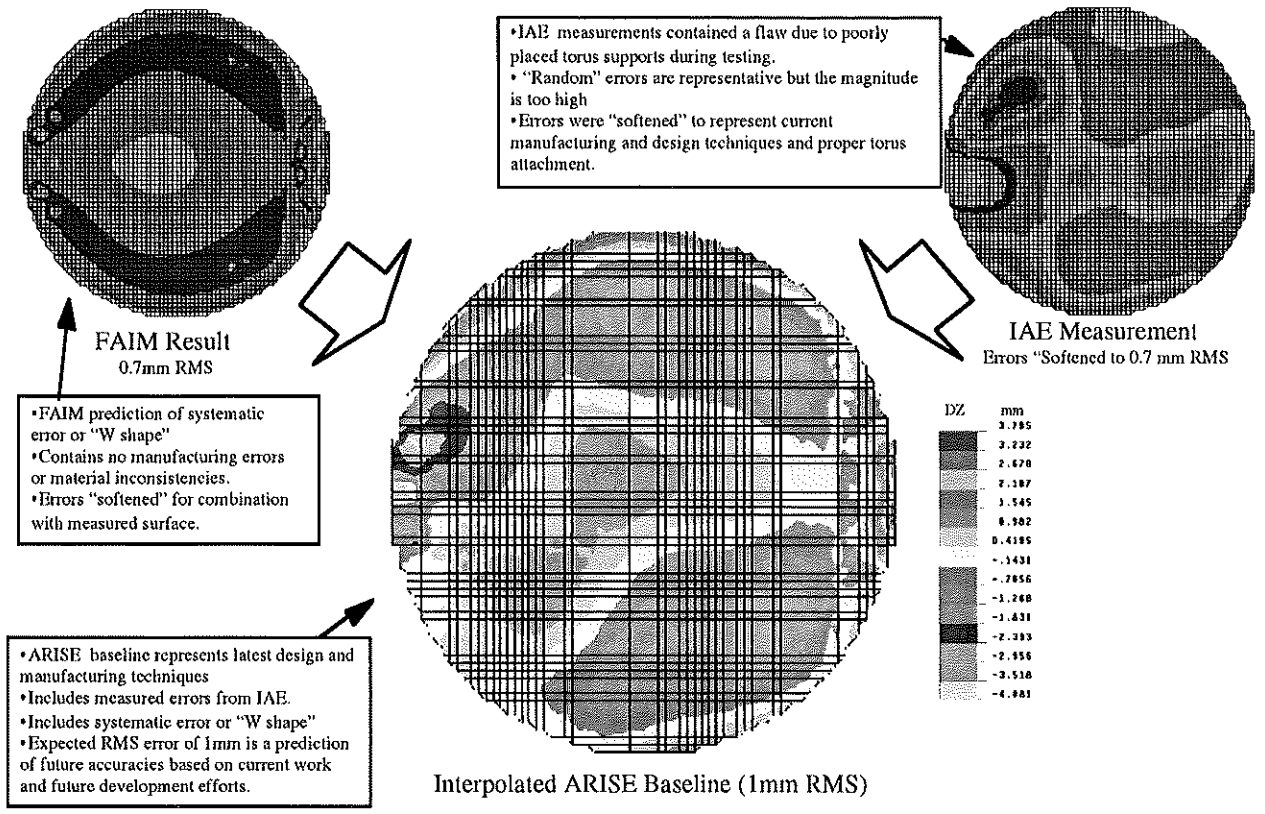

Figure 4.8: ARISE Reflector Precision Projection

4.5 Inflation system

The inflation system for the ARISE mission must provide gas for initial inflation of the struts, torus, envelope (reflector/canopy assembly), and solar array booms, and make-up gas for the envelope over the life of the mission. A range of options was considered, including tanked gas, chemical gas generation, and combinations of these. The baseline specifications for the inflatable antenna are 3.0 kg necessary for initial inflation plus the appropriate amount of make-up gas required over a three-year mission life, and an envelope operating pressure of 10E-4 psia.

The system as currently configured utilizes tanked gas for initial inflation and catalytic hydrazine decomposition for make-up gas. The tank masses are based on scaling relations from a prior study (Thunnissen 1995). No redundancy is incorporated into this conceptual design. The gas tank is 0.24m-dia, T-1000 aluminum-lined graphite-epoxy, initially contains 0.4 kg He gas at 6000 psia, and has a mass of 1.4 kg. The hydrazine tank is 0.40 m-dia titanium, initially contains 23 kg LHZ at 500 psia, and has a mass of 2.4 kg. Estimated mass of catalyst, valves, regulators, filters, orifice, and associated plumbing is 1.2 kg, yielding a total wet mass of 28 kg. With the plumbing items located between the two tanks, the system will fit into an envelope of approximately 0.11 m^3. The components are essentially off-the-shelf items, although some development of the catalyst bed is anticipated to minimize the ammonia content of the products, to provide the minimum molecular weight possible. (The masses listed here assume 100 percent decomposition of the N2H4 into N2 and H2.) Jeff Maybee of Primex Aerospace has been consulted about the design of a minimal-ammonia hydrazine catalyst.

Operation of the system begins by actuating the pyro-valve (or latch valve) at the exit of the gas tank (Fig. 4.9). Regulated helium gas is then introduced into the struts and torus (controlled by a series of solenoid valves), with the cooling of the gas over the duration of the fill assumed to be within acceptable parameters for the cold-rigidized portions of the structure. The initial inflation of the structure is assumed to have a 5-minute duration (worst case). The next operation will be pressurization of the solar array booms to sufficient internal pressure (8 psia) to extend and rigidize, followed by inflation of the antenna envelope to operating pressure. The isolation valve between the hydrazine tank and gas tank is then opened, allowing the gas tank to serve as a reservoir for the products of the hydrazine catalyst bed. The gas tank is of sufficient volume to maintain an approximately one-day supply of make-up gas at nominal conditions, at 5-atm tank pressure. (See section 6.1 for a description of the full launch sequence).

Further definition of the inflation system is dependent on refined estimates of the operational requirements. If the expected catalyst bed exit temperature of 800K is within the allowable temperature range of the spacecraft structural elements, it may, for example, prove feasible to eliminate the gas tank and use the hydrazine system for both initial inflation and make-up. While this does not provide a significant mass advantage, the resulting system will have fewer components. Additionally, the leakage rate at the end of the mission determines the catalyst size and allowable quiescent period for the science mission, unless the fill operation can be done concurrently with data acquisition. The current configuration incorporates a catalyst of 0.2 kg, which is estimated to be sufficient to provide a gas flow rate of 0.6 kg/min.

Potential issues which have yet to be quantitatively addressed include integration of the inflation and propulsion systems, possible absorption of signals by the inflation gas (especially ammonia), possible ionization of inflatant gases caused by large electrical potential gradients between the canopy and reflector (and resultant effect on data collection), and condensation of inflation gases at minimum-temperature conditions.

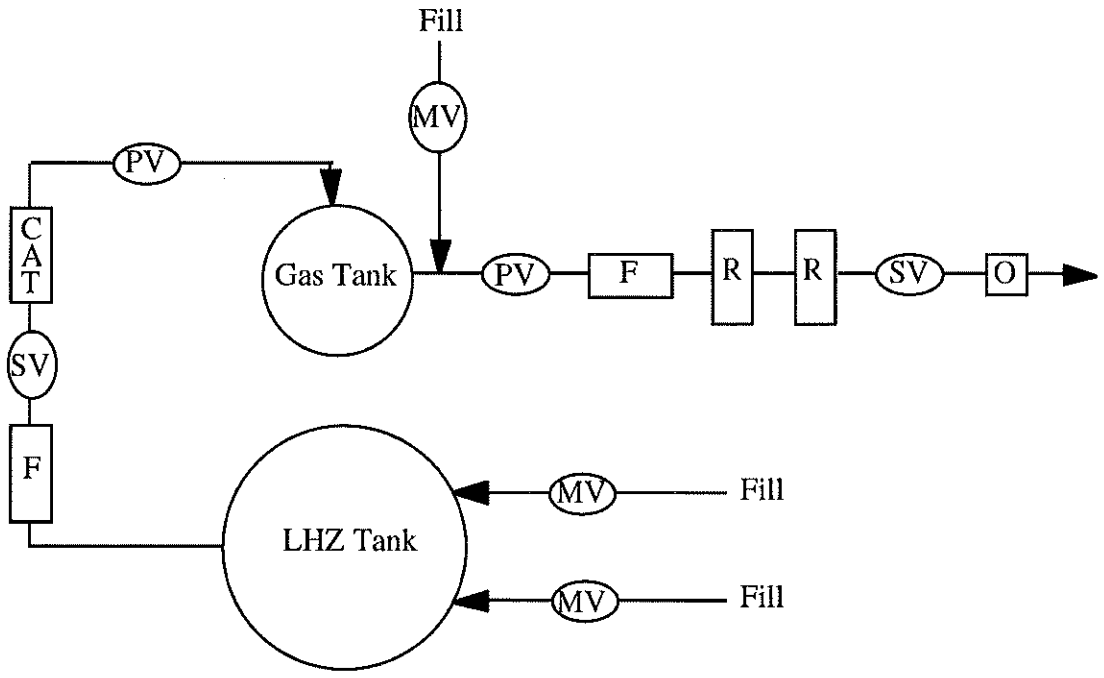

Figure 4.9: ARISE Inflation System: MV = manual valve; SV = solenoid valve; PV = pyro valve; F = filter; R = regulator; O = orifice

4.6 Deployment sequence and Canister design

L'Garde has developed a new flexible enclosure canister as shown in Figure 4.10 and 4.11. The concept promises significant weight savings over the solid canister designs. The lenticular and torus are stored inside a membrane container designed to withstand the increased internal pressure during ascent of the payload. Upon deployment, the top portion of the membrane is released by a pyrotechnic. The petals open, releasing the lenticular and torus. Some residual gas in the lenticular is possible (as was experienced in the IAE flight experiment) and the lenticular is expected to billow out slightly to relieve any internal pressure. After initial deployment the LDDs or L'Garde Deployment Devices are initiated. The next picture in the sequence shows the LDDs deploying the struts. Note, the torus and lenticular are still uninflated and suspended between the extending struts. The next pictures show the struts at full deployment and the torus partially inflated. The lenticular is still not inflated. The solar array gets deployed followed then by the inflation of the lenticular structure. Development of the deployment sequence draws extensively on the lessons learned from the IAE flight experiment.

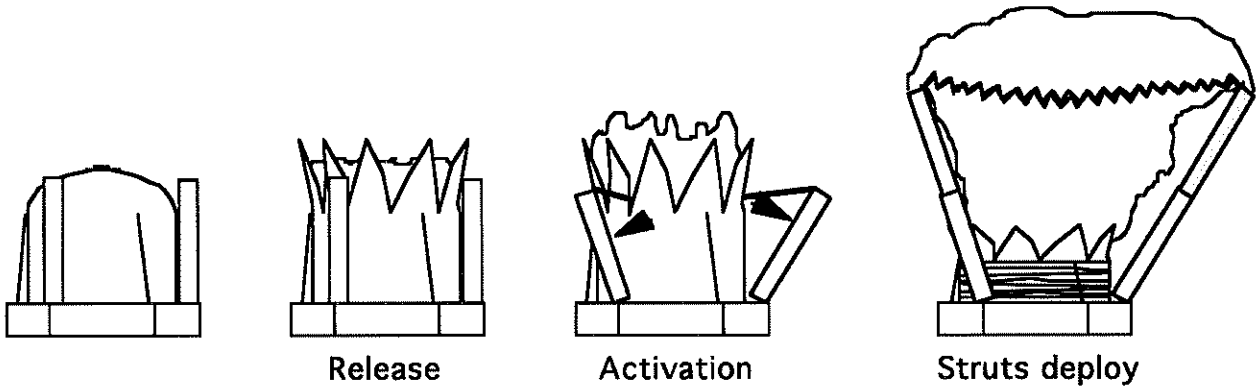

Figure 4.10. ARISE Canister Concept

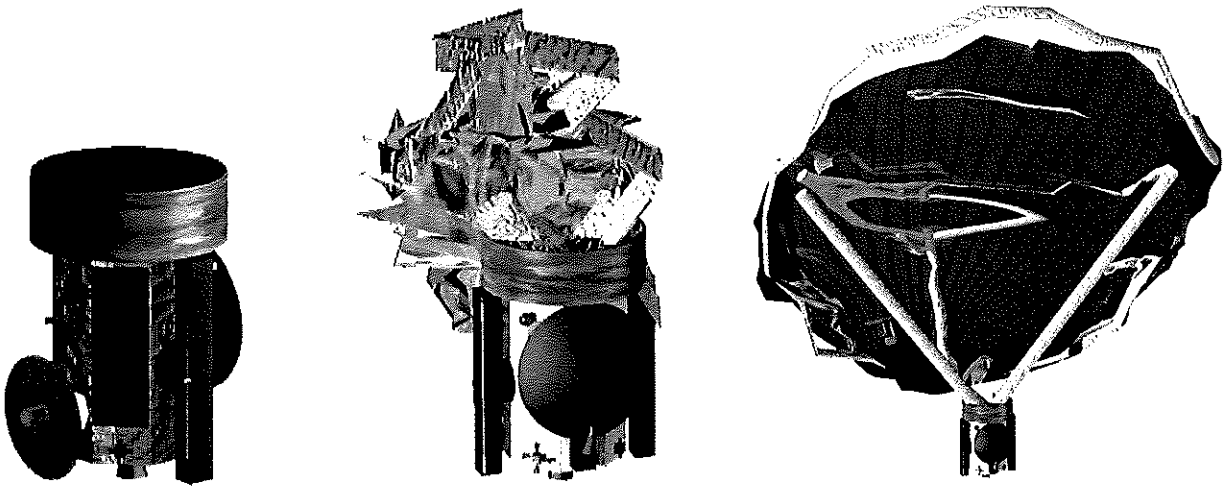

Figure 4.11. Inflatable Antenna Deployment Sequence (by TDM Inc.)

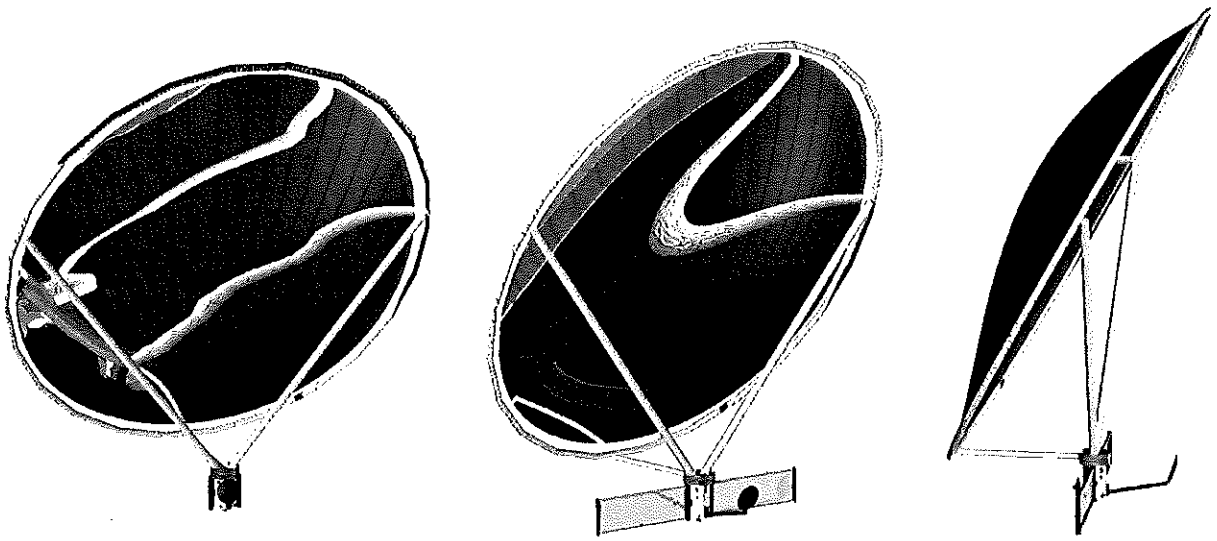

Figure 4.11. Inflatable Antenna Deployment Sequence (by TDM Inc.) (continued)

4.7 Subreflector description

The basic configuration and RF error budget for the ARISE radio telescope assumes that the deviations from an ideal surface figure in the primary mirror (or reflector) will be compensated in large part by changing the shape of the secondary reflector. Present assumptions suggest that this correction may have to be done as often as once every fifteen minutes, but not at a frequency of cycles per second. There is work presently underway at Composite Optics Inc. (COI) in tunable radio frequency reflectors in the one to two meter diameter range. Moreover, work is being done on SBIR contracts by a number of vendors to solve the actuator requirements of the Next Generation Space Telescope (NGST). Given this work in progress the assumption is that an actuated, tunable reflector with the desired optical characteristics may be manufactured at reasonable cost, by building on the work in progress at COI and NGST.

There are six basic problems to be resolved with the ARISE secondary mirror task. These are:

- Mirror Skin Design
- Actuator Selection
- Strong Back
- Mass
- Software
- Integration & Launch Packaging

Mirror Skin Design

COI has completed a Phase One SBIR for ground based tunable reflectors of comparable size to ARISE's subreflector. These reflectors have a composite surface, and are adjusted with screw jacks on the back surface of the mirror. COI has recently been awarded a phase two SBIR contract to extend this work. Of particular relevance to the ARISE work is the amount of finite element modeling which is being done under these contracts, and the confirmation of these FEM models in full size test mirrors. The models comprise a set of basic design tools which COI can employ, at modest cost, on a prototype design of the ARISE reflector. A request for contract numbers, and relevant technical publications is pending with COI, as of this writing.

Actuator Selection

To shape the surface of the secondary reflector, a set of cryogenically adapted, precision, linear motors is required. NGST requires more than 2000 cryogenic actuators, some of which must have a travel of millimeters, and others of which must have a resolution in the 10's of nanometers. NGST is presently funding research at the level of around $800,000 per annum in mechanism development. These mechanisms are being studied in the Low Temperature Science & Engineering cryogenic mechanisms laboratory at JPL. From this work there is a high degree of certainty that actuators suitable for ARISE will be produced. A significant candidate for this actuator is a cryogenic lead-screw designed by Thermetrex Corporation of San Diego. This actuator is tentatively scheduled for test at JPL this fall.

Strong Back

The actuators that shape the secondary need a stable, structural reaction surface behind the mirror. For lightness and strength this should probably not be inflatable, unless it is a self-rigidized inflatable of some type, perhaps with filled epoxy. A composite strong back structure should work well. Because COI has experience in understanding the composite mirror loads, they are the logical company to design a strong back structure that accurately reacts to those loads. The required mass for such an assembly is not known as of this writing. A small study may be sufficient for COI to adapt their present SBIR work to the ARISE problem. This should probably be done sooner rather than later, in case the mass of the strong back is greater than that included in the present ARISE mass budgets.

Mass

Generating an adequate predictive model on the mass budget for the secondary mirror assembly is a task that requires some attention at this point. The strong back, actuator, actuator electronics, cables, supporting structure and the mirror masses are not known at this time to any degree of specificity.

Software

Various organizations have largely resolved the problem of feeding wave-front error into optical surface adjustments over a broad range of wavelengths and response frequencies. A brief survey of the established methods for doing this should be undertaken, in order to select the most appropriate to be adapted to the needs of ARISE.

Integration and Launch Packaging

Significant economies in mass, and other types of performance advantage can often be achieved by cleverly resolving the design trades in the integration and packaging task. For instance, it may be possible to reduce mass, and launch package volume by designing a strong back / mirror surface system in which a primary and secondary inflatable structure are used. The primary structure might hold the mirror / actuator assembly in place. An inflatable, epoxy-cure-upon-deployment strong back could be designed to provide needed strength to the system.

These design trades are often best done at the early phases of system conceptualization. Therefore a brief integration design-trade study, with a view to mass and volume reduction should be conducted in the very near future.

5. Science Payload

5.1 Science requirements

The ARISE top level science requirements can be summarized as:

1. Source detection: the spacecraft must be able to detect sources that have strength of about 10 mJy at 43 GHz, and about 3 mJy at 22 GHz.
2. Spacecraft - ground telecom data rates: 8 Giga bits per second (Gbps), driven by sampling at Nyquist rate (2 samples/sec/Hz) and digitizing at 1bit/sample or 2 bits/sample.
3. Observation duration: the spacecraft must be able to observe a single source for 12-24 hours, at one or several frequencies. One coherent integration time is between 15 and 350 seconds.
4. Sampling duty cycle: the fraction of time that science data is gathered during one observation is at least 70 %. That leaves 30% for other spacecraft duties.
5. Gain variation: the gain in the direction of the source cannot vary more than 2-5% during one coherent integration time.

Table 5.1 to 5.12 provide a more complete set of default parameters for the ARISE mission, together with possible ranges for those parameters. Telescope parameters for the Green Bank Telescope (GBT) have been taken from the GBT web site, while VLBA telescope parameters are taken from the VLBA web site, with some assumptions made about improved system temperatures by the time of ARISE launch. The possible ranges of many parameters are educated guesses. It is unlikely that phase-referencing will be possible at the higher (or any) frequencies for ARISE. However, the tables include the possibility of achieving equivalently long coherence times by means of atmospheric calibration at the ground telescopes (using water vapor radiometers, phase referencing of the ground telescopes, or similar techniques). Finally, in the calculation of spectral-line sensitivities, a channel width of 0.5 km/sec has been assumed in all cases. This was chosen as a compromise among the various types of spectral-line science that might be done, and can easily be scaled for other assumptions by the square root of the channel width.

Table 5.1: Radio Telescope

Quantity	Nominal	Possible Range
Diameter	25 m	15 - 25 m
Structure	Inflatable	Others
Optics	Off-axis Gregorian	On-axis; Cassegrain
Sun-Avoidance Angle	30 deg	20 - 50 deg
Pointing Accuracy	3 arcsec	2 - 6 arcsec
Slew Rate	2 deg/min	1 - 4 deg/min
Phase Referencing	None	5 - 8 GHz
Surface Accuracy	0.5 mm (target)	0.2 - 1 mm
Corrected Surf. Acc.	0.25 mm	0.2 - 0.5 mm

Table 5.2: Observing System

Quantity	Nominal	Possible Range
Freq. Coverage	8, 22, 43, 60, 86 GHz	No 8 & 60; add 1.6 & 5
Polarization	Dual Circular	Single Circular
Polarization Purity	< 3%	1-6%
Sampling	1 or 2 bit	2 bit
Calibration Accuracy	2%	1% - 3%
IF channelization	TBD	TBD

Table 5.3: Sensitivity vs. Frequency - 8 GHz

Quantity	Nominal	Possible Range
Frequency Span	8 - 9 GHz	5 - 9 GHz
T_{sys}	12 K	8 - 15 K
Aperture Efficiency	0.50	0.4 - 0.6
System Equivalent Flux Density (SEFD)	130 Jy	75 - 590 Jy
Coher. Time (C=0.9)	350 sec	100 - 2000 sec
Data Rate	4 Gbit/sec	1 - 4 Gbit/sec

Table 5.4: Sensitivity vs. Frequency - 22 GHz

Quantity	Nominal	Possible Range
Frequency Span	21 - 23 GHz	18 - 23 GHz
T_{sys}	16 K	12 - 25 K
Aperture Efficiency	0.38	0.3 - 0.5
SEFD	240 Jy	130 - 1280 Jy
Coher. Time (C=0.9)	150 sec	60 - 1000 sec
Data Rate	8 Gbit/sec	1 - 8 Gbit/sec

Table 5.5: Sensitivity vs. Frequency - 43 GHz

Quantity	Nominal	Possible Range
Frequency Span	42 - 44 GHz	40 - 45 GHz
T_{sys}	24 K	20 - 35 K
Aperture Efficiency	0.24	0.2 - 0.35
SEFD	560 Jy	320 - 2700 Jy
Coher. Time (C=0.9)	60 sec	20 - 400 sec
Data Rate	8 Gbit/sec	1 - 8 Gbit/sec

Table 5.6: Sensitivity vs. Frequency - 60 GHz (single dish only)

Quantity	Nominal	Possible Range
Parameters	TBD	TBD

Table 5.7: Sensitivity vs. Frequency - 86 GHz

Quantity	Nominal	Possible Range
Frequency Span	84 - 88 GHz	80 - 90 GHz ?
T_{sys}	45 K	30 - 80 K
Aperture Efficiency	0.08	0.08 - 0.2
SEFD	3200 Jy	850 - 16,000 Jy
Coher. Time (C=0.9)	15 sec	5 - 100 sec
Data Rate	8 Gbit/sec	1 - 8 Gbit/sec

Table 5.8: 7-sigma continuum sensitivity to 1 VLBA antenna

Quantity	Nominal	Possible Range
8 GHz	1.9 mJy	0.6 - 15 mJy
22 GHz	4.5 mJy	1.3 - 46 mJy
43 GHz	15 mJy	4.4 - 162 mJy
86 GHz	120 mJy	25 - 1400 mJy

Table 5.9: 7-sigma continuum sensitivity to GBT

Quantity	Nominal	Possible Range
8 GHz	0.4 mJy	0.1 - 3.6 mJy
22 GHz	0.8 mJy	0.2 - 8.3 mJy
43 GHz	2.5 mJy	0.7 - 28 mJy
86 GHz	26 mJy	5.5 - 300 mJy

Table 5.10: 7-sigma spectral line sensitivity to VLBA antenna (0.5 km/s channel)

Quantity	Nominal	Possible Range
8 GHz	0.5 Jy/ch	0.2 - 2.2 Jy/ch
22 GHz	1.0 Jy/ch	0.3 - 3.8 Jy/ch
43 GHz	2.5 Jy/ch	0.7 - 9.5 Jy/ch
86 GHz	14 Jy/ch	2.9 - 57 Jy/ch

Table 5.11: 7-sigma spectral line sensitivity to GBT (0.5 km/s channel)

Quantity	Nominal	Possible Range
8 GHz	0.1 Jy/ch	0.04 - 0.5 Jy/ch
22 GHz	0.2 Jy/ch	0.06 - 0.7 Jy/ch
43 GHz	0.4 Jy/ch	0.1 - 1.6 Jy/ch
86 GHz	3.1 Jy/ch	0.6 - 12 Jy/ch

Table 5.12: Additional mission information

Quantity	Nominal	Possible Range
Launch Date	2008	2007 - 2012
Lifetime	3 yr	2 - 5 yr
Comm. Link	38 GHz	80 GHz or optical
Tracking Stations	5	4 - 7

5.2 Receivers/Amplifiers

The ARISE receiver design is critical to the final performance of the instrument. By providing the lowest noise possible, requirements on the size and performance of the primary mirror can be bound to achievable goals. Cryogenic InP High Electron Mobility Transistors (HEMTs) provide the lowest possible noise for receivers from 1-100 GHz operating at temperatures above 4 K.

In addition InP HEMT transistors operate with the lowest power dissipation of any three ternimal device, which is critical for thermal load on the cryocooler.

The baseline ARISE receiver has channels at 8, 22, 43 and 86 GHz. The receiver front end is cooled to 20 K. The front end (Figure 5.1) is comprised of an antenna, orthomode transducer and an InP HEMT amplifier. The front end is nominally designed to have a noise figure of 5 times quantum limited noise at all four frequencies. This noise temperature has already been achieved at 8, 22 and 43 GHz using InP HEMT amplifiers with discrete transistors. This goal at 86 GHz is expected to be met by a cryogenic amplifier program at JPL and is consistent with the goals of the ESA's Planck Surveyor, Low Frequency Instrument. The use of InP monolithic millimeter-wave integrated circuit (MMIC) technology allows for state-of-the-art performance and ease of integration at 86 GHz. This will be crucial should the adaptive array be utilized on ARISE.

Parameter	8 GHz	22 GHz	43 GHz	86 GHz
Noise (K)	8	12	19	39
Bandwidth (GHz)	2	2	4	4
Cryo power (mw)	64	23	15	8

Table 5.13 Performance of the ARISE Receivers.

The cryogenic portion of the radiometer front end is connected to a warm back end via stainless steel waveguide or coaxial cable. The signals are then passed through an image reject filter and mixed down to an IF bandwidth of DC-4 GHz. The mixer will utilize a phase locked local oscillator (PLLO) with phase locking derived from a stable crystal oscillator. Should an adaptive array be implemented, each feed in the array will have its own front end and mixer, the IF signal will be passed into an array processor which will trim the phase of the PLLO on each element individually and adjust the IF amplifier gain. The output of the array processor will be a single IF channel with a "clean" effective beam.

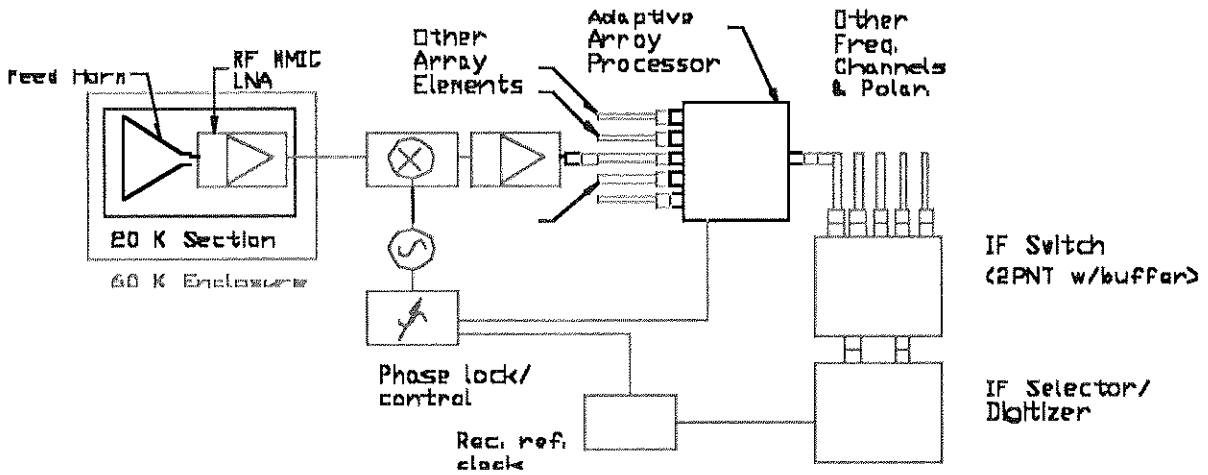

Figure 5.1: ARISE Receiver Schematic.

Following the array processor, the IF signals are sorted by frequency and polarization and digitized. A tone provided by a ground based source is digitized along with the signal to provide an accurate phase reference for the signal.

Two approaches towards digitization may be taken. The first option is to build on the current VLBA digitizers which multiplex many 32 MHz A/D converters to build a larger bandwidth. The advantage of this scheme is that it takes advantage of the current VLBA equipment, potentially reducing overall program costs. A second approach is to utilize modern high speed A/D converters operating at frequencies in excess of 1 GHz. The advantage to this technology is a greatly reduced digitizer mass and power, but the development costs to populate VLBI telescopes could be significant.

5.3 RF adaptive compensation

At all the operating frequencies, the radiation performance of ARISE has been evaluated using a vector diffraction computer program, which employs Physical Optics on both the main reflector and the subreflector. For the operating frequencies at 43 GHz and 86 GHz, array feeds are utilized to electronically compensate for the performance deterioration caused by surface distortions and beam pointing error. At both operating frequencies, a 19 element array feed is used with 0.86 λ inter-element spacing. Investigations into adaptive methods to optimally combine the signals received by the individual array elements are currently under way. Utilization of circularily polarized compensation is also under investigation, and it is expected that although results will not change, hardware and software implementation will be more complex.

5.3.1 Feed layout and array configuration

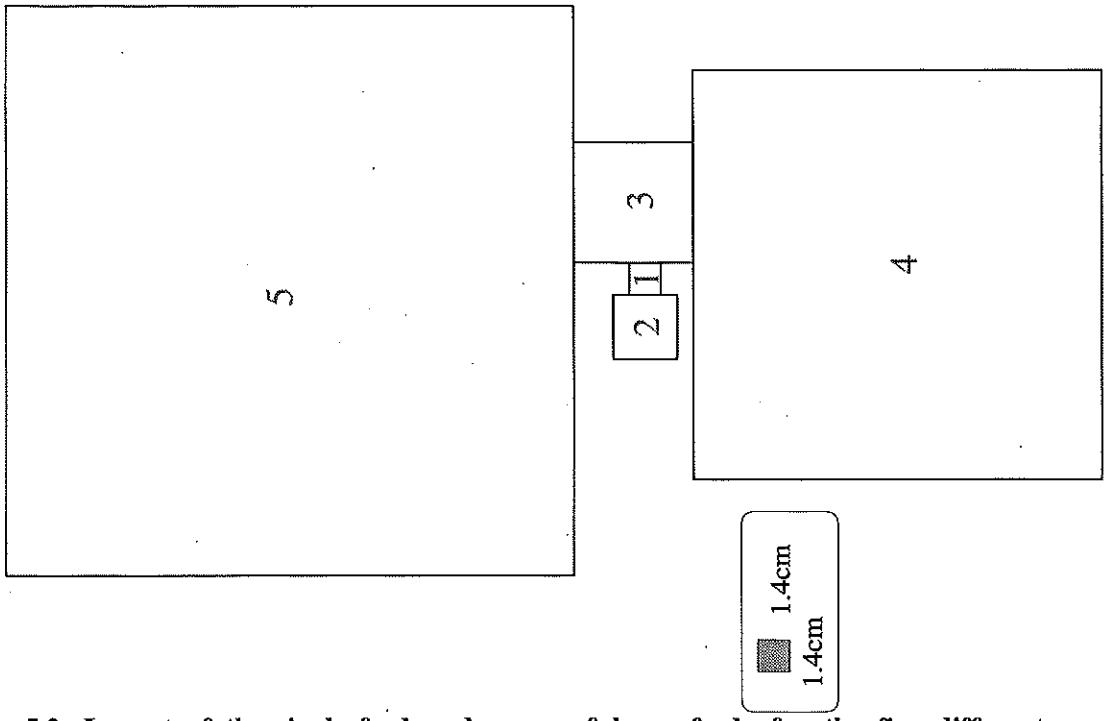

Figure 5.2: Layout of the single feed and array of horn feeds for the five different operating frequencies. The numbers refer to 1 = 86 GHz, 2 = 43 GHz, 3 = 22 GHz, 4 = 8 GHz and 5 = 4.85 GHz (Size of scaled square corresponds to size of the 86 GHz feed).

The layout of the horn feeds and array of horn feeds in the focal plane of the reflector are displayed in Figure 5.2. The numbers in this figure refer to the operating frequencies of the respective feed, i.e.

1 = 86 GHz
2 = 43 GHz
3 = 22 GHz
4 = 8.0 GHz

At both 43 GHz and 86 GHz a 19-element array feed is used. Both array feeds are hexagonal based. The feed geometry is displayed in Figure 5.3. The usage of a 37-element array feed is also contemplated. This array feed is similarly hexagonal based and its feed geometry is displayed in Figure 5.4. For the RF performance shown in the following paragraphs, an array inter-element spacing of 0.86 λ is assumed. This array spacing is still a subject of ongoing research.

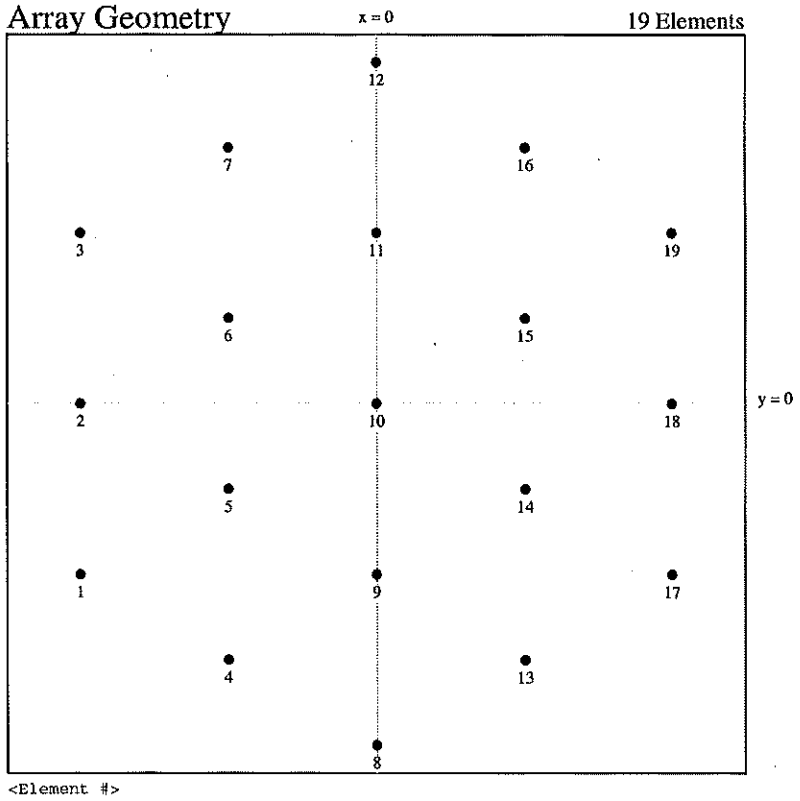

Figure 5.3: Geometry of the hexagonal based 19-element array feed. The array spacing is at 0.86 λ, which is 6 mm at 43 GHz and 3 mm at 86 GHz.

5.3.2 Surface distortions and un-wanted beam tilt

Due to material, manufacturing and deployment imperfections, limitations and errors, surface distortions are introduced in the primary reflector. Because of the unique characteristics of the inflatable membrane structure, these distortions are slowly varying in nature. In order to accurately simulate the RF system performance, the assessment of these distortions in terms of their effects on the radiation characteristics is imperative.

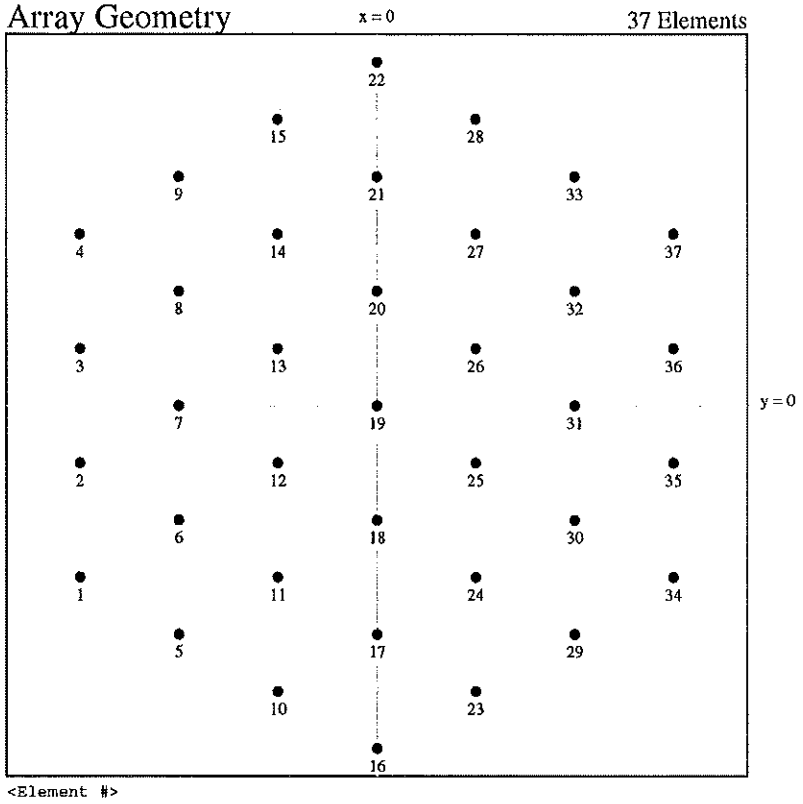

Figure 5.4: Geometry of the hexagonal based 37-element array feed. The array spacing is at 0.86 λ, which is 6 mm at 43 GHz and 3 mm at 86 GHz.

As an analytic distortion model, a functional dependency of the form:

$$z = \tau * \rho^3 * \sin(3 * \varphi)$$

was considered. (ρ, φ) are the coordinates in a polar coordinate system, τ denotes the center-to-peak height of the distortion. A surface plot of this analytic distortion model is displayed in Figure 5.5. A surface RMS value of 0.5 and 1 mm was considered, which resulted in a center-to-peak height of 1.5 and 3 mm in the distortion model described above.

A surface plot of the most recently supplied discrete surface distortion data by L'Garde is displayed in Figure 5.6. This distortion has a surface RMS value of approximately 1 mm.

A further source of RF performance degradation is un-wanted beam pointing. A beam pointing error of only one beamwidth reduces the directivity and antenna efficiency significantly. At higher frequencies the beamwidth becomes more narrow, which makes the accurate pointing more difficult and necessitates the usage of an array feed and corrective feed array excitation to achieve the required RF performance.

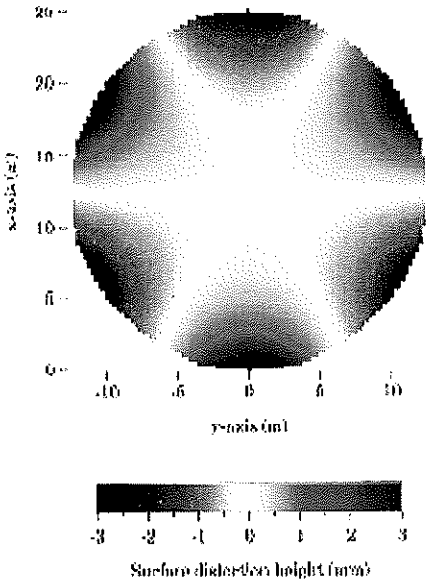

Figure 5.5: Surface plot of the analytic surface distortion model. The center-to-peak height is 3 mm, which yields a rms of approximately 1 mm.

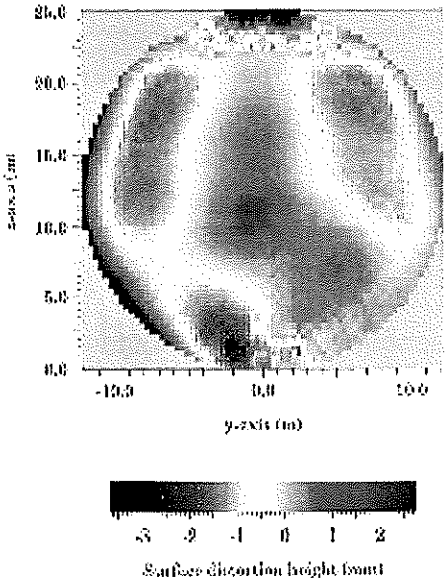

Figure 5.6: Surface plot of the discrete surface distortion data as supplied by L'Garde on 04/06/98.

5.3.3 RF performance using single feeds

At first the RF system performance is evaluated using single feeds at each of the five operating frequencies. This approach is less costly and easier in its implementation complexity. The key ARISE RF performance parameters for an undistorted and distorted surface (analytical distortion model) using single feeds at each frequency are displayed in the following table. For the analytic distortion model, an RMS value of 1 mm has been considered. Additionally at the operating frequencies 43 GHz and 86 GHz, a surface RMS value of 0.5 mm has been investigated.

Frequency [GHz]	Configuration	D [dB]	AE [%]	BW [deg.]
8.0	ideal	65.52	81.0	0.110
	distorted (1 mm)	65.19	75.3	0.110
22.0	ideal	74.30	81.0	0.036
	distorted (1 mm)	71.95	47.3	0.045
43.0	ideal	80.19	81.0	0.018
	distorted (0.5 mm)	77.87	48.4	0.022
	distorted (1 mm)	73.79	18.2	0.033
86.0	ideal	86.14	81.0	0.009
	distorted (0.5 mm)	79.82	19.0	0.017
	distorted (1 mm)	76.66	9.1	0.019

Table 5.14: RF performance of ARISE, using a single feed at each of the operating frequencies.

In Table 5.14, D denotes the directivity in dB, AE the antenna efficiency (including taper and illumination efficiency) and BW the half-power beamwidth in degrees. Note that the efficiency referred to here includes only taper and illumination efficiency. Other efficiency numbers due to losses caused by effects such as mismatch, feed network, finite surface conductivity, local surface rms, blockage or polarization mismatch are not considered in the antenna efficiency. The ultimate efficiency will be somewhat lower than the value recorded in this table.

It is apparent from the previous table, that the deteriorating effects of the surface distortions increase with frequency. While the losses in directivity and, hence, antenna efficiency are acceptable up to a frequency of 22 GHz, the losses at 43 GHz and 86 GHz are too severe for the RF system performance requirements assuming a RMS value of 1 mm. New ways to achieve the requirements are needed.

5.3.4 RF performance using array feeds

At both 43 GHz and 86 GHz, array feeds are used to compensate for surface distortions and beam pointing errors. In the following, the RF performance at 43 GHz and 86 GHz is discussed using an array feed as displayed in part 5.3.1 of this section. At first, analytic surface distortions as displayed in Figure 5.5 are considered. In the following table, the three cases 'ideal' (no surface distortions), 'distorted' (analytic surface distortion model) and 'compensated' (using corrective feed array excitation) are considered.

For the discrete surface distortion data as supplied by L'Garde and shown in Figure 5.6, the RF performance at 43 GHz is investigated. With these surface distortions, the directivity reduces to 72.01 dB, where the beam tilts by 0.029 degrees. With a 19-element array as displayed in Figure 5.3 for distortion compensation, the directivity changes to 70.27 dB and the beam tilt reduces to 0.025 degrees. Using a 37-element array as displayed in Figure 5.4, the directivity increases to 73.31 dB and the unwanted beam tilt is fully compensated for. To avoid the usage of a 37-element array, subreflector shaping in combination with a 19-element array compensation is currently under investigation.

Frequency [GHz]	Config.	D [dB]	AE [%]	BW [deg.]
43.0 (RMS=0.5mm)	ideal	80.19	82.40	0.018
	distorted	78.11	51.07	0.022
	compensated	78.38	54.32	0.022
43.0 (RMS=1mm)	ideal	80.19	82.40	0.018
	distorted	74.34	21.42	0.032
	compensated	75.36	27.12	0.030
86.0 (RMS=0.5mm)	ideal	86.18	81.87	0.009
	distorted	80.34	21.32	0.016
	compensated	81.67	29.01	0.015
86.0 (RMS=1mm)	ideal	86.18	81.87	0.009
	distorted	77.17	10.29	0.019
	compensated	78.63	14.41	0.018

Table 5.15: RF performance of ARISE at 43 GHz and 86 GHz, using 19-element array feeds with corrective feed array excitation coefficients.

For the beam pointing error, an unwanted beam tilt in the amount of the half-power beamwidth is considered. At an operating frequency of 43 GHz, the half-power beamwidth is 0.018 degrees. Given a beam tilt of the same amount (0.018 deg.), the directivity and antenna efficiency at boresight without array compensation reduces to 67.13 dB and 4.08%, respectively. With the array compensation, the beam tilt is reduced to 0.006 degrees and the maximum directivity at that location is at 79.1 dB. For an unwanted beam tilt of 0.012 degrees, the array compensation can fully compensate for the tilt. The directivity for the uncompensated and the compensated case are 75.12 dB and 79.64 dB, respectively.

5.3.5 Representative farfield patterns

The operating frequency for the following four cases is at 43 GHz. In Figure 5.7 a), the beam contour pattern of an undistorted ARISE reflector surface is displayed. In Figure 5.7 b), the distorted beam contour pattern is displayed using the discrete surface distortion data supplied by L'Garde (see Figure 5.6). A single feed is used in these two cases.

In Figure 5.8 a), a 19-element array is used to compensate for the surface distortion effects. In Figure 5.8 b), a 37-element array is used to compensate for the surface distortion. The improvement using array feed compensation with 19 elements and especially 37 elements is clearly visible in these figures.

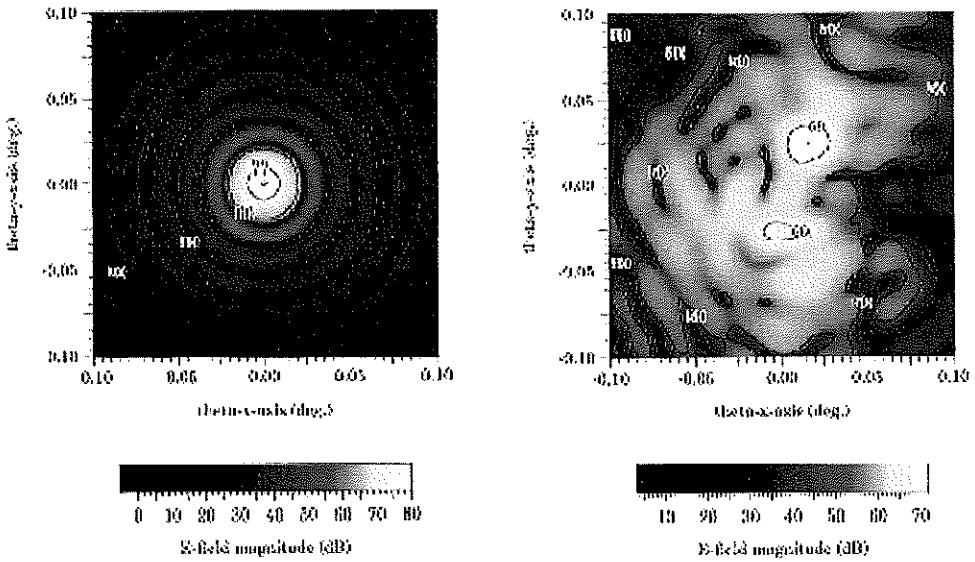

a) b)

Figure 5.7: Beam contour pattern of ARISE at 43 GHz. a) No surface distortions. Single feed. b) Discrete surface distortion model as shown in Figure 5.6. Single feed.

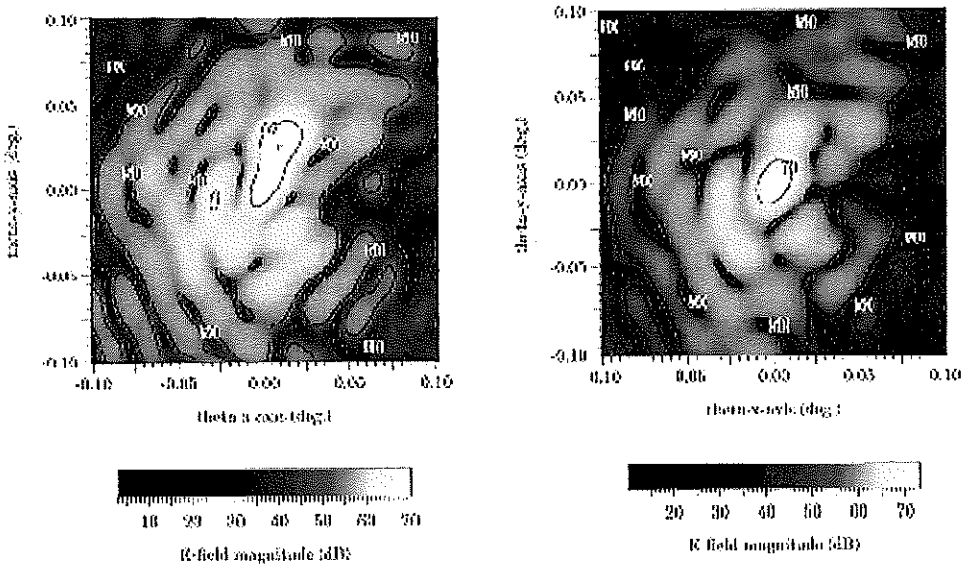

a) b)

Figure 5.8: Beam contour pattern of ARISE at 43 GHz. Discrete surface distortion model as shown in Figure 5.6 a) Feed array compensation using a 19-element array feed. b) Feed array compensation using a 37-element array feed.

5.4 RF system performances

One of the most critical parameter to assess on ARISE is the overall antenna efficiency. For a 25-m diameter aperture, the science requirements ask for a 7 σ sensitivity of about 3 mJy at 22 GHz and about 10 mJy at 43 GHz. It is then desirable that the antenna efficiency be at least 0.55 at 22 GHz, at least 0.2 at 43 GHz, and the highest possible at 86 GHz. The RF adaptive compensation scheme described above allow for an increase in antenna efficiency that includes distortions of the main reflector, aperture taper, feed spillover and polarization efficiencies. However, other losses should be taken into account. A preliminary assessment of these other system efficiencies is summarized in Table 5.16 for each frequency of interest. The canopy transmittance is based on testing of a 0.5-mil CP-1 sheet coated with 100 Ang. of ITO, which is currently the candidate material. The reflector material is a 0.5-mil sheet of Kapton coated with Aluminum. The pointing error is an estimate from the spacecraft and antenna ACS analysis.

Efficiency	8 GHz	22 GHz	43 GHz	86 GHz
Adaptive compensation (computed) Antenna distortions Aperture taper Feed spillover Polarization	0.753 (Single feed)	0.473 (Single feed)	0.271	0.144
RF path attenuation				
Shadowing (struts + S/C)	0.94	0.94	0.94	0.94
Canopy transmittance (twice)	0.93^2	0.91^2	0.88^2	0.85^2
Meteoroid shield (twice)	0.95^2	0.95^2	0.95^2	0.95^2
Reflector reflectance	0.98	0.98	0.98	0.98
Surface local rms (specular)	0.98*	0.98*	0.98*	0.98*
Feed displacement	0.98*	0.98*	0.98*	0.98*
Pointing error	0.98*	0.98*	0.98*	0.98*
Surface ohmic efficiency	0.99*	0.99*	0.99*	0.99*
Feed network loss	0.95*	0.95*	0.95*	0.95*
Margin	0.97	0.97	0.97	0.97
Total efficiency	**0.46**	**0.28**	**0.15**	**0.07**

Table 5.16: Projection of the overall aperture efficiency *: estimated efficiency

The prediction of the antenna distortions results from an ACS/dynamics, structural analysis (described in the inflatable antenna section and spacecraft design section) and thermal steady state worst case scenario analysis. The amplitude of the distortions are summarized in Table 5.17. More work needs to be done to assess/confirm these antenna distortions.

Distortions type	Amplitude (peak to valley) (mm)	RMS (mm)	Comments
Manufacturing / Wrinkles	3	1	Predicted
Dynamics	< 0.1		Reaction Wheels effects
Thermal	TBD		Not compensated - Steady
ESD Lofting	TBD		Unknown at this stage
Make up gas waves	TBD		Unknown at this stage
Total			

Table 5.17: Projection of the inflatable antenna distortions

Assuming the aperture efficiencies stated in Table 5.16, the science system performances then provide a 7 σ sensitivity summarized in Table 5.18.

Frequency	8 GHz	22 GHz	43 GHz	86 GHz
ARISE diameter	25 m	25 m	25 m	25 m
ARISE efficiency	0.46	0.28	0.15	0.07
ARISE Tsys	12 K	16 K	24 K	45 K
VLBA diameter	25 m	25 m	25 m	25 m
VLBA efficiency	0.72	0.52	0.36	0.15
VLBA Tsys	30 K	60 K	80 K	100 K
Data rate	4 Gbps	8 Gbps	8 Gbps	8 Gbps
Coherence time	350 s	150 s	60 s	15 s
7 σ limit	2.0 mJy	5.2 mJy	19.0 mJy	130 mJy

Table 5.18: ARISE Science System Performance Projection

Sensitivities of the antenna efficiency to the final detection threshold is under investigation.

6. Spacecraft Description

6.1 Spacecraft configuration

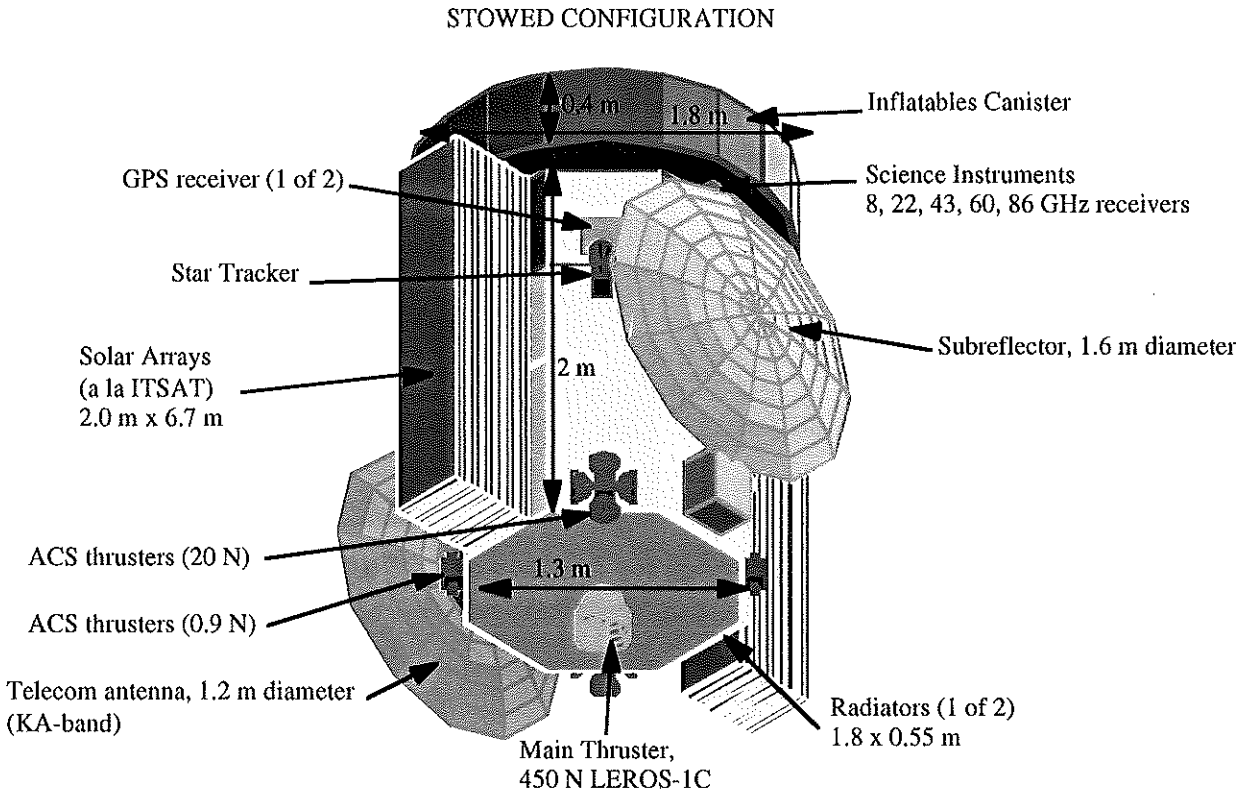

Figure 6.1: ARISE spacecraft in the stowed launch configuration

The spacecraft design is based on an octagonal shaped bus 1.3-m large and 2-m high. Figure 6.1 shows a conceptual external configuration of the ARISE spacecraft. Figure 6.2 shows the conceptual layout of the interior of the spacecraft bus. The octagonal structure supports the inflatable antenna canister on the top, as well as the inflatable solar arrays on two of the side panels. The other panels support a deployable 1.2-m diameter RF Ka-band telecom antenna, a deployable 1.6-m diameter secondary (sub-) reflector, and various other spacecraft equipment (ACS thrusters, GPS receivers, star scanners, radiators, omni-antennas...). The science receivers described in the science subsystem section are located at the focal plane and on the same panel as the sub-reflector and below the canister in a way that no blocking of the receivers occurs. The canister was designed to be part of the bus structure as much as possible (to reduce its structural mass) and to minimize blocking/shadowing of the main reflector.

The spacecraft volume and maximum dimensions were mostly driven by the Delta II 7925 9.5-ft diameter three-stage configuration fairing. The interior dimensions of the fairing are 2.5-m diameter at the base (same diameter for a height of 2-m) and about 4.6-m high. The canister diameter was constrained by the width of the shroud. In the current design, there is about a 0.3-0.4 m radial margin with respect to the shroud for the lower part of the spacecraft (everything below the canister).

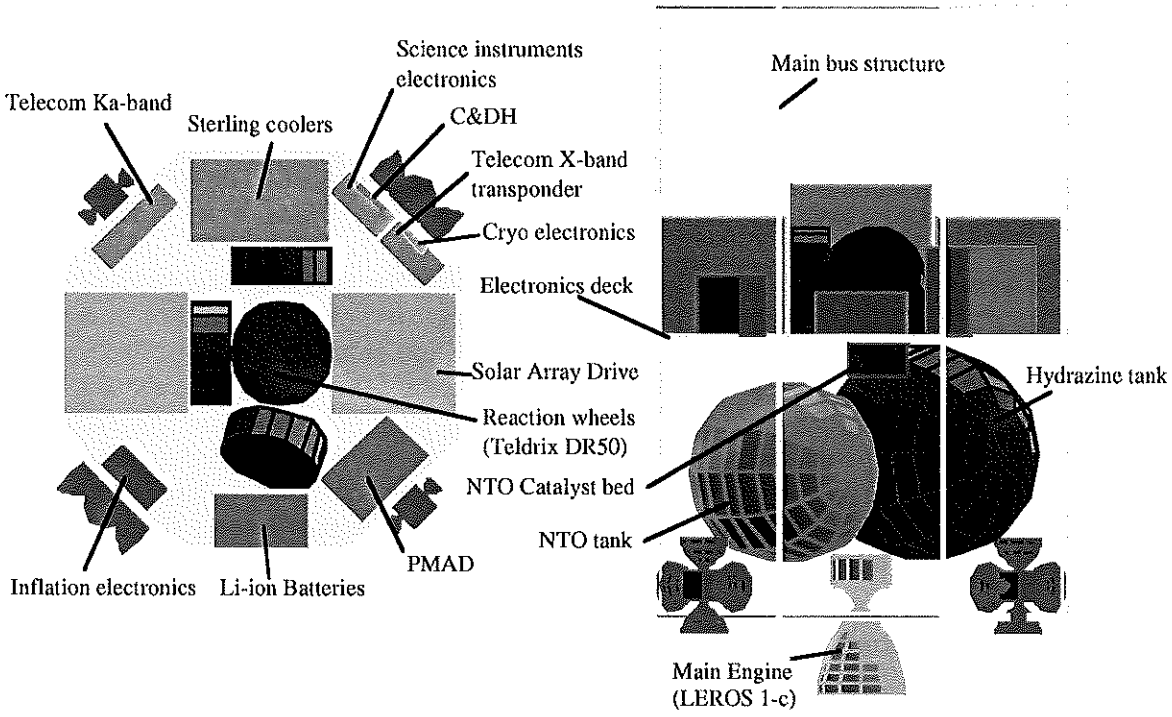

Figure 6.2: Inside layout of the ARISE spacecraft

The interior layout of the spacecraft was driven by the Delta II 7925 Cg requirement, which must be located about 1.2 m above the separation plane (see Fig. 6.2). The fairing separation plane corresponds to the bottom plane of the spacecraft bus where the adapter will be located. The lower third of the spacecraft bus contains mainly the propulsion module with the Hydrazine, Nitrogen Tetroxide, Xenon and pressurant tanks, feed systems, main engine and mounting, inflation catalyst bed and various hardware associated with the inflation system. About 295 kg of fluids will be initially loaded, and about 128 kg of propulsion dry mass (no contingency) will be mounted in this first third of the spacecraft bus. The middle third will house the electronics deck, with the Telecom, Data system, Power, Attitude Control and Science hardware and electronics. This deck also includes the two cryocooler stages, with the Sorption cooler mounted at the bottom of the inflatable antenna canister. No or little effort was done to integrate the electronics with the structure as per the Lookheed Martin Multifunctional Structures bus design. By 2008, it is to be anticipated that such an integrated bus will be current technology and thus the spacecraft design will have to be revisited to take this technology into account (a projected 20% reduction in total spacecraft mass could be applicable then). The top third of the spacecraft bus holds the inflatable antenna canister which is integrated with the bus structure.

About 6.9 hours after launch, a perigee raise maneuver will occur at the GTO (Geo Transfer Orbit) apogee. Then several sequences of deployment will happen. First, due to its large size, the inflatable antenna will be deployed. This deployment will be controlled and will take between 5 and 20 minutes. The struts will be inflated first, then the torus. The struts and torus will be rigidized through a thermal phase change of the material (cold rigidization). To simplify the inflation system, the inflatable solar arrays will be deployed (on 2 wings) next. This scenario enables the combination of the antenna inflation system, solar arrays inflation system and the attitude control/propulsion system, thus reducing system dry masses. Only once the solar arrays are in place does the reflector/canopy assembly get inflated. The spacecraft will be running on batteries

until solar arrays deployment and will be telecommunicating with the Earth with two omnidirectional antennas. The third deployment will be the sub-reflector one. A rigid astro-mast type arm will be used to carry the sub-reflector to about 3.6 m from the spacecraft. A gimbal system at the end of the mast will then align the sub-reflector with the main reflector. The last deployment will be that of the 1.2-m diameter telecom antenna. This antenna needs to be deployed downward with respect to the spacecraft bus in order to get a clear half-space field of view and also to minimize coupling of Ka-band telecom antenna with the main reflector. A gimbaling system will allow the antenna to rotate and cover a whole half space.

A challenge in the spacecraft design was to take into account all the pointing and field of view requirements. During science observations, the main reflector can be pointed anywhere in the sky except for a 30 deg. cone around the Sun. At the same time the solar arrays must be pointed toward the Sun to provide the 2.4-kW needed (see power budget in section 6.2), and the Ka-band telecom antenna must be pointed toward the Earth for continuous science data downlink. To achieve these requirements, the solar arrays will be one-axis gimbaled and the telecom antenna is deployed and 2 DOF gimbaled to cover a half-space. At this time it is believed that this configuration should allow for almost continuous coverage of the telecom ground stations but a more thorough analysis should be done to evaluate the effective coverage.

6.2 System description, mass and power budgets

A top level mass budget of the ARISE spacecraft is summarized in Table 6.1. A more detailed mass budget can be found in Appendix A. A 30% mass contingency was applied to the spacecraft dry mass. The propulsion module was sized using the launch vehicle injected mass. The main GTO perigee raise maneuver is done with the NTO/Hydrazine 450 N Leros 1-C, which features an Isp of 325 seconds. A ΔV of about 380 m/s is achieved. Height (8) 22 N thrusters will be used for main burn trajectory correction, and height (8) 0.9 N thrusters will be used for coarse attitude control maneuvers.

Subsystem	Mass (kg)
Inflatable antenna	192
Telecom	32
C&DH	13
Power	142
ACS	82
Thermal Control	159
Structures/Mechanisms	204
Propulsion (+ACS) system	128
Science instruments	81
Spacecraft dry mass	**1033**
Contingency (30%)	310
Propellants/Fluids	295
Launch Vehicle adapter	46
Total spacecraft mass	**1684**
Launch vehicle capability (@ i=36 deg.)	**1691**

Table 6.1: ARISE spacecraft mass budget

Twelve (12) mini ion thrusters (3-cm diameter, see description in Appendix D) will be used on the inflatable antenna torus to overcome and correct for solar pressure torques. These mini-ion thrusters still need to be developed, and 3 sets of the more mature Field Emission Electric Propulsion (FEEPs) could be used instead for about the same dry mass. One concern though with the FEEPs is that they use liquid metal as propellant and therefore contamination of the canopy and main reflector might be an issue. However, more analysis needs to be done to determine the implications of having ion thrusters on the inflatable antenna torus, both on an ACS and structures points of view. The attitude determination of the spacecraft will be done with star trackers, sun sensors and 2 GPS receivers. Fine pointing will be done with reaction wheels. It is to be anticipated that a closed loop between the science receivers (feed array) and the ACS system will have to be designed in order to achieve the 3-50 arcsec pointing requirements of the main reflector.

The science data requirements are quite demanding (8 Gbps) and an early trade-off between optical and RF downlinks was done. In view of the technology development programs, it was decided that the RF system was a "safer" candidate and therefore chosen as the telecommunication system for the ARISE spacecraft. This choice could be revisited later on. Thus, a 1.2-m diameter Ka-band antenna transmitting 30 W RF will be used to downlink science data at a rate of 8 Gbps. Both polarizations and a high order modulation technique such as the Quadrature Amplitude Modulation will enable the data to be transmitted within the tight 1 GHz bandwidth available at Ka-band. A parallel X-band transponder will be used to uplink commands and valuable time information for VLBI processing. X-band receivers are two patch antennas that will cover near 4π steradian coverage.

Mode / Subsystem	Launch + post-launch	Orbit insertion	All deploy-ments	Science	Stand by, slewing	Eclipses
ACS	133.5	133.5	133.5	228.5	228.5	133.5
Propulsion	60	60	70	520	10	10
C&DH	9	9	9	12	9	9
Inflatable antenna	82	82	82	5	5	5
Power	20	20	20	72	40	40
Mechanisms	0	0	80	80	80	50
Telecom	36	36	36	303	36	36
Thermal control	70	70	70	450	70	70
Science	0	0	0	75	0	0
Subtotal (W)	**410.5**	**410.5**	**500.5**	**1745.5**	**478.5**	**353.5**
Contingency (30%)	123.1	123.1	150.1	523.7	143.5	106.1
Battery recharge				125	125	
Total (W)	**533.6**	**533.6**	**650.6**	**2394.2**	**747**	**459.5**
Source	Primary battery	Secondary battery	Primary battery	Solar array	Solar array	Secondary battery
Duration (hrs)	6.8	0.5	2			0.75

Table 6.2: Power budget in Watts per mission modes

The power sources encompass a set of primary Li/SO_2 batteries for post-launch activities (about 5 kWhr), a set of secondary Li-ion batteries (about 350 Whr, with 125 W of recharge power) for power generation during eclipses and a 2-wing inflatable solar array for main power generation.

The array is sized to provide 2.4 kW during science observation (most constraining mode). The inflation system of the solar array is integrated with the main reflector inflation system and propulsion/ACS hardware to reduce dry mass. Power demand per mission modes is summarized in Table 6.2 (see Appendix B for more details). A 30% power contingency was used on all modes. The larger power consumers are the cryo-coolers, the reaction wheels, the telecom 8 Gbps downlink and the mini-ion engines. Also, since the power requirements are large during the science mode, no science will be done during eclipses. Details on all subsystems are given next sections.

6.3 Gain and observation duration budget

As part of the science requirements, it was prescribed that for valuable science to occur, the gain of the antenna should not vary more than 2-5% during the sampling period and that the science data acquisition should take at least 70% of the observation duration. In an attempt to address both requirements, lists of potential perturbation during sampling and spacecraft duties during observations were established. Potential perturbations include ACS reaction wheels, cryocooler, thermal and dynamics, lenticular pressure maintenance, and ESD Lofting. Spacecraft duties are summarized in Table 6.3. Both list are evolving as our understanding of the spacecraft, mission and antenna improves.

Task	Frequency (per orbit)	Total Duration (min)
Earth occultation	0-1	30-40
Antenna calibration		
Bright source pointing	1-2	2-4
Antenna stabilization	1-2	TBD
Subreflector focusing	1-2	TBD
Adaptive array calibration	1-2	TBD
Source data acquisition		
Target source pointing	1-2	2-4
Antenna stabilization	1-2	TBD
New source pointing	1	19
Telecom ground station switching	1-3	5-15
Telecom link establishment	1-3	2-6
Reaction wheels unloading	32	32
Cryos set-up	1-2	TBD
Antenna gas maintenance	3-?	TBD
Miscellaneous		
Effective total		**TBD (120+)**
Total required	30% of orbit	**245**
RF data acquisition	70% of orbit	**571**

Table 6.3: Observation duration timeline

6.4 Spacecraft Data Flow

6.4.1 Avionics

Requirements and Assumptions

The Command & Data Subsystem (CDS) for the ARISE spacecraft is required to operate for a primary mission life of 3 years. The dual string block redundant design will transfer real time science data to the Telecom subsystem at a rate of 8 Gbps. The CDS will receive periodic uplink commands at rate 2 kbps. An 8 GHz uplink tone will be distributed to the science instrument. The electronics must operate through an equivalent radiation environment of 315 krads behind 100 mils of aluminum. The mass storage element in the CDS is not required to store or process the high speed science data.

Design Implementation and New Technology

The CDS required functions are performed by either CDS block redundant strings. Redundancy provides a high level of reliability to meet the primary and extended mission high speed data throughput performance requirements. All of the key elements in the CDS design are new technology.

Real time science data is transferred to the Telecom subsystem via four channels simultaneously. Each FireWire IEEE 1394.B channel will operate at 2 Gbps. High speed First In First Out (FIFOs) registers insert header data and State Of Health (SOH) data into the downlink data frames. The FIFOs may be provided by UTMC or Honeywell. Uplink commands are processed at 2 kbps. The Lockheed Martin PowerPC 750 processor verifies and processes uplink commands, stores time tag commands & GPS data, controls the spacecraft fault protection, routes the science data, distributes the spacecraft time and collects SOH data. Lockheed Martin PowerPC 405 microcontrollers may be used as needed. The flight code and SOH data are stored in flash non-volatile memory. Redundant low power serial busses provide an interface to control and monitor the health of the other subsystems. The flight software code is written in ANSI C or C++. The ACS pointing and control algorithms are supported in the CDS software.

The 14 Multi-Chip Modules (MCMs) in the CDS design have a mass of approximately 4 kg. Each CDS string dissipates 9 watts. One CDS string is active at any given time, while the other string is in a cold sparing mode. Commercial rad-tolerant electronics are shielded behind 100 mils of Tantalum. The shielding mass is 8.7 kg. The effective radiation environment is 19.5 krads Total Ionizing Dose (TID). The electronic devices are immune to Single Event Latch-up (SEL) and immune to Single Event Upset (SEU) to 75 MeV/mg-cm^2.

CDS Avionics Caveats

The IEEE 1394.A FireWire serial bus is presently being developed by the X2000 Team. Their plan is to provide a fixed rate (100 Mbps) data bus design. Although this does not meet the needs for the ARISE mission, the X2000-2 Team could leverage from the X2000 design team effort to develop an IEEE 1394.B FireWire serial bus. The advanced FireWire design would operate up to 3.2 Gbps. Both FireWire designs require some modification to provide electrical isolation between functional subsystems. Commercial high speed rad-tolerant electronics will be a challenge to develop.

6.4.2 Telecommunications

Requirements

The ARISE spacecraft will orbit around the Earth in a LEO orbit with perigee of 5000 Km and apogee of 40,000 km. The telecom system needs to downlink data at up to 8 Gbps with bit error rate (BER) less than 10^{-4}. The observed data is not stored on the spacecraft and needs to be downlinked immediately. The spacecraft is expected to perform science measurements approximately 70% of the time. Link availability is required to be greater than 70 % during observation. Dedicated ground receiving stations are needed. The telecom system also needs to support a command link at 2 Kbps or less and a housekeeping telemetry link at 2 Kbps or less. Two-way Doppler measurements need be performed for accurate time-stamping of the data..

Candidate Systems

The candidate telecom system designs consist of an X-band transponder for command, housekeeping, and two-way Doppler tracking and a separate high data rate downlink system. Both optical and RF systems have been considered for the high rate downlink.

An optical system was initially recommended because optical systems do not have to meet any spectral usage requirements. The candidate system employs four wavelength-multiplexed lasers, each with output power of 2 W. This is designed to match the four channels of radio science data. The aggregate output is fed to a 30 cm telescope on the spacecraft. With the help of a laser beacon from the ground receiving site, the spacecraft telescope transmit to the ground station which has a one-meter telescope. Initial calculation shows that the lasers can provide over 7 dB of link margin.

The high rate RF system needs to operate in the 37-38 GHz spectrum allocated by the FCC for space VLBI missions. To meet the 8 Gbps downlink requirement with 1 GHz of bandwidth, the candidate RF system implements two 4 Gbps links using left-handed circular polarization (LHCP) and right-handed circular (RHCP) polarization. The high rate RF system transmits at 30 W RF in each polarization to a 34-m DSN antenna. The link margin is about 6 dB.

Optical system offers excellent capability that will greatly benefit ARISE. The ARISE preproject will work closely with the optical communications technologists to monitor the progress of the technology development. It is hoped that the optical telecom technology will become sufficiently matured and that there will be enough operating experience for ARISE to revisit optical communication systems at a later date.

Current baseline

The current telecom design consists of an X-band transponder for command, housekeeping, and two-way Doppler tracking and a Ka-band system at 37 GHz band for high data rate downlink.

The X-band transponder design is based on the Spacecraft Transponding Modem (STM). Two X-band patch antennas are needed for near 4-π steradian coverage. A 0.5 W SSPA provides sufficient downlink margin. An ovenized oscillator is included to provide accurate Doppler measurement. The ROM cost is $ 3.3 M. The cost, however, does not include DSN support. DSN cost is included in a separate ground systems development and operation cost estimate.

With 1 GHz of bandwidth at 37-38 GHz, only high order modulation techniques such as quadrature amplitude modulation (QAM) can be considered to support the high downlink data rate. A block diagram of the high data rate transmitter is shown in Figure 6.3. 256-QAM is

chosen for the current baseline. Each transmitted symbol is selected from one of 256 possible waveforms and represents eight bits of information. As alternates to the current baseline of 256-QAM, it is possible to use square-root raised cosine filtering to increase the number of symbols per hertz, thus allowing the use of smaller QAM constellation such as 16-QAM and 32-QAM which are less risky. It is also worthwhile to investigate other spectrally efficient modulations such as GMSK and FQPSK which allow the use of power-efficient non-linear ampliers on the ARISE spacecraft, but require more spectrum. All of the above options will be examined more closely in future work.

Thirty (30) watts of RF power is needed through a gimbaled 1.2 m high-gain antenna to support up to 4 Gbps using 34-m DSN stations with 6 dB of link margin. A link budget is shown in Table 6.4. A shaping filter at the transmitter is needed to meet FCC's spectral usage requirements. This filter, however, introduces intersymbol interference (ISI) which corrupts the transmitted signal. An equalizer is needed at the ground receiver. The maximum data rate depends on the FCC requirements and the complexity of the shaping filter and equalizer. No channel coding is used. Since the spacecraft also carries a GPS receiver, the gimbaled antenna is expected to be able to point at the receiving DSN sites without the aid of a beacon from the ground.

The throughput of the 1 GHz bandwidth can be doubled through the use two orthogonal polarizations -- left-handed circular polarization and right-handed circular polarization. Further study is needed, however, to see if the polarizations can provide enough separation to satisfy the high signal-to-ratio requirement of 256-QAM. In addition, depolarization of the signal in the presence of water vapor in the atmosphere can cause the two polarizations to interfere with one another. An equalizer can be used to alleviate the effects of depolarization.

The cost for the high-rate system only includes telecom system on the spacecraft and comes up to about $ 15 M. It does not include the necessary upgrades of the DSN sites such as new RF front-end at 37 GHz, high rate baseband receiver, and equalizer. All ground station development cost and operation expenses are kept separately in the ground systems cost estimate. The ARISE spacecraft needs to orient itself to point the inflatable antenna at the observed objects. One gimbaled antenna is needed to meet the 70% availability requirement. The gimbaling system will allow for a half space view of the Earth (180 deg. 2 DOF capability).

There are many challenges for using 256-QAM as the 8 Gbps system. High order modulations such as 256-QAM has thus far only been used in very stable communication channels like wire-line systems. Atmospheric effects can make reliable transmission of 256-QAM difficult. The effect of water vapor at 37 GHz can be significant especially in heavy rain at low elevation angles. Highly linear power amplifiers at 37 GHz need to be developed. There are also proposed lunar missions with whom ARISE is expected to share the 37-37.5 GHz spectrum. Although the overlapping of telecom coverage areas on the Earth is not expected to be significant, ARISE will have to coordinate with these missions to avoid mutual interference. A separate transmitter using only the 37.5-38 GHz spectrum can be added to provide downlink during overlaps, albeit at a lower data rate.

We expect the advances in high data rate commercial RF systems will solve many of the problems described above by 2004. The risk of the RF system can also be significantly reduced if the required data requirement is lowered to 2 or 4 Gbps. One problem which deserves immediate attention that the current stage of the design effort has not been able to address is the cross coupling of the 1.2-m telecom antenna and the 25-m inflatable antenna. The downlink frequency of 37-38 GHz of the telecom system is very close to two of the ARISE observation bands at 43 GHz and 22 GHz. The transmit signal of the telecom system is many orders of magnitude larger than the observed signal at 43 and 22 GHz and the transmit power spectrum of the telecom system may not undergo sufficient attenuation at these 43 GHz and 22 GHz. Cross coupling of the transmit signal to the 25-m antenna can contaminate the signal in the observed bands. Judicious placement of the antenna and the use of absorbing material and other techniques should be investigated.

Transmitter power	30.00	Watts
Transmitter power	44.77	dBm
Transmitter losses	-2.00	dB
Antenna gain	53.00	dBi
Antenna Efficiency	-2.22	dB
Pointing loss	-3.00	dB
EIRP	90.55	dBm
Distance	4.00E+04	km
Link Frequency	3.75E+10	Hz
Atmospheric attenuation	-5.00	dB
Space losses	-215.96	dB
Ground receiver parameters		
Polarization losses	-1.00	dB
Receive antenna gain	80.00	dBi
Receiver cable/feeder losses	-2.00	dB
System Noise Temperature	80.00	K
Noise spectral density	-179.57	dBm/Hz
Received power Summary		
Received total power	-53.41	dBm
Received Pt/No	126.16	dB-Hz
Data Rate	4.00E+09	bps
Eb/No	30.14	dB
Eb/No Threshold (uncoded)	24.00	dB
Link Margin	6.14	dB

Table 6.4. Link budget of the 8 Gbps downlink. The link is consist of a RHCP and a LHCP each at 4 Gbps.

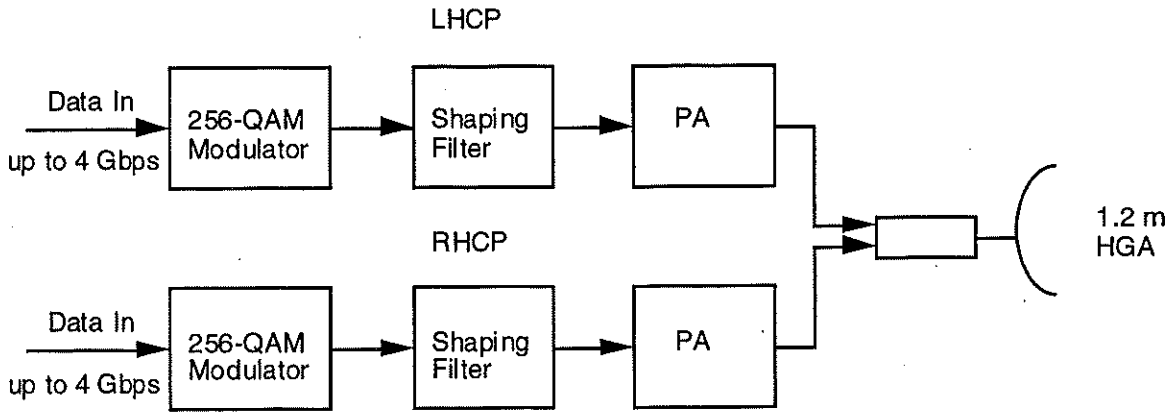

Figure 6.3. Block diagram of the 8 Gbps downlink transmitter

6.5 Spacecraft thermal design

The thermal control system for the ARISE spacecraft consists of two specific elements: 1) the cryocooler stage, and 2) the bus thermal control.

6.5.1 Cryocoolers stage

The cryocooler stage will consist of a three stage cooler system, which is required to provide the science instruments with a 20 K temperature. The first stage will be a Stirling mechanical cooler, while the second cooler stage will be a Sorption cooler. The first stage will operate between about 295 K to 60 K, while the Sorption stage will bring the science detector to 20 K. This system will require 350 watts of electrical power, and will have a mass of about 90 kg.

6.5.2 Bus Thermal Control

The other spacecraft systems that affect the Thermal Control System are: the Power system, because of the batteries, and Solar Array requirements; the Propulsion System, because of the temperature requirements of the propellants; and the systems that require electronics components, because of their temperature limits. Further the thermal design requires a knowledge of the structure because its material (thermal conduction) and configuration (radiation) effect the thermal exchange between spacecraft elements.

The TCS must control the temperature of the spacecraft elements within allowable limits for this spacecraft, which has an electrical power level of about 2400 watts, has a cold zone, which must be maintained at 20 K. The design uses standard passive thermal control elements, and will use technology that is available at the technology cut off date. Multilayer Insulation (MLI) blankets will control the thermal radiation between the spacecraft and space as well as between spacecraft elements. Thermal surfaces will be used to control the thermal balance between the spacecraft and the environment. Thermal conduction control will be used to maintain thermal gradients as required. Also required are electric heaters and controllers for temperature sensitive elements such as the batteries, and propulsion elements.

To maintain the science elements at 20 K, a two stage cryogenic cooler system is required, and will consist of a Stirling cooler, and a Sorption cooler system. The design must incorporate thermal isolation between the spacecraft bus elements and science stage, which will require thermal conduction and radiation isolation. The thermal energy from the cryogenic coolers will be transferred to thermal radiators with looped heat pipes that are mounted on the spacecraft bus. The thermal radiators will be constructed from high performance composite material and will also incorporate heat pipes.

The thermal control of the inflatable elements will use passive means, plus heaters, if necessary for storage, deployment and rigidization. Several optional rigidization techniques are being evaluated, one technique is cold rigidization. This technique requires that the inflatable elements be kept below 225 K. An initial analysis shows, that with the correct external thermal surface, in this case FEP-Aluminum or FEP-Silver, this temperature level can be achieved. To provide the uniformity required, a simple 5 layer MLI blanket will be necessary. The inflatable elements must be kept above the rigidization temperature during launch and prior to deployment, and this will be accomplished with a MLI cover, and a small heater. The deployment must be accomplished rather rapidly, as the inflatable elements will cool to 225 K between 3 to 20 minutes. Figure 6.5 summarizes thr thermal control system elements for ARISE.

System Elements	Mass (kg)	Electrical Power (watts)
Bus Elements		
Multilayer Insulation (MLI)	14.0	
Thermal Conduction Control	3.0	
Thermal Control Surfaces	2.0	
Thermal Radiators	11.0	
Thermal Louvers	4.0	
Looped Heat Pipes	3.0	
Electric Heaters/Thermostats	5.0	
Instrumentation	2.5	100 Avg.
Misc.	20.0	
Cryocooler Elements		
cryocooler	90.0	350
TOTAL	**154.5**	**450**

Table 6.5: Thermal Control System Elements

6.6 Spacecraft attitude control

The ACS system (in conjunction with propulsion) has to perform changes in velocity (delta-V). In addition, it must determine and control spacecraft attitude and rate to allow science observations. It must do this in the presence of various external and internal disturbances. To verify performance, models must be built for both static and dynamic analysis. Below we discuss the requirements, choice of components, cost, and analysis including modeling.

ACS Requirements

The ARISE pre-deployment requirements include, from the ACS standpoint, a 380 m/s delta-V (approximately 34 minutes duration given a 450 N main engine). The science requirements are described as follows:

- calibration requires a 2 degree slew in 60 seconds;
- a slew of 180 degrees in 60 minutes to 2 hours is desirable (slew rate 1 to 4 degrees in 60 seconds);
- keep the boresight to within +/- 30 degrees from the Sun;
- a quiescent phase during observing time of a duration from 2 to 20 minutes (depending on the observation frequency);
- pointing accuracy during observation of 2 to 6 arcseconds.

The ARISE stability requirements, as a function of frequency, are shown in Table 6.6.

While maintaining these requirements the ACS must also counteract external disturbance torques consisting of Earth's gravity gradient forces and moments, and solar pressure forces and moments. In addition there are internal disturbance sources such as the ACS components themselves (thrusters or reaction wheels) and other devices such as certain coolers (sorption coolers will be quiet, but Stirling can be quite noisy).

Frequency [GHz]	Motion [arcsec]	Time Scale [sec]	Stability [arcsec/sec]
5	**50**	**350**	**0.042**
8	**29**	**350**	**0.024**
22	**11**	**150**	**0.020**
43	**5**	**60**	**0.028**
86	**3**	**15**	**0.025**

Table 6.6: Stability Requirements

Components

To satisfy these stringent requirements and perform routine ACS operations, one set of reaction wheels and two sets of thrusters with different thrusting capability are envisioned as the actuators. One star tracker, one Sun sensor, one Inertial Reference Unit, and one GPS receiver are envisioned as on-board attitude sensors. These may be redundant for reliability as desired. These components are described in Table 6.7.

The ACS design is driven by the tight requirements and low structural frequencies of the antenna, which dictates reaction wheels for fine pointing. These are sized by the torque and momentum capability required for slewing and counteracting environmental torques.

Vibration isolation components may be necessary, depending on the design of the cooling system, and the results of more detailed dynamics simulations. These can either be passive, as the isolation used for the Hubble Space Telescope reaction wheels, or active, as for STRV2.

These components can meet the accuracy requirements for the spacecraft bus itself. However, to point the optical boresight to these same accuracy will require calibration of the alignment between the optical axes and the bus axes. In addition, the stability of this calibration is an issue since it may not be possible to calibrate during observations. Thermal variations and material aging may cause significant perturbations requiring periodic re-calibration. This issue may require a closer interaction between the RF and ACS subsystems. This may also require an active metrology system for calibration during observations.

Component	Type	Mass [Kg]	Power [W]	Number
Reaction Wheels	Teldix DR50	12	150/15	4
Electronics		2	30/5	4
Star Tracker	CT601 class	8	12	1
IRU	HRG	5	22	1
Sun Sensor	Electronics Head	0.5	0.5	1
0.9 N Thrusters		2.5	5	8
22 N Thrusters		2.5	5	8
ACS Computer				
TOTAL		62	122	

Table 6.7. ACS Hardware Components

Performance Analysis

Some calculations have been done to size the disturbance environment and quantify the pointing problem. A finite element model of the ARISE spacecraft has been built in Matlab using the IMOS software (Integrated Modeling of Optical Systems) . This has been refined by using NASTRAN data for consistency with the structural design. The finite element model features all the structural dynamic components of the spacecraft, with the exception of the bus and the subreflector, which are assumed to be rigid. The solar panels and the subreflector boom are, however, modeled using finite elements. See Figure 6.4 for the model. Therefore, we have beam elements for the support struts and the hard truss, and membrane elements for the reflector and the canopy. The inflatable torus, modeled as a circular ring, is connected to the reflector/canopy through a set of pretensioned constant force springs. The membrane elements are linear, with no pretension. All material properties are homogeneous and isotropic. The finite element model has 1876 degrees of freedom (132 beams, 72 constant force springs, 396 membranes, 24 multipoint constrained degrees of freedom, 472 massless degrees of freedom obtained through Guyan reduction), of which 1382 are retained for the dynamic analysis. A model for the reaction wheels, including saturation at 0.2 Nm, is also included in the structural model. The model also describes input forces and torques, such as those derived from gravity gradient, solar pressure, thruster forces, and reaction wheel torques. Static and dynamic deformation under open loop or closed loop control can be produced.

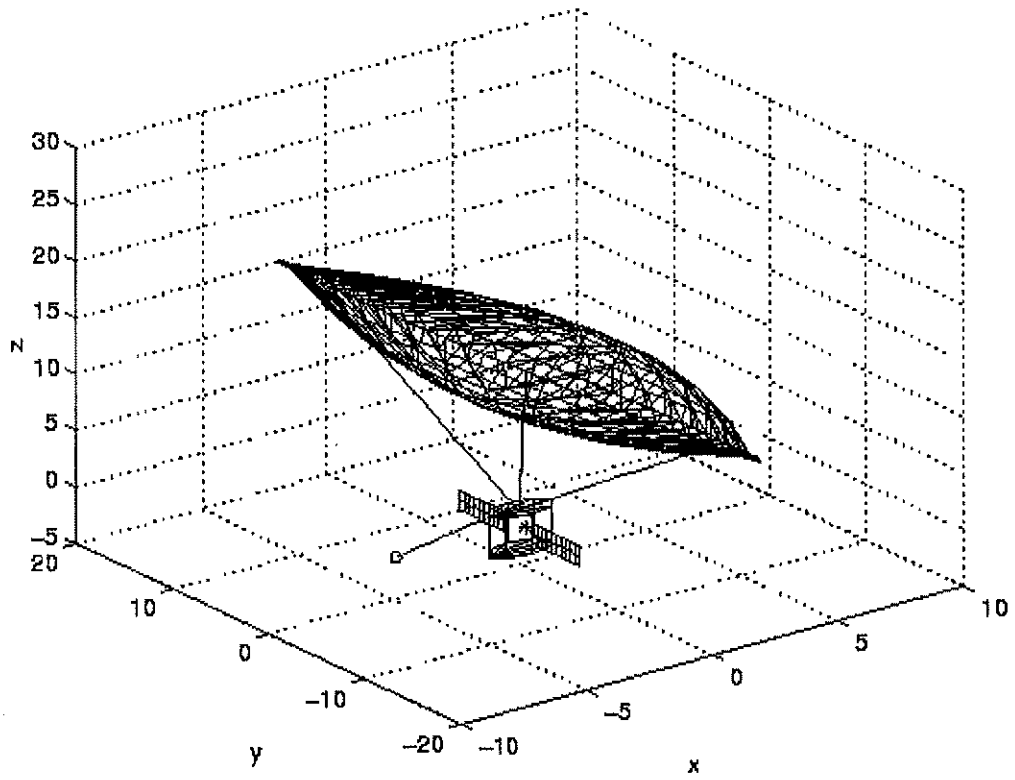

Figure 6.4.

Disturbances

Given the inertia matrix, it is easy to determine the gravity gradient torque for arbitrary spacecraft orientations. The worst case gravity gradient torque is less than 5.12E-3 Nm. IMOS also has the capability of determining the gravity deformation forces that also result from the gradient; these are less than 4.5E-4 N. The solar force direction in the spacecraft frame of reference has an angle with the boresight (theta), and an angle of rotation around the boresight (alpha). The impact of the force on the antenna can be determined and the forces and torques determined for various geometries. See Figure 6.5.

Preliminary analyses show that the solar force is less that 3.7E-3 N, the solar torque is less than 0.05 Nm, the gravity gradient force is less than 4.5E-4 N, and the gravity gradient torque is less than 5.12E-3 Nm. Of interest is the distance between the center of pressure and the center of mass, equal to [-6;-7.5;-14.0] m. Also, see Figures 6.6, 6.7, 6.8, and 6.9 for the various dynamic quantities of interest during the solar torque unloading maneuver.

Cooler disturbance data is not yet available, but an example of the possible magnitude of the disturbance is given by work on STRV2. In that case, a 1 watt TI cryogenic cooler was used. It produced forces of about 5N at various harmonics of the 55 Hz drive frequency. If the ARISE cryocooler produces forces of this magnitude, it is very likely that it will have to be isolated at least by a passive system similar to that used on Hubble.

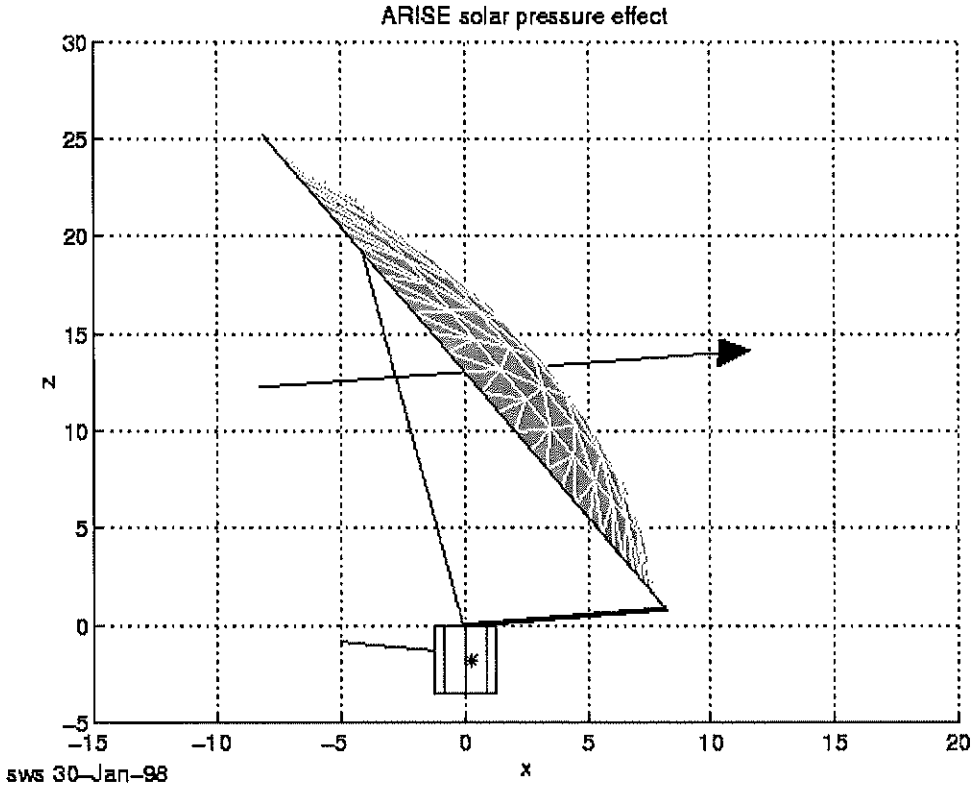

Figure 6.5

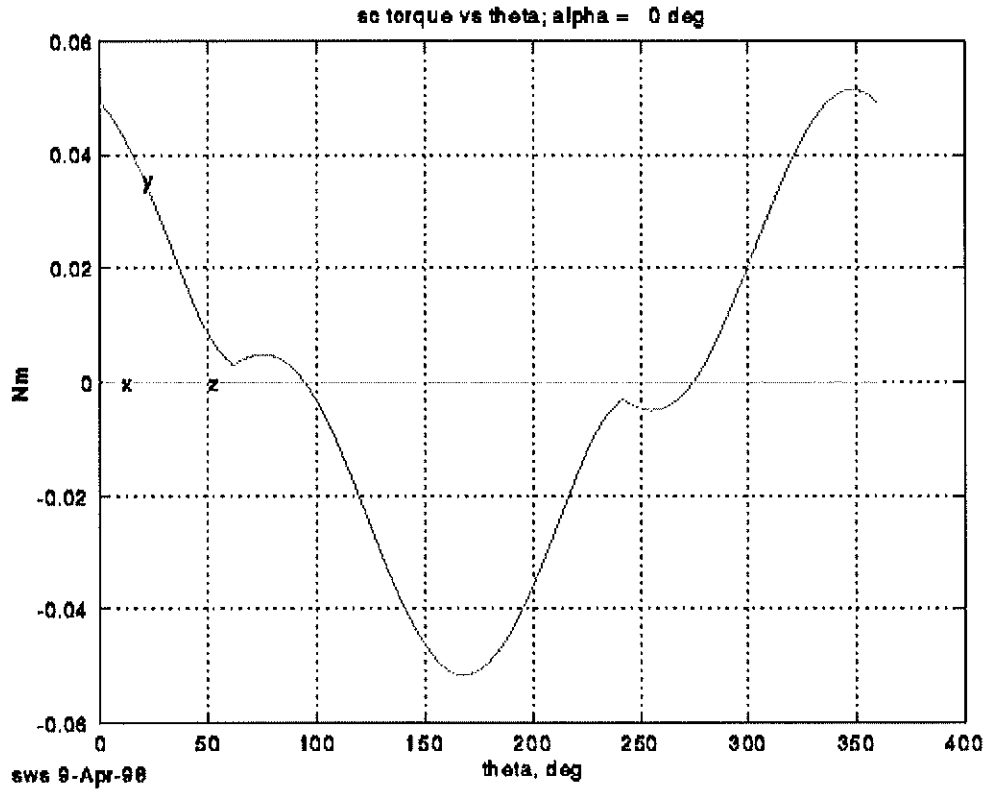

Figure 6.6

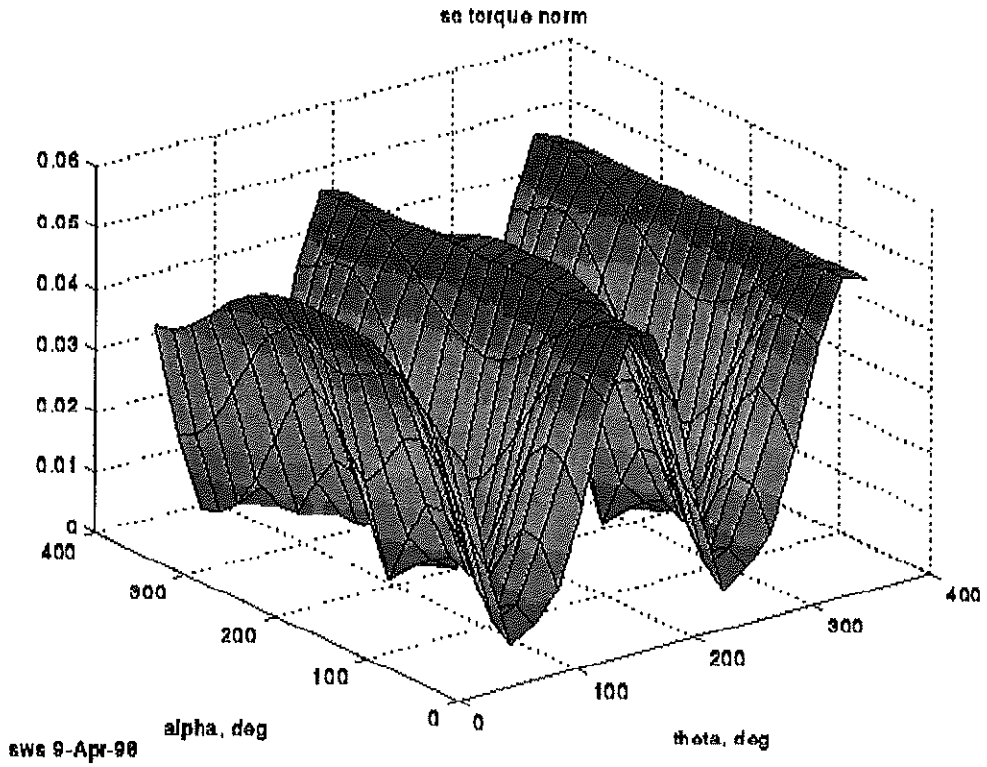

Figure 6.7

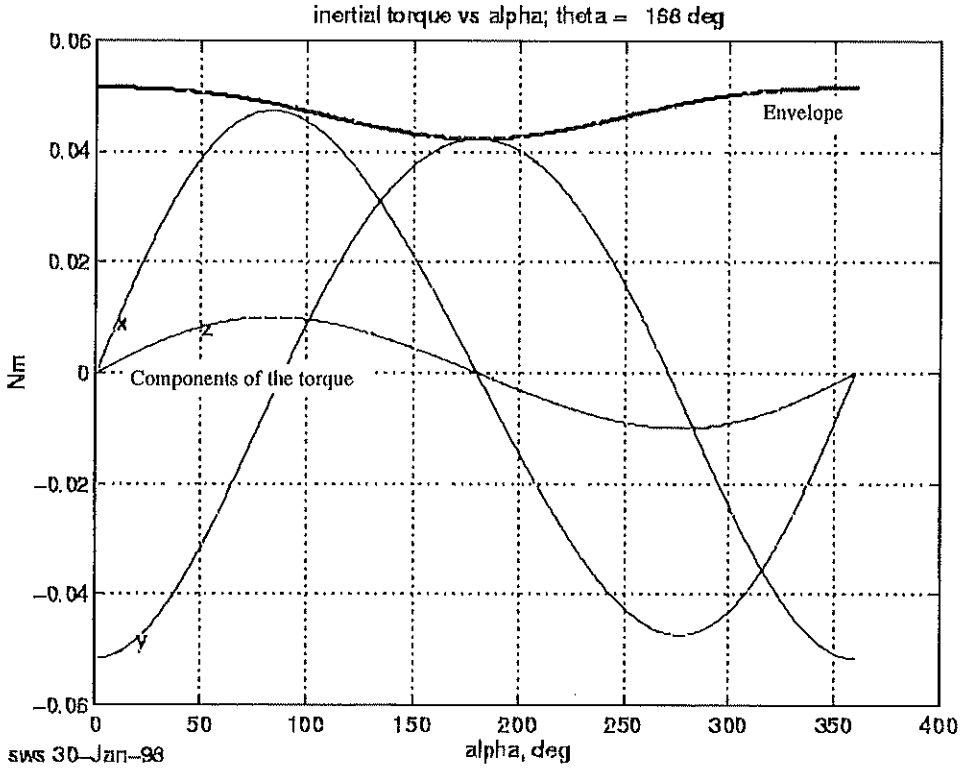

Figure 6.8

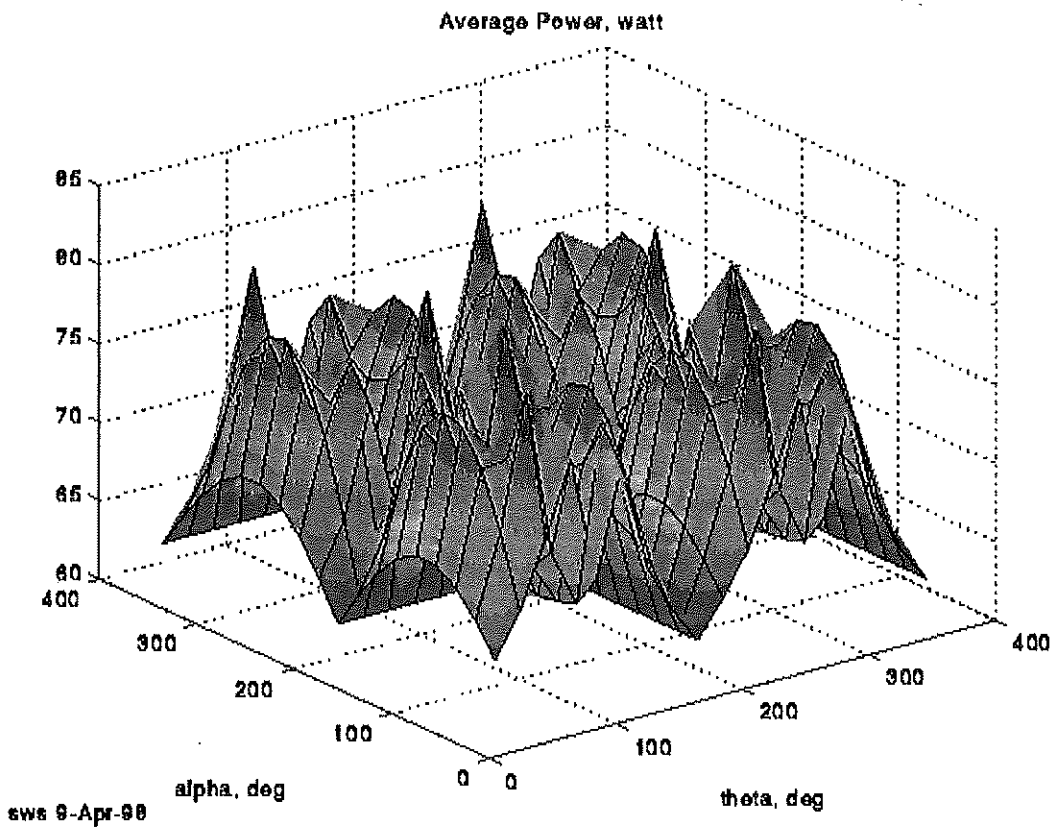

Figure 6.9

Momentum Management

After examining various options for reaction wheels, we have chosen the following wheel:

Teldix DR 50:

- torque: 0.3N
- max momentum: 300 Nms
- max wheel speed: 6000 Rpm
- power: 150/15/3 watt
- mass: 12 kg
- size: 0.15 m x 0.5 mD

Given the maximum torque, we can wait as long as 99 minutes before unloading the wheels, which certainly is longer than required. The wheels will then be spinning at maximum speed (6000 RPM) and drawing maximum power. A better choice seems to be to unload if the wheels reach about 1/4 of their momentum capability, which requires much less power. This also leaves a large margin for observational flexibility. In addition, the reaction wheel disturbances are functions of the square of the wheel speed, so minimizing the speed improves the pointing performance.

The power usage, considering all solar angles is given in table 6.6. The max power is the power required for all 3 wheels just before unloading, minimized over all solar incidence angles. This assumes we unload all wheels at once. The maximum average power is the power for all 3 wheels, averaged over one cycle, taking the maximum over all solar incidence angles. When the antenna is

pointing at 30 degrees from the sun (worst case requirement), it can stay at minimum torque capability of the reaction wheels for a total of 31 minutes, before unloading. To be able to sustain the solar torque disturbance, it can spin at 1.2 mrad/s for about 12 hours.

Table 6.8. Power for reaction wheels during observations.

option	time before unloading (min)	H at unloading (Nms)	max power (watt)	max average power (watt)
A	99	300	314	180
B	26	80	117	81

The wheels can perform 2 degree slew in about 118 seconds and a 180 degree slew in about 19 minutes. Both of these are well within the requirements.

Unloading the solar torques can require a significant amount of hydrazine. This amount can be reduced by using ion thrusters. This amount can also be reduced by rotating the whole spacecraft about the boresight, but this maneuver would affect the power collection and telecommunications subsystems, and to some extent even the science data gathering.

Dynamic Analysis and Control

While we do not want to use the thrusters during science observations, it will be necessary to unload the reaction wheels periodically and so we want to quantify the disturbance this will cause.

Preliminary analysis of a 2 second firing of a pair of 0.9 N thrusters resulting in a couple about the vertical axis of the spacecraft (z), shows that the maximum relative deformation at the joint between the torus and a rigidizable struts is never exceeding 20 mm, and the residual vibration rapidly dies out because of the high structural damping present in the inflatable structure (3% structural damping). See Figures 6.10, 6.11 and 6.12.

Figure 6.13 shows the attitude control block diagram used in the simulations. Figure 6.14 and Figure 6.15 show open loop simulation done with the Hubble reaction wheel model, at 500 rpm and 2000 rpm, respectively. What is shown is the angle due to deformation at the torus-strut attachment point when the wheels are operating. Based on test data, the wheels produce disturbance forces and moments due to imbalance, motor cogging, and ripple. For the 2000 rpm case we can still meet the requirements. This indicates that isolation of the wheels may not be needed. Note that we may obtain additional margin by keeping the wheels at a lower speed by unloading more often, which is quite possible as the observation times for the radio frequencies requiring the highest precision are only about 2-3 minutes. If we unload every 10 minutes for the maximum disturbance torque, then the peak wheel speed is only about 600 rpm.

Closed loop analysis was made of a 2 degree slew in 200 seconds maneuver about the x-axis of the spacecraft, using reaction wheels. The results show this to be a very benign maneuver. Figure 6.16 shows the spacecraft slew angle, Figure 6.17 the reaction wheel torque profile, and Figure 6.18 the displacement at the strut-torus attachment.

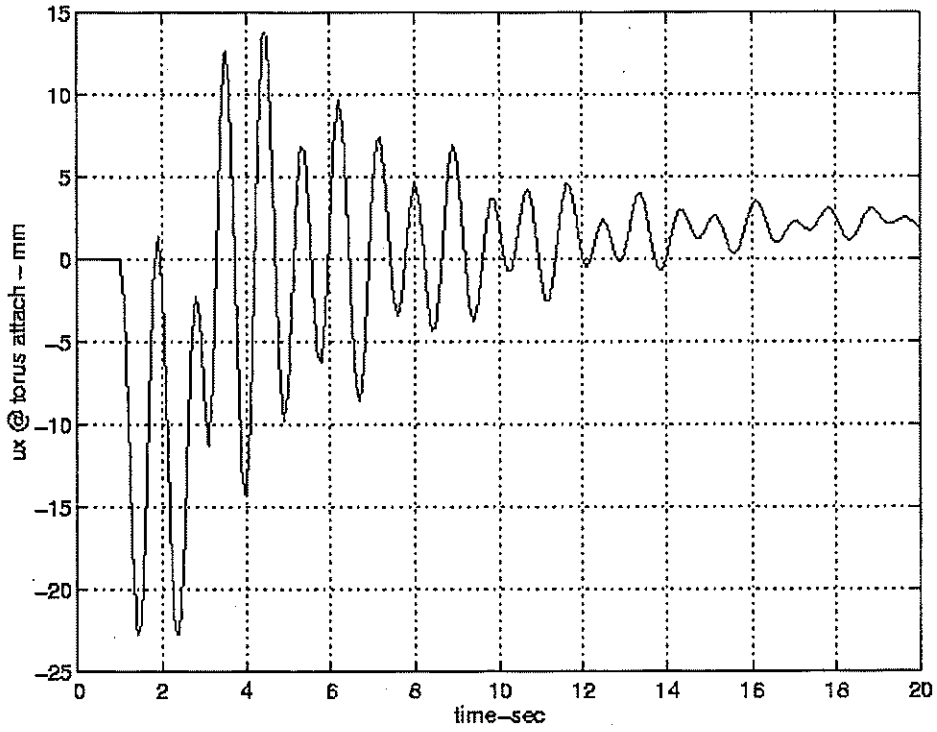

Figure 6.10

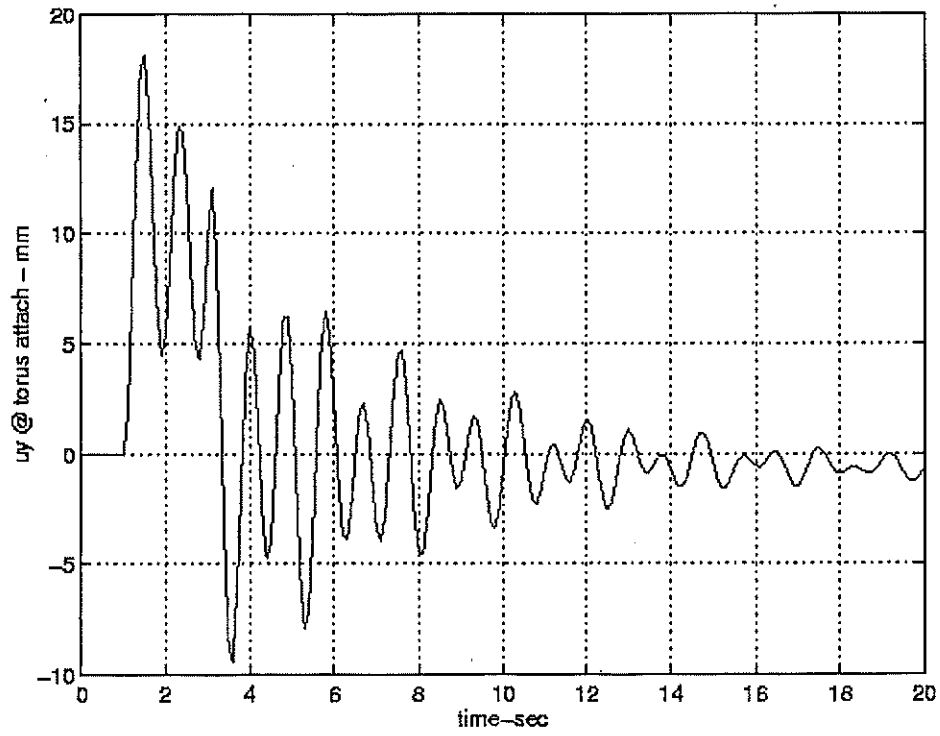

Figure 6.11

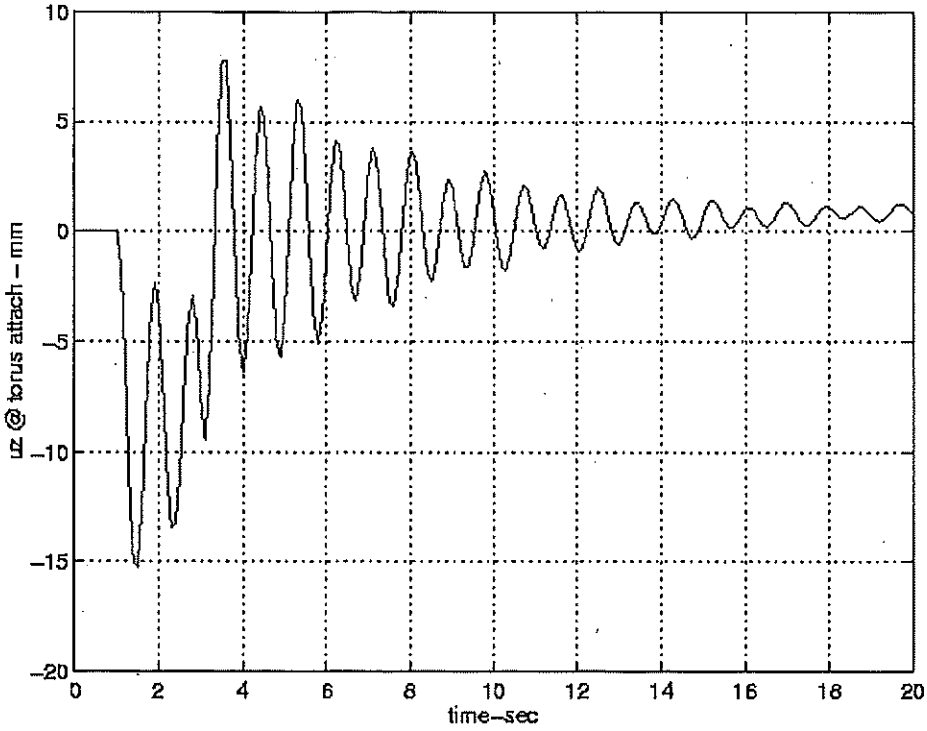

Figure 6.12

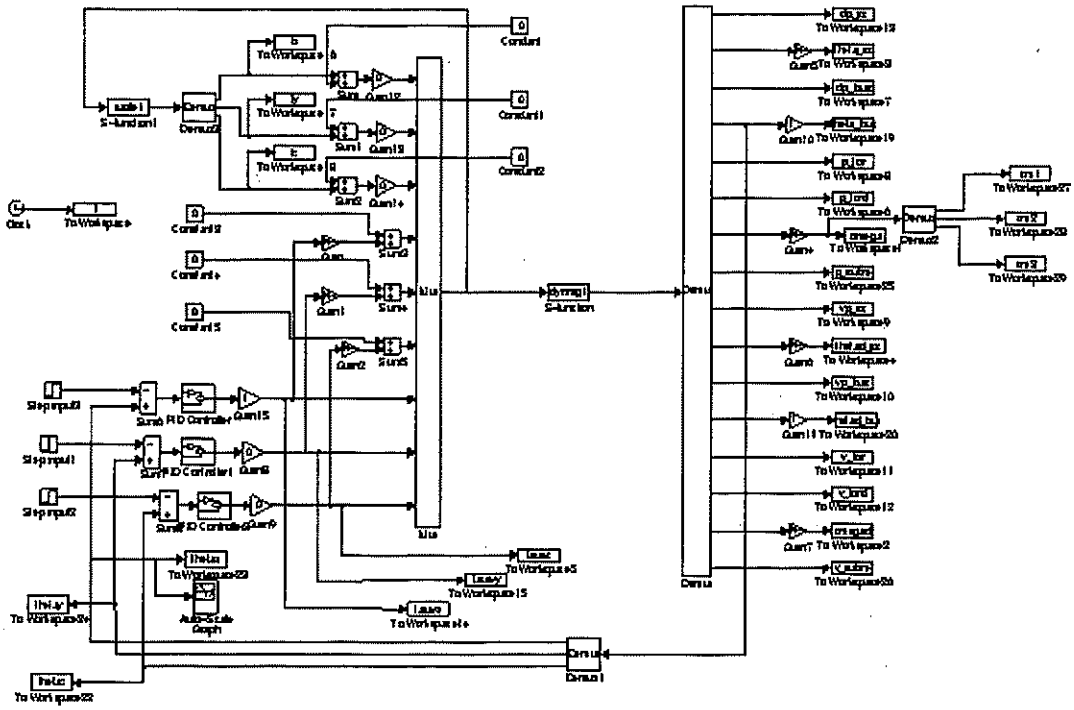

Figure 6.13

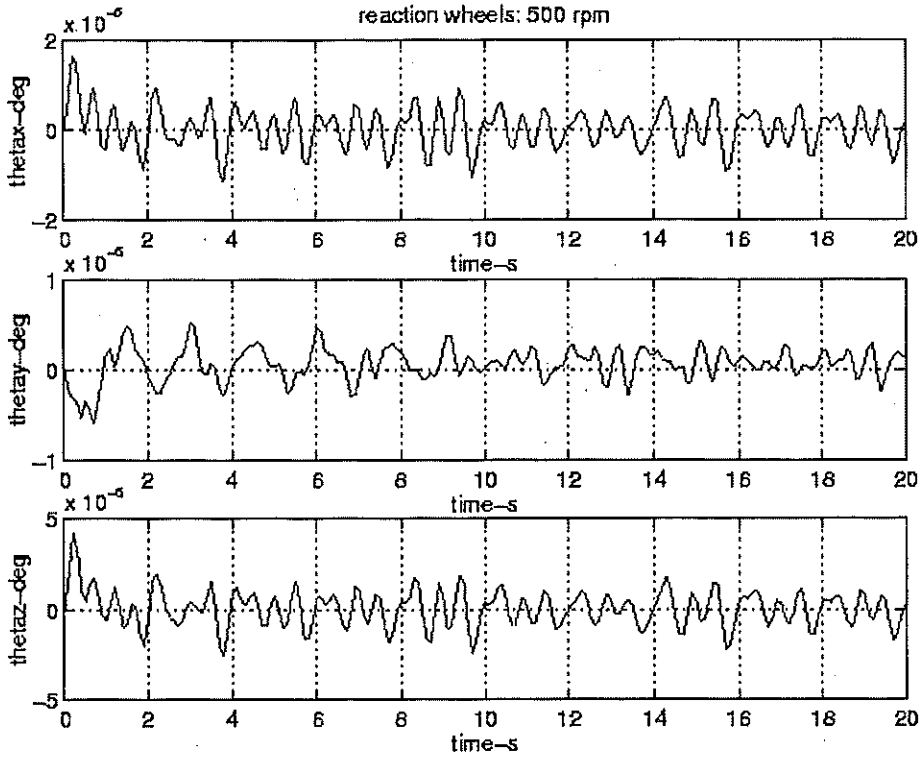

Figure 6.14

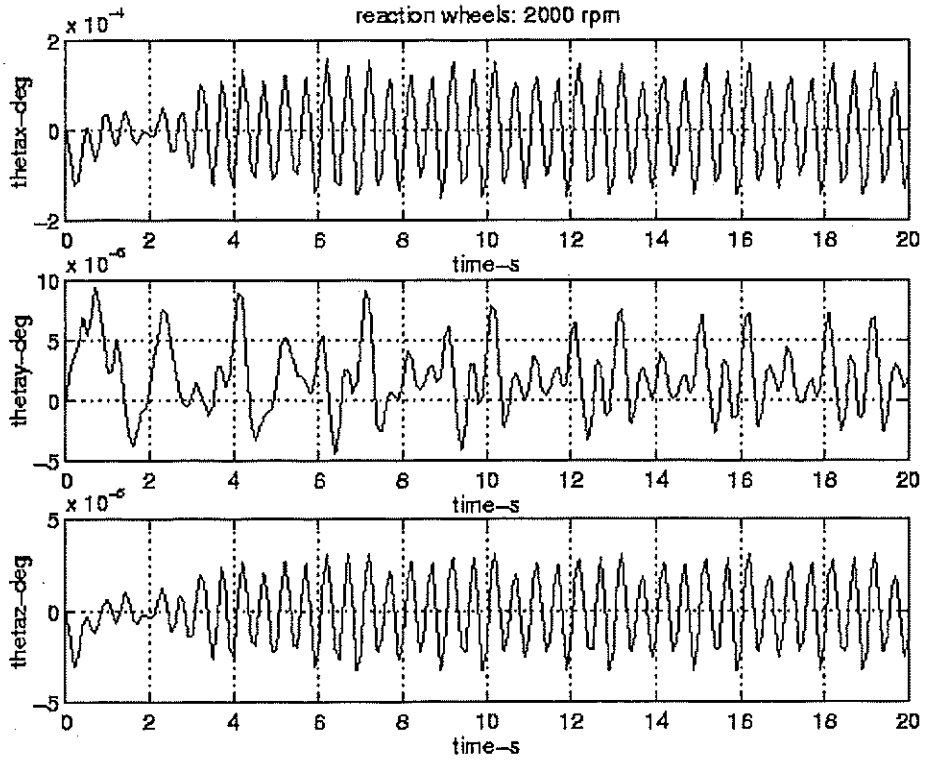

Figure 6.15

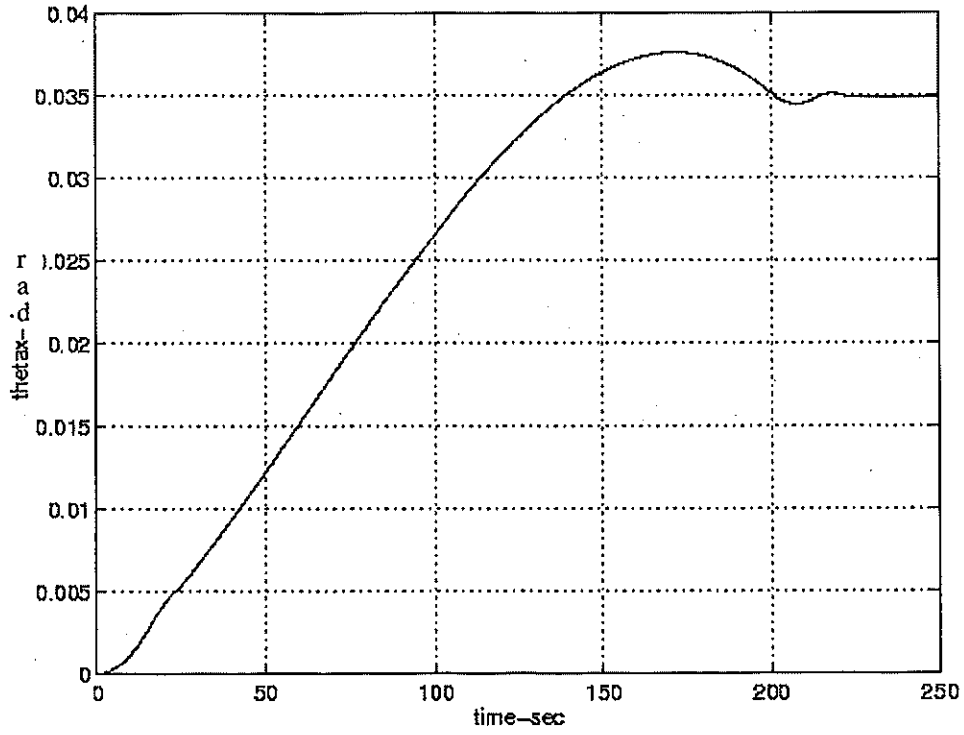

Figure 6.16

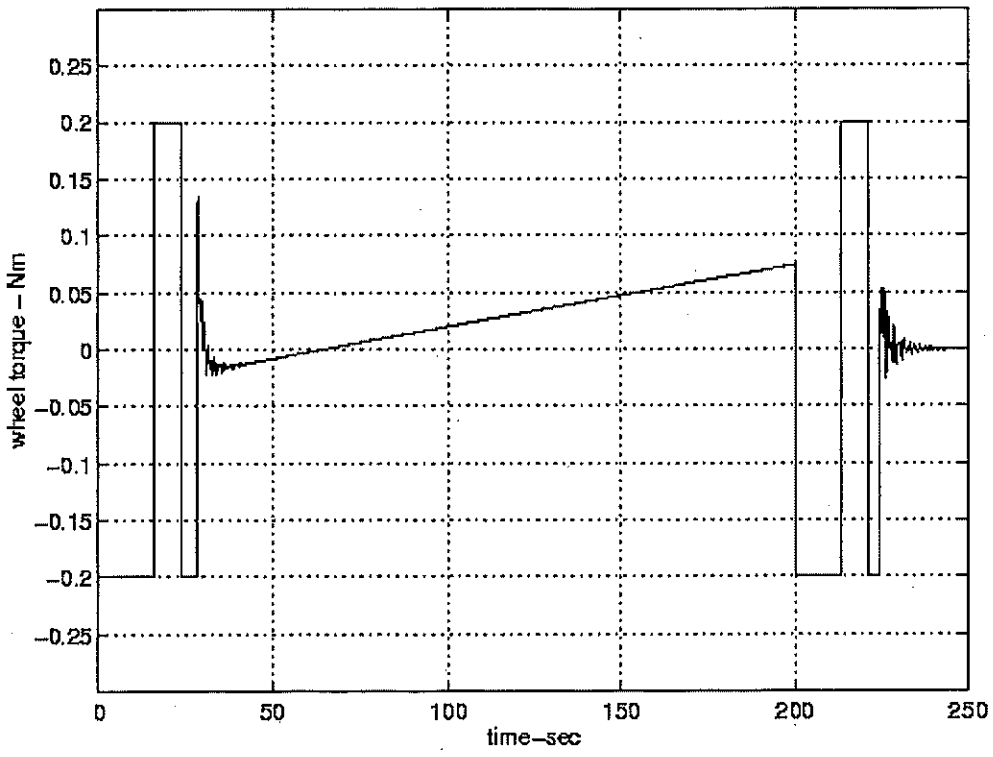

Figure 6.17

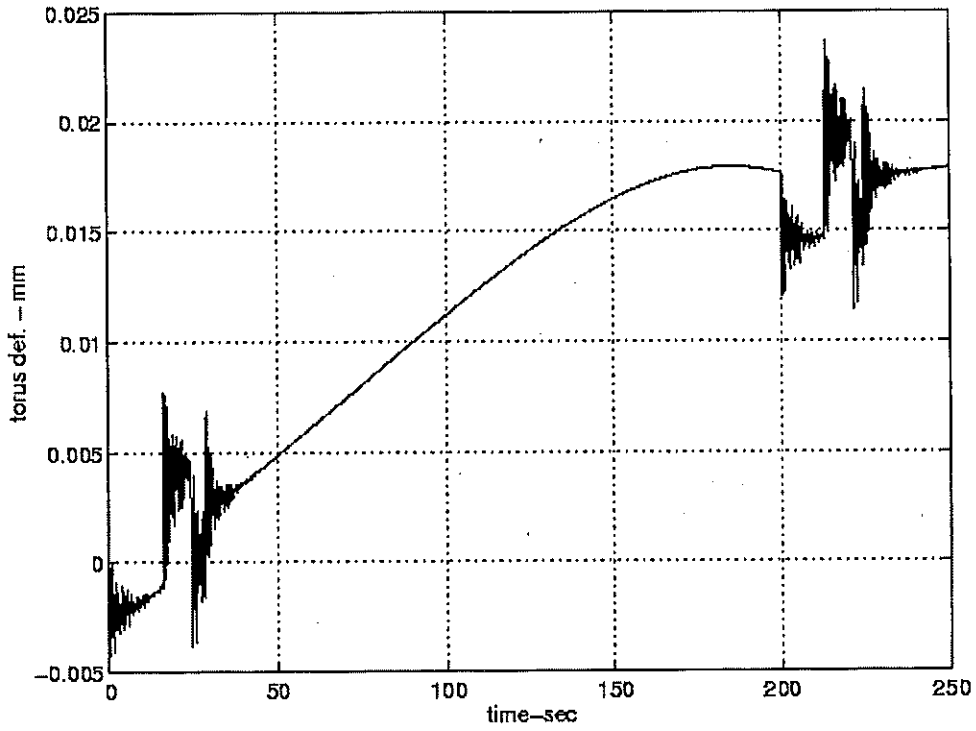

Figure 6.18

6.7 Structures and mechanisms

As discussed in the spacecraft configuration section, the spacecraft bus has an octogonal shape 2 m long and 1.3 m wide. It was not attempted in this study to define and design the bus material and thickness. A mass of 10% of the spacecraft dry mass minus propulsion and inflatable antenna subsystem masses was allocated for the spacecraft bus structure, which rounds up to about 71 kg. Masses for the mechanisms, such as subreflector truss and deployment, solar array gimbals, telecom antenna boom and deployment, were estimated. Cables and connectors were taken as 7.5% of the spacecraft dry mass minus propulsion and inflatable antenna subsystem masses. An allocation of 10 kg was also made for additional radiation shielding of sensitive parts of the spacecraft (C&DH shielding was bookkept separately).

6.8 Power subsystem

The power system has three major parts. The solar array provides power during sunlit periods. The battery provides power during eclipses, supplements the solar array during peak power periods, and provides power during the immediate postlaunch period, before the solar arrays are deployed. The PMAD system provides power management and distribution. It includes the peak power tracker; distribution, regulation and control electronics; and pyro.

Calculations of the estimated solar array area and mass were based on spacecraft requirements of 2270 W EOL, which includes 30% contingency. Until further details are available on the spacecraft power profile, it was assumed that the solar array would handle all power needs during sunlit periods. Adding an estimated 125 W to recharge the Li-ion secondary battery, the overall

array sizing assumed a net 2400 W EOL requirement. The results for six of the leading cell candidates are detailed in Table 6.9. These mass and area numbers include the cells; thin coverglass (3 mil), with the exception of the copper indium diselenide (CIS) cells which do not include coverglass; wiring, terminals, connectors, and substrates. As is customary, they do not include additional contingency (this is carried at the system level), nor do they include the support structure (connection to the spacecraft), deployment, drive or housing. Overall, the most reasonable compromise between area, mass, cost and availability was projected to be the inflatable array (ITSAT type) using high-efficiency Si cells at a specific power of 86 W/kg BOL. The array area would be 16.3 m^2 and the array mass would be 32.8 kg.

	Area (m^2)	Mass (kg)
GaAs	14.9	46.3
2-junction (GaInP/GaAs)	13.3	41.1
3-junction (GaInP/GaAs/Ge)	11.1	32.6
CIS (LMA est.)	36.9	34.3
CIS (L'Garde est.)	36.9	25.2
High efficiency Si	16.3	32.8

Table 6.9: Calculated Solar Array Area and Mass for 2400 W EOL
GaAs = gallium arsenide on Ge substrates
GaInP/GaAs = two junction cell on Ge substrate
GaInP/GaAs/Ge = three junction cell on Ge substrate; includes active Ge junction
CIS = copper indium diselenide

Calculations of the estimated secondary battery mass and volume assumed that the battery would be used only during eclipses (460 W for 45 min, or 345 Whr). The primary battery requirements cover a 8.8 hr period immediately postlaunch (4930 W-hr). Until further details are available on the spacecraft power profile, it was assumed that the solar array would handle all active power needs during sunlit periods. It was assumed that neither science data collection nor telecom would not occur during eclipse. It was also assumed that the mission lifetime would be limited to about 3 years, in order that a Li-ion battery could handle the required number of cycles. The numbers do not include battery mass or battery volume contingency, which would be carried at the system level. The required 25 Ahr Li-ion secondary battery would have a mass of 7.3 kg and a volume of 6 liters. It is evident that a large mass and volume penalty would result if a Ni-based battery were to be substituted.

Calculations of the estimated PMAD mass were based on extrapolations from the Phase A Light SAR calculations performed at JPL in 1996. It was assumed that the ARISE EOL solar array power would be 2400 W and the secondary battery capacity would be 25 Ahr. The calculated mass of the peak power tracker would then be 13.9 kg, and the mass of the distribution, regulation and control electronics would be 66.7 kg, for a total PMAD mass of 80.6 kg. The corresponding EOL PMAD specific power would be 30 W/kg. This corresponds favorably to the 30 W/kg anticipated for the JPL X-2000 PMAD second delivery. The results are detailed in Table 6.10.

Several key technology challenges for the power system were identified. First, the advanced solar array technologies (multijunctions and CIS) must be scaled up without appreciable efficiency loss if they are to compete effectively with Si and GaAs. Second, deployment mechanisms for ultralightweight solar arrays need to be flight qualified. Third, Li-ion secondary batteries need a flight demonstration; they also need to be demonstrated in large sizes (over 20 Ahr). Fourth, the PMAD mass can only be reduced if the projected parameters of the X-2000 3rd delivery

(approximately 200 W/kg) can be demonstrated and scaled up. The X-2000 3rd delivery is planned for a very small (10 W) power system.

Extrapolated from LightSAR case:

	LightSAR	ARISE
Solar array power (EOL)	782 W	2400 W
Battery capacity	44 Ahr (Ni)	25 Ahr (Li)
Peak power tracker	6.4 kg	13.9 kg
Dist, Reg & Cntrl Electronics*	15.0 kg	66.7 kg
Total PMAD mass	21.4 kg	80.6 kg
PMAD specific power (EOL)	36.5 W/kg**	30 W/kg***

Table 6.10: Calculated PMAD Mass
*Estimate based on EOL array power corrected for environmental degradation only (EOL/0.85)
**LightSAR assumed a very bare-bones system
***30 W/kg is approximate value for X-2000 PMAD 2nd delivery

In summary: Size estimates, including mass and area, have been generated for the ARISE solar array. Size estimates, including mass and volume, have been generated for the ARISE battery. A ROM estimate of power electronics mass and specific power has been calculated. Several key needs were identified. First, more data on the planned orbit and eclipses are needed in order to refine the power system sizing. Second, more data on the spacecraft power profile vs. time are needed in order to determine the proper role of the battery in supplementing the solar array. Third, the calculations assume a moderately benign radiation environment, which may not actually be the case in the planned ARISE orbit; more data is needed on the radiation environment in order to properly size the power system, particularly the solar array which is relatively difficult to shield. Planned near-term activities include: updating the power system design in accord with evolving system requirements; continuing to reduce the power system mass; refining the PMAD mass and cost estimates; and establishing a power system design and fabrication schedule.

Backup data are available in the tables in the Appendix G (Tables A through G).

6.9 Propulsion subsystem

The propulsion module is a bipropellant dual-mode propulsion system that is used to perform a ~380 m/s periapse raise, reaction control during the periapse raise, and attitude control for the duration of the mission.

The bipropellant dual-mode propulsion system uses nitrogen tetroxide (NTO) and hydrazine (N_2H_4) as the oxidizer and fuel, respectively. The periapse raise is performed using a 445 N Royal Ordinance LEROS-1c main engine that is qualified for these propellants exclusively. Two titanium tanks (one for the oxidizer and one for the fuel) are used to store the propellant. The oxidizer and fuel tanks are pressurized via separate high-pressure helium feed systems (two pressurant tanks). The separate feed systems eliminates any possibility of propellant migration. Eight 22 N and eight 0.9 N monopropellant (hydrazine) thrusters are assumed for thrust vector and roll control. Conventional technology components are assumed.

This design has two possibilities for combining the inflation system with the propulsion system. One option is to have an NTO inflation system feeding off a line downstream of the oxidizer tank. Liquid NTO decomposes into gaseous N_2 and O_2 through a two-step reaction. Another option is to have an N_2H_4 inflation system feeding off a line downstream of the fuel tank (feeding off the RCS system). Liquid N_2H_4 decomposes into gaseous NH_3, N_2, and H_2 through a two-step reaction. Since there are separate pressurization feed systems for both the oxidizer and the fuel, both tanks remain pressurized for the entire mission. No pyrotechnic firings are necessary after the periapse raise.

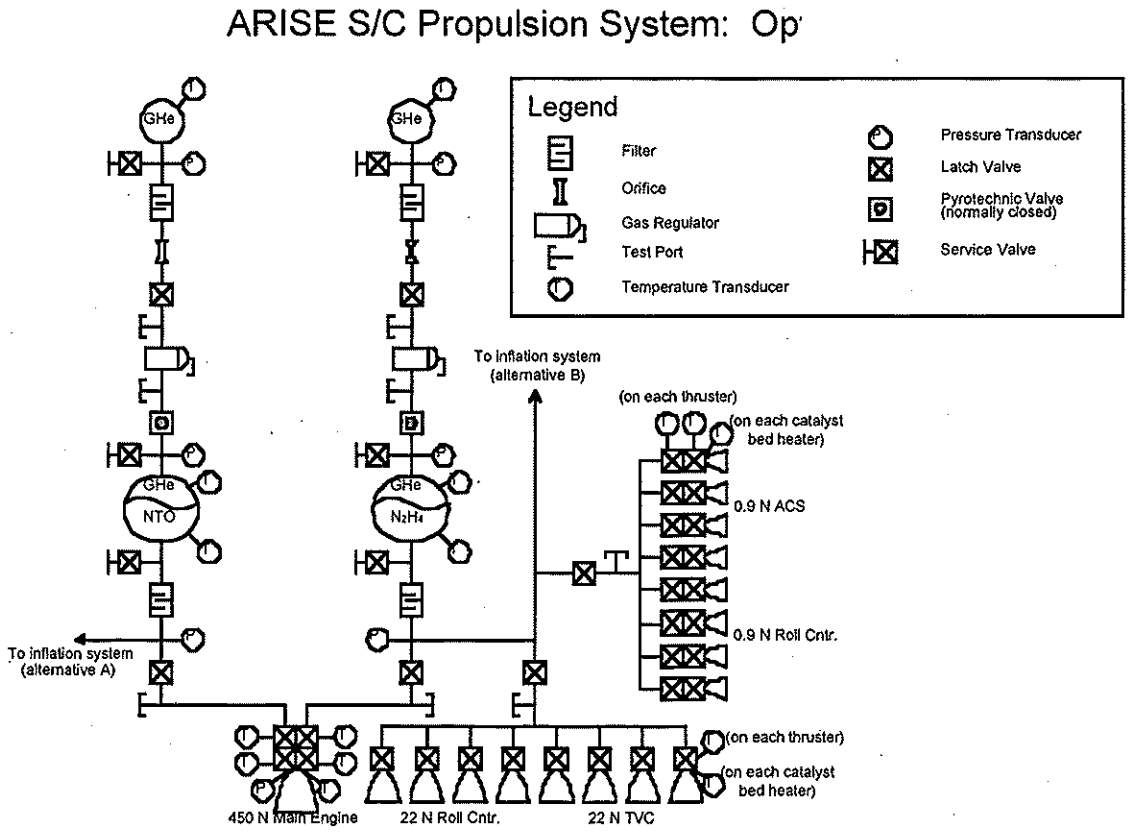

7. Ground systems and mission operations

The FY'98 work focused on the space segment of ARISE. The issues and design considerations associated with the ground segment will be studied in more detail in FY'99. This section summarizes the current understanding of the ground system and mission operations.

Operations and data handling scenario

The ARISE Mission carries out observations on an approximately 70% duty cycle. During observations instrument data are immediately sent to the ground, so the spacecraft must be tracked during all observation periods. Instrument data loss of up to 20% is tolerable during these tracking periods. Instrument data is transmitted at 8 Gbps over a Ka-Band link to a set of dedicated ground terminals. It is recorded at 8 Gbps on tapes which are then shipped to a VLBI data processing center. This instrument data flow is shown on the lower part of Figure 7.1. The upper part of the figure shows the downlink and uplink flows for engineering telemetry and spacecraft commands. Engineering data is recorded on-board the spacecraft and is played back once a week over a DSN 34 meter tracking pass. During this pass the commands to control the next week's worth of observations are transmitted to the spacecraft. These commands are the result of the planning of science and engineering activities needed to achieve the mission goals. A coordinated set of observation plans are sent to radio telescopes on earth to direct the collection of concurrent observations to be correlated with the observations conducted from the spacecraft. Details of the ground system components needed to operate the mission are discussed in the next section.

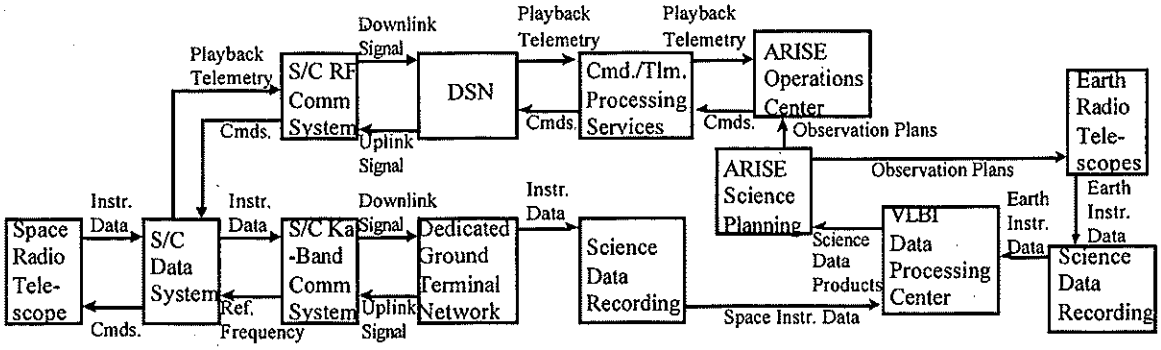

Figure 7.1: End-to-End Data Flow

Ground system design

Figure 7.2 illustrates the ground system design for ARISE. The ARISE ground system is above and to the right of the dashed line in the figure. The VLBI science observations are planned to be executed by concurrent use of the spacecraft-based radio science instrument and a set of earth-based radio science instruments. The coordinated observation plans are issued from the science planning function shown on the far right hand side of Figure 7.2. Observation plans for the spacecraft are translated at the ARISE Operations Center into a set of commands to be uplinked through the DSN's multimission command processing service once a week. During this once a week DSN track the spacecraft plays back the last week's worth of recorded engineering telemetry which is delivered by the DSN's multimission telemetry processing service. The ARISE Operations Center analyzes the engineering data to assess the performance of the spacecraft and generates any ancillary data about the spacecraft status needed to support VLBI data processing.

ARISE will use a dedicated ground terminal network to handle the instrument data downlink. The network will consist of 3 terminals distributed at sites around the world so as to make coverage almost continually available to the orbiting spacecraft. The terminals will be remotely controlled from the ARISE Operations Center, except for maintenance and tape loading, unloading, and shipping operations. The instrument data from space will be recorded on 2 to 4 tapes for each observation. The tapes will be played back at the VLBI Data Processing Center, along with tapes containing radio science instrument data from concurrent earth-based observations. The VLBI Data Processing Center will perform correlation, fringe fitting, image processing, and data archiving.

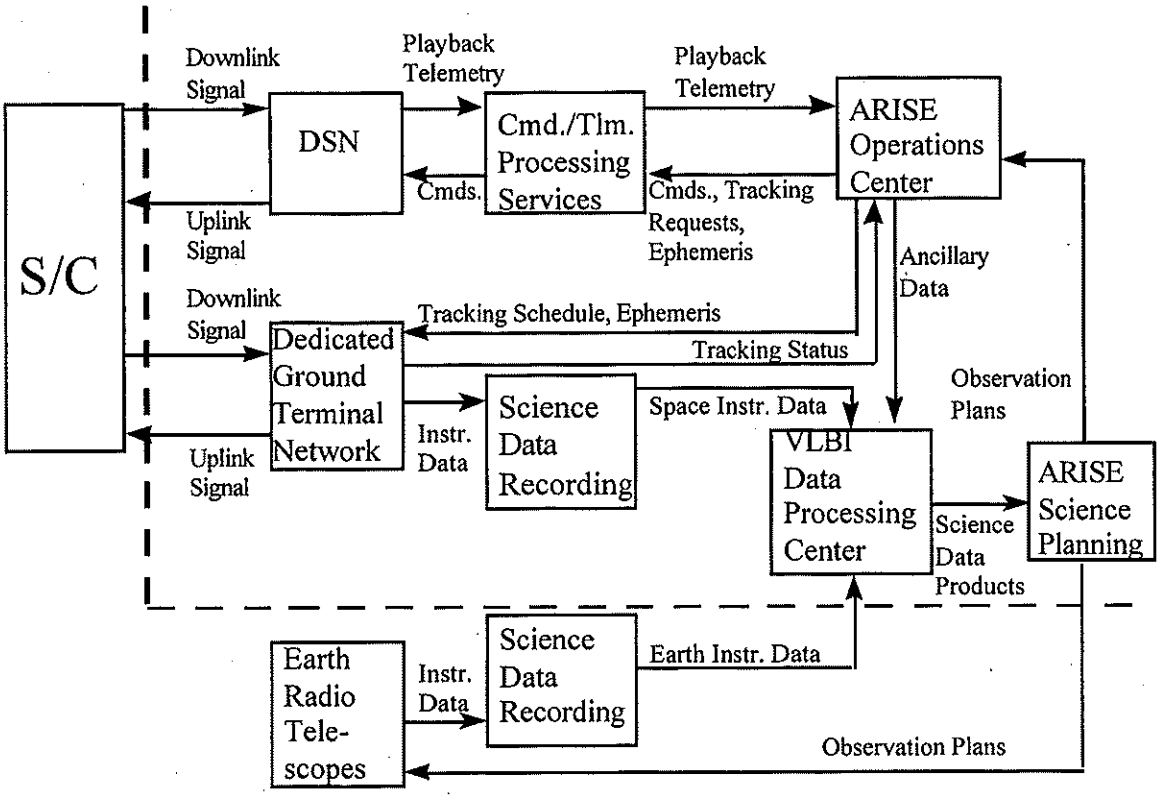

Figure 7.2: Ground System Functional Block Diagram

8. Costs

The ARISE cost used JPL's Team X cost estimation tools. Comparison of the ARISE cost profile with other current flight mission profiles were done to validate its applicability. The Team X model build for ARISE uses quasi grass roots estimates for the spacecraft subsystems, mission operations, science team and launch vehicle. It uses historical estimate models for other mission components. These costs assume a 20% reserves on phase A-D and 10% on phase E. They also assume a phase A duration of 18 months, phase B duration of 18 months, phase C/D of 48 months, and phase E of 39 months. Redundancy is typical and the costs are estimated in FY'98 dollars. Table 8.1 summarizes the ARISE cost breakdown. More details can be found in Appendix H. The known subsystem grass roots cost estimates are given below.

	Phase A-D	**Phase E**
Project Management	12.3	0.7
Science	2.8	1.3
Project & Mission Engineering	5.4	
Payload (science instruments)	27.4	
Spacecraft	**144.1**	
System management	1.7	
System Engineering	2.5	
Inflatables	6.0	
ACS	32.0	
C&DH	6.0	
Telecommunications	25.3	
Power	11.0	
Propulsion	12.0	
Structure/thermal/cabling	24.7	
Thermal control	2.9	
Cryocoolers	11.0	
Software	7.0	
LV adapter	2.0	
ATLO	20.1	
Mission Operations	35.0	17.0
Launch Vehicle	60.0	
Reserves	49.4 (@ 20%)	2.0 (@ 10%)
Total	**356.6**	**21.0**

Table 8.1: ARISE cost breakdown in FY'98 dollars

Ground system development cost and operations cost

The costs for the ARISE ground system development and ARISE mission operations are summarized below. Each of the components of the ARISE ground system pictured in Figure 7.2 are listed in the left hand column (see Table 8.2). The next 3 columns show the cost in FY 98

dollars for technology development, ground system development (Phase C/D) and mission operations (Phase E). There is no need to provide advanced technology development funds for any of the elements of the ARISE ground system. All technologies will be fully developed and ready for use by the beginning of Phase C/D. The Phase C/D development costs are estimated to total approximately $35M. The Phase E operations costs are estimated to total approximately $17M for 3 years of operations.

Component	Technology Development Costs ($M)	ARISE Development Costs ($M)	Operations Costs (3 Years, $M)
DSN Tracking	0	0	0.8
Cmd./Tlm. Processing Services	0	0.5	0.2
ARISE Operations Center	0	3	7.5 (17 operators)
Dedicated Ground Terminal Network	0	6 (1 terminal with control system at each of 3 sites = 3, 1 high rate receiver and equalizer at each site = 3)	4.5 (6 operators, tapes and shipping for 3300 tapes [2 - 4 tapes per observation])
Science Data Recording	0	9 (1 decoder at each site = 3, 2 recorders at each site = 6)	Included in DSN Ground Terminal Network Costs
VLBI Data Processing Center	0	16 (1 VLBI correlator and image processor = 6, 10 recorders = 10)	3 (5 operators)
ARISE Science Planning	0	0.5	1
Totals	**0**	**35**	**17**

Table 8.2: Estimated Development and Operations Costs

Telecom system cost

System	Costs ($ k)
RF X-Band	
Transponder	400
SSPA	400
Oscillator	500
Antenna	300
Diplexor	300
Cables and connectors	100
Power supply	600
Testing and support	300
RF Ka-band	
Modulator + shaping filter	800
Power Amplifier	3,750
Antenna	4,000
Misc. electronics	2,000
Cables and connectors	200
Power supply	600
Testing and support	300
Total	13,750

Thermal control system cost

Workforce *	(11 WY x $ 150 K)	1,650 K
Multilayer Insulation Mat/Fab/Instl	(14 kg)	700 K
Thermal Conduction Control		100 K
Thermal Control Surfaces		200 K
Thermal Radiator (includes heat pipes)		400 K
Thermal Louvers (4 units)		800 K
Loop Heat Pipes		1,000 K
Electric Heaters/Thermostats		200 K
Instrumentation		100 K
cryocooler		3,200 K

*This costing does not utilize the DNP process

Table 8.3: Estimated Thermal Control Subsystem Cost

Attitute control system cost

ACS Subsystem cost information is shown in Table 6.14.

ACS Subsystem Description	Cost [K$]
System Engineering	660
Controls & Analysis	770
Software	1288
I & T	7007
GSE	2908
H/W Engineering	2789
Flight Hardware	16107
TOTAL ACS COST	31529

Table 8.4: ACS Subsystem Cost

Power system cost

A rough order of magnitude (ROM) cost estimate for the power system was generated. The details are provided in Table 8.5. The estimated cost of the solar array was $3.5 M including the array subcontract, JPL engineering support and all burdens. The estimated cost of the battery was $1.3 M including the battery subcontract, JPL engineering support and all burdens. The PMAD cost was not yet defined since the details of the PMAD system were not yet available; however, it was noted that the LightSAR PMAD system, for a smaller (782 W EOL) power system, was estimated to cost $5.9 M including labor, engineering support and burdens.

Table 8.5: Power System Cost Estimate

- Solar array
  - GaAs $2K/W x 1700 W = $3.4 M
  - Si or CIS $1K/W x 1700 W = $1.7 M
  - High effic Si $1.5 K/W x 1700 W = $2.55 M

    - CIS potentially even less expensive but not yet demonstrated
  - Multijunction $2.5 K/W x 1700 W = $4.2 M
  - Add JPL engineering support ($200 K/yr) + proc/general burdens
  - Assume high efficiency Si baseline
    - ((2.55*1.027) + (0.75*0.200) + (2*0.200) + (0.75*0.200))*1.058 = $3.5 M
- Battery
  - Li-ion batteries = $170 K apiece x 3 batteries = $0.51 M (2005 est.)
    - need flight, spare and qualification units
  - Add JPL engineering support ($200 K/yr) + proc /general burdens
    - ((0.51*1.027) + (0.75*0.200) + (2*0.200) + (0.75*0.200))*1.058 = $1.3 M
- PMAD
  - LightSAR $5.9 M incl. labor + engineering support + burdens
  - ARISE being calculated

APPENDICES

APPENDIX A

ARISE Mass Budget

Subsystem Component	Flight units #	Mass (kg) /unit CBE	Mass (kg) CBE Total	Power (W) Average	Power (W) Peak	Dimensions	FOV, pointing, thermal... requirements	Other Comments
Inflatable Antenna		**Total:**	**192.3**	**11.0**	**82.0**			**Off-axis Gregorian**
Reflector	1	10.80	10.80			28.4 x 25 m		0.5-mil Al-Ka-Au (100 psi membrane stress)
Canopy	1	10.80	10.80					0.5-mil CP-1
Meterold shield	1	10.80	10.80					
Struts	3	18.47	55.40		40.00			Cold rigidized, 16 in diam, 14-mil thick (estimate for 3 struts)
Struts joints reinforcement	3	3.00	9.00					
MLI for inflatable struts	1	5.40	5.40					
Torus (with MLI and constant force springs)	1	21.40	21.40	10.00	40.00			Cold rigidized, 10.5 in diam, 12-mil thick + 306 constant force springs
Canister & mechanisms new design	1	45.25	45.25					Save ~ 12 kg. Use of the S/C structure + inflation system combined with propulsion + no
Additional tubing for NTO to canister	1	1.00	1.00					
Hardware	1	18.40	18.40					
Electronics	1	4.00	4.00	1.00	2.00			
Telecom		**Total:**	**31.5**	**28.0**	**303.0**			**RF system**
Modulator + shaping filter Ka-band	2	1.00	2.00		2.00			
Ka-band PA	1	3.50	3.50		240.00			30 W RF TWTA at 25% efficiency
1 set of microwave components Ka-band	1	7.00	7.00		13.00			
Ka-band antenna (high gain)	1	4.50	4.50					1.2 m diam antenna for 8 Gbps at Ka-band, 30 W RF
Transponder X-band	2	0.50	1.00	10.00	10.00			
X-band power amplifier SSPA	2	0.10	0.20	1.43	1.43		6 W thermal load	
X-band Encoder/Decoder	1	0.50	0.50					
1 set of microwave components X-band	1	4.00	4.00	3.61	3.61			
Antennas (patch)	1	0.50	0.50			20 x 20 cm		2 antennas
Oscillator	1	0.50	0.50	3.00	3.00			
GPS receivers	2	3.90	7.80	10.00	30.00			Mass and power from VSOP
C&DH		**Total:**	**12.7**	**9.0**	**12.0**			
Dual string architecture	1	4.00	4.00	9.00	12.00			
Tantalum enclosure	1	8.70	8.70					
Power		**Total:**	**141.6**	**40.0**	**72.0**			
Solar Array	1	32.80	32.80			32.8 m2 = 2 wings of 1.8x4.5 m2		High efficiency SI cells, 2.4 kW EOL
Power Management and Distribution								Estimate from Gene Wester
Distribution, regulation & control unit	1	66.70	66.70	20.00	20.00			gives ~ 30 W/kg expected for X2000
Peak power tracker	1	13.90	13.90	20.00	52.00			
Pyro initiation unit	1	1.00	1.00					guesstimate
Secondary battery	1	7.26	7.26					LI-ion batteries, 3 year mission, 45 min eclipses/orbit for 3 months/year, 3.5 hr recharge
Primary batteries	1	18.96	18.96					LISO2 primary battery, 260 Whr/kg
Battery enclosure	1	1.00	1.00					guesstimate
ACS		**Total:**	**82.1**	**133.5**	**228.5**			
Star trackers/camera	2	8.00	16.00	24.00	24.00			CT 601 class, 1 arcs, 12 W
Sun sensor	5	0.32	1.60	2.50	2.50			MGS/MPF type, 5 heads, 0.5 W
Sun sensor electronics	1	0.50	0.50					
Rate sensor (IRU)/gyro	1	5.00	5.00	22.00	22.00			Cassini class, 0.25 urad, 22 W
Wheel driver assembly	1	2.00	2.00					
Interface electronics	2	0.50	1.00					
Reaction wheels	4	12.00	48.00	80.00	150.00			teldix dr50
Electronics	4	2.00	8.00	5.00	30.00			
Thermal Control		**Total:**	**159.5**	**70.0**	**450.0**			

Cryocooler	1	95.00	95.00		350.00	20 K: .75 x .75 x .1 m3, 60 K: .56 x .42 x .28 + elect of 200mm3		2 Sterling (25 kg) + 1 Sorption (45 kg) active cooling, 0.5 W cooling power @ 20 K, 1 W @
Radiator	1	11.00	11.00					K1100, ~ 1cm thick, ~1 m2
Heat pipes from cryocooler to radiator	1	5.00	5.00					from Bob Miyake
Pump cryocooler heat pipes	1	5.00	5.00		30.00			from Bob Miyake
MLI+coatings+heaters+louvers for bus	1	14.00	14.00	28.00	28.00			from Bob Miyake
Heat pipes for bus	1	3.50	3.50					from Bob Miyake
Pump bus heat pipes	1	3.50	3.50	30.00	30.00			from Bob Miyake
Temperature sensors	10	0.20	2.00	2.00	2.00			from Bob Miyake
Thermal conduction control electronics	1	0.50	0.50	10.00	10.00			from Bob Miyake
Misc.	1	20.00	20.00					
Structures / Mechanisms		**Total:**	**204.3**	**50.0**	**160.0**			
Main bus + general structures	1	71.28	71.28					10% of S/C dry - propulsion - inflatable antenna
Subreflector truss	1	4.60	4.60					3.9 m Gr/Ep deployable
Subreflector boom mechanism	1	2.00	2.00		50.00			guesstimate
Subreflector (not adaptive)	1	11.00	11.00					Elliptical Gr/Cyanate 1.2x1.65-m, e=0.555
Solar array gimbals/drive	2	8.00	16.00		30.00			guesstimate
Solar array deployment + housing	2	10.00	20.00		30.00			get estimates from LightSAR (same as Carol)
Telecom antenna boom	1	6.00	6.00					
Telecom antenna deployment drive/gimbal	1	10.00	10.00	50.00	50.00			
Radiation shielding	1	10.00	10.00					guesstimate
Cables	1	35.64	35.64					5 % S/C dry - propulsion - inflatable antenna
Connectors	1	17.82	17.82					50 % cable mass
Propulsion System (+ ACS)		**Total:**	**128.3**	**520.0**	**520.0**			**81.3 for 252 kg of propellant, 86.2 kg for 330 kg of propellant**
Oxidizer tank(s)	1	6.18	6.18					Titanium tank; 320 psia MEOP; 1.5 factor of safety; includes 0.5 kg PMD
Fuel tank(s)	1	6.18	6.18					Titanium tank; 320 psia MEOP; 1.5 factor of safety; includes 1 kg PMD
Pressurant tanks	1	7.56	7.56					0.5 kg of He => 0.084 m radius by 0.495 m high cylindrical COPV
Service valve, HP	2	0.18	0.36					1.0 kg of He => 0.104 m radius by 0.613 m high cylindrical COPV
Latch valve, HP	1	0.34	0.34					
Filter, HP gas	1	0.14	0.14					
Metering orifice	1	0.10	0.10					
Pyrotechnic valve, NO, 1/4"	1	0.18	0.18					
Pressure transducer, HP	2	0.18	0.36					
Pressure transducer, LP	6	0.18	1.08					
Test port	6	0.09	0.54					
Gas regulator	1	0.74	0.74					
Quad redundant check valves	2	1.80	3.60					
Service valve, LP	5	0.18	0.90					
Latch valve, 3/8"	0	0.68	0.00					
Pyrotechnic valve, NC, 3/8"	2	0.18	0.36					
Latch valve, LP 1/4"	4	0.31	1.24					
Filter, O & F 3/8"	3	0.36	1.08					
Filter, N2H4 1/4"	0	0.14	0.00					
Temperature sensors	53	0.01	0.53					
Variable liquid regulator	0	1.12	0.00					Currently under development
Main engine	1	3.75	3.75					LEROS 1-c
TVC thruster, 22 N Monoprop	8	0.35	2.80					
Turning/RC thruster, 0.9 N	8	0.28	2.24					
Main engine heat shield	1	1.87	1.87					
Engine mounting plate	1	1.87	1.87					
Thermal blankets	1	7.00	7.00					
Thermal hardware & RHUs	1	1.50	1.50					
Wiring; pigtails & connectors	1	2.00	2.00					
Misc. (lines, fittings, etc.)	1	3.00	3.00					

Propulsion support structure	1	31.31	31.31					
Inflation gas tank	1	1.40	1.40					5% of propulsion wet mass
Inflation catalyst, valves, regulators, filters, c	1	1.20	1.20	10.00	10.00			What about any electronics, or Pressure Control Unit (PCU)?
SEP ACS system	1	36.88	36.88	510.00	510.00			
Science		**Total:**	**81.0**	**75.0**	**75.0**			
Adaptive array (19 elts, all f)	1	70.00	70.00	50.00	50.00			estimate Todd
Supporting electronics IFs	1	11.00	11.00	25.00	25.00			estimate Todd
Spacecraft Dry Mass			**1033.3**					
Contingency: 30%			310.0					
Subtotal			1343.3					
Fluids		**Total:**	**295.4**					
Nitrogen tetroxide (N2O4) oxidizer	1	109.43	109.43					main engine burn - 252 kg total burn
Hydrazine (N2H4) fuel	1	128.47	128.47					main engine burn
Inflation He	1	0.40	0.40					
Make-up gas (hydrazine)	1	23.00	23.00					
Residuals	1	6.52	6.52					2.5% of the oxidizer and fuel
Pressurant (gazeous Helium)	1	2.80	2.80					100% margin included
Xenon SEP for ACS	1	24.77	24.77					
Adapter		**Total:**	**45.4**					
LV adapter	1	45.40	45.40					Delta II specs
Spacecraft Total Mass			**1684.1**	**kg**				
Launch Vehicle capability: 5% margin			**1691**	kg -	Delta II 7925H @	36	deg. inclination	(propellant mass for the DV is based on this mass)

76

APPENDIX B

ARISE Power Budget

Description of the power phases/modes:

Mode 1:	Launch duration + post-lauch operation
Mode 2:	DV burns, orbit insertion phase
Mode 3:	Inflatable antenna + other deployments
Mode 4:	Science data collection + telecom
Mode 5:	Non science mode, repositioning, slewing
Mode 6:	Eclipses

Power Budget: REQUIRED S/A OUTPUT

Assumption:	1.5 kW Solar Array EOL			**ALL NUMBERS IN WATT**			Mechanisms/mode:		
								1	- None
Subsyst.\Modes	**1**	**2**	**3**	**4**	**5**	**6**		2	- None
Attitude control ACS				228.5	228.5			3	- Subreflector
Propulsion				520	10				- then Ka-band antenna
C&DH				12	9			4	- Solar arrays gimbal
Inflatable antenna				5	5				- then Ka-band antenna gimbal
Power				72	40		no recharge	5	- Solar arrays gimbal
Mechanisms				80	80				- then Ka-band antenna gimbal
Telecom				303	36			6	- Ka-band antenna gimbal
Thermal control				450	70				
Science				75	0				
Subtotal				**1745.5**	**478.5**				
Contingency (30%)				**523.65**	**143.55**				
Total				**2269.15**	**622.05**				
				(end of life)					

Power Budget: TRANSCIENT EVENTS ON BATTERIES

Subsyst.\Modes	**1**	**2**	**3**	**4**	**5**	**6**	
Attitude control ACS	133.5	133.5	133.5			133.5	
Propulsion	60	60	70			10	
C&DH	9	9	9			9	
Inflatable antenna	82	82	82			5	
Power	20	20	20			40	
Mechanisms/Pyro	0	0	80			50	
Telecom	36	36	36			36	
Thermal control	70	70	70			70	
Science	0	0	0			0	
Total	**410.5**	**410.5**	**500.5**			**353.5**	
Contingency (30%)	**123.15**	**123.15**	**150.15**			**106.05**	
Total	**533.65**	**533.65**	**650.65**			**459.55**	
Duration (hrs)	6.8	0.5	2			0.75	
Battery Whr requirement	3628.8	266.8	1301.3			344.7	1 orbit is 13.6 hours
Battery type	primary	secondary	primary			secondary	

APPENDIX C

ARISE Structures and Thermal Analysis

ARISE Finite Element Model

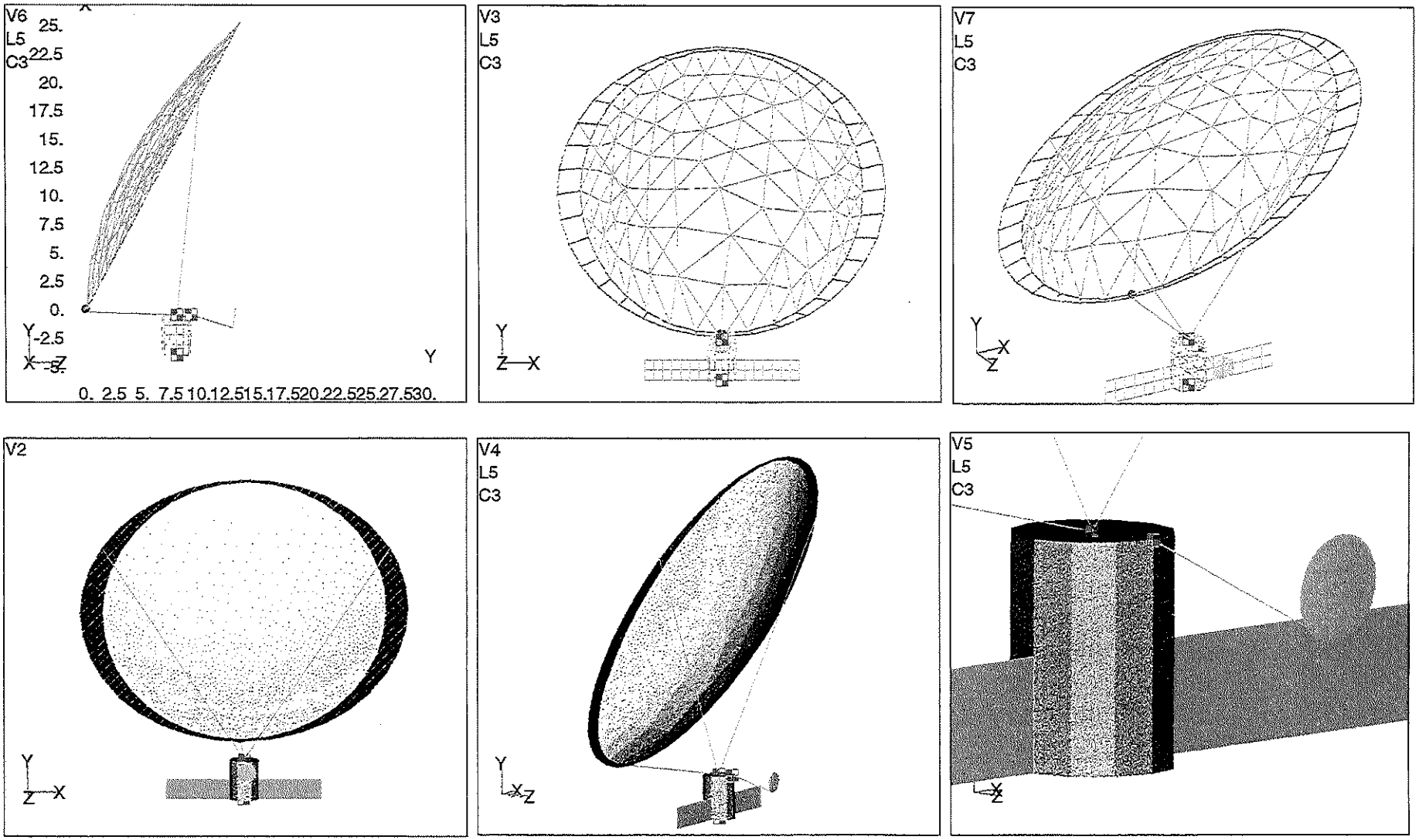

Off-Axis Gregorian, f = 11.55m, D = 25m, f#p = 0.23

ARISE On-Orbit Temperature Profiles

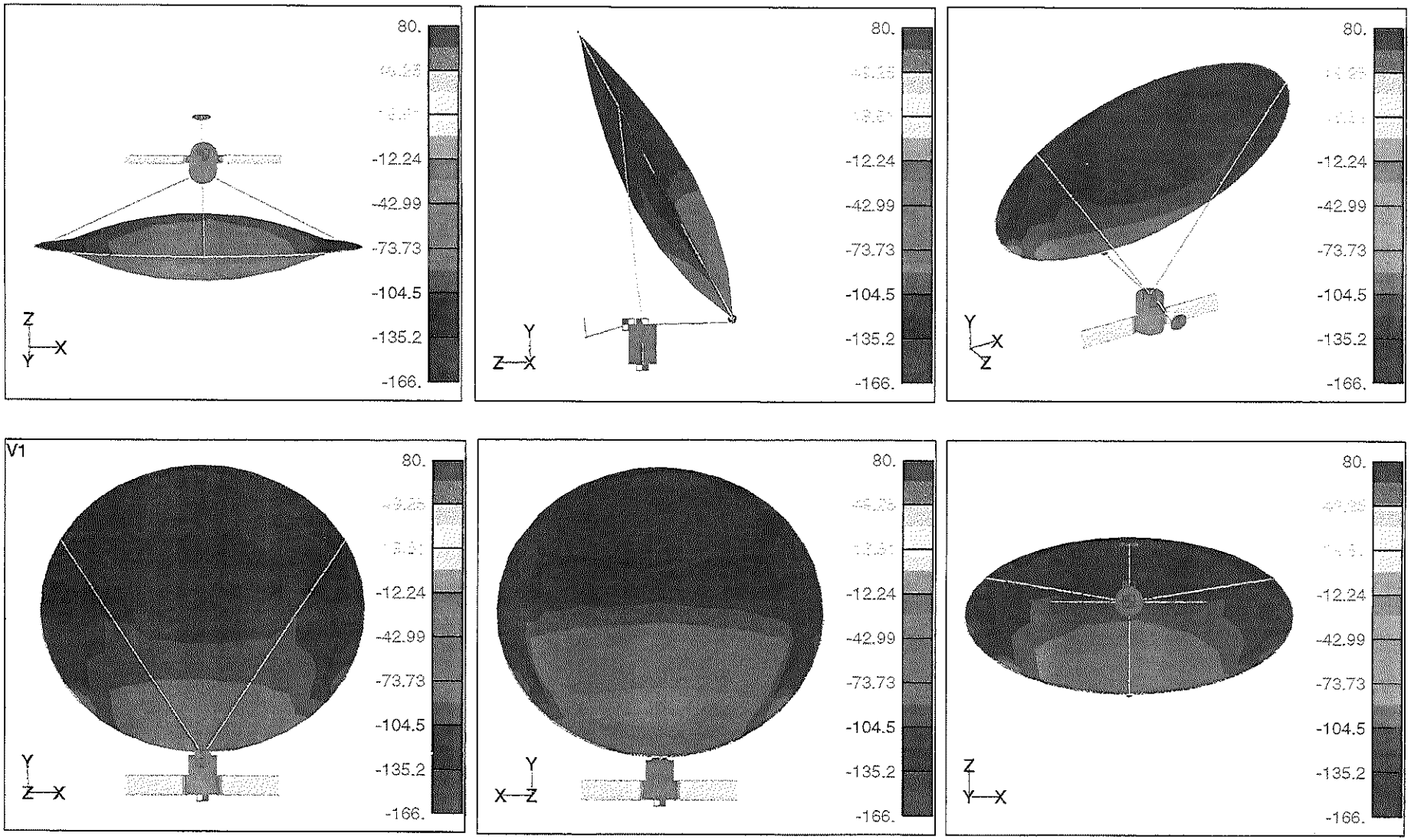

Edge-On Solar Loading Case with Earth's Albedo/IR

APPENDIX D

SEP System

Micro Ion thrusters system								
Total propellant usage:								
Number of operating axis:	2	/ 6						
Number of operating thrusters per axis:	3			85	W/engine at PPU input (assumes η=30%)			
Number of years:	3			510	W total			
Total propellant mass:	24.2	kg		1	mN			
Torque to counteract:								
Average torque:	0.05	Nm (max 0.05 Nm)						
Average arm length:	16	m						
Thrust required:	3.1E-03	N						
Isp:	2500	s						
Propellant mass flow rate:	1.27551E-07	kg/s						
Total propellant mass / year:	4.0	kg/year						
System masses:								
Item	**QTY**	**Mass/unit**	**Mass (kg)**	**Conting. (%)**	**Total Mass (kg)**			
Ion Engines	12	0.1	1.2	0	1.2			
Ion PPUs	6	2.8	17.1	0	17.1			
Gimbals	0	0.0	0.0	0	0.0			
Gimbal drive electronics	0	0.5	0.0	0	0.0			
PPU Thermal control	6	0.2	1.0	0	1.0			
PPU Micrometeroid protection								
DCIU	1	*0.3*	0.3	0	0.3			
Propellant Tank (10% propellant)	1	2.5	2.5	0	2.5			
Fixed Feed System	1	*3.0*	3.0	0	3.0			
Feed System per Engine	12	*0.1*	1.2	0	1.2			
PMAD specific to SEP stage	1	0.5	0.5	0	0.5			
Structure/cabling per Engine	0	4.0	0.0	0	0.0			
Subtotal 1					***26.7***			
Cabling (10% of Subtotal)	0	10%	2.7	0	6.8	+ struts cabling:	4.1	kg
Structure/Mecanisms (7.5% of Subtotal)	0	7.50%	2.0	0	2.0			
Thermal (5% of Subtotal)	0	5%	1.3	0	1.3			
Subtotal 2					***36.9***			
Solar Arrays (80W/kg)	1	6.4	6.4	included	6.4			
S/A support structure	1	10%	0.6	30	0.8			
S/A drive	1	10%	0.6	30	0.8			
Subtotal 3					***44.9***			
Residuals (2.5%)	1	0.6			0.6			
Total propellant	1	24.2			24.2			
SEP TAL TOTAL					***69.7***			

APPENDIX E

ARISE radiation environment

JET PROPULSION LABORATORY

INTEROFFICE MEMORANDUM
5052-98-024
February 3, 1998

TO: Muriel Noca

FROM: D.R.Croley

SUBJECT: Radiation Environmental Comparison of Four Potential ARISE Orbits

Summary

The radiation risk to a spacecraft encountered in four highly inclined orbits is discussed. The most significant radiation hazard is from trapped magnetospheric charged particles (protons and electrons). The contribution from solar and galactic cosmic rays is also discussed. The radiation dose to a thin-polymer, inflatable antenna is analyzed using a simple model and a radiation transport code.

Introduction

The ARISE orbits under consideration are all 5000 km perigee x 40000 km apogee. The inclinations considered are 30° and 60°. Two arguments of perigee are also considered: 0° and 90°. The lower (more equatorial) inclination orbits stay in the radiation belts over a greater part of the orbit than the higher (more polar) inclination orbits. Also, orbits which have their apogee near the equator have a greater radiation exposure than when apogee is more polar. Since the apogee is at very high altitude, out past geosynchronous orbit, solar flare particles and galactic cosmic rays have easy access to the spacecraft. There are two main radiation issues addressed: Total ionizing dose in silicon to address electronics issues and the dose acquired by the inflatable antenna which is constructed from a very thin polymer. The radiation dose received by the thin polymer is enormous because of the absence of shielding. The major concern should be potential changes in material properties due to radiation exposure.

Total Ionizing Dose

Figure 1 gives the trapped particle radiation dose in silicon vs aluminum shield depth for the four orbits under consideration. The worst case dose for 100 mils Al shield is 150 krads/year using a 4π spherical shield geometry. This dose is accumulated on every pass through the radiation belts.

Solar flare and galactic cosmic rays are shielded from earth to a large extent by the geomagnetic field. Although the galactic cosmic ray background is continuous, solar flare particles occur randomly in time , magnetude and composition. The apogee of these orbits is in a region where the earth's magnetic field is weak so solar flare and galactic cosmic rays have easy access. Over the lower parts of the orbit, particles of some energy will penetrate. Average penetration factors for these orbits, which are energy dependent, have been calculated and applied to the solar proton fluence for a 3-year mission. Figure 2 gives the dose due to these penetrating solar flare protons. The dose is small compared to that due to trapped

magnetospheric particles. However, this is an average calculation and could be deceptive. Figure 5 gives the solar flare proton flux time profile for the October 1989 solar flare as seen by a GOES spacecraft at geosynchronous orbit . There are roughly two orbits per day for the 5000 x 40000 km orbit. It can be seen that the actual proton dose will depend on the phasing of the spacecraft apogee time with the solar proton flux time profile.

Trapped Particle Fluence

The scale size of microelectronics parts is decreasing making parts more radiation sensitive. Many parts now are susceptible to displacement damage. The damage cross sections are given as a function of total proton fluence (protons/cm^2). Figure 3 is the integral proton fluence per year for these orbits. Figure 4 is the integral electron fluence per year for these orbits which might figure in solar cell degradation considerations.

Figure 6 is the peak trapped proton flux for the worst case orbit. If an electronic part has an upset cross section threshold less than about 15-20 MeV-cm^2/mg, it will be vulnerable to energetic protons. Upset will occur during passage through the inner radiation belt. The upset rate will be highest in regions of peak proton flux.

Galactic Cosmic Ray Background

A continuous radiation background due to Galactic Cosmic Rays (GCR) is composed of an energetic proton component and an energetic heavy ion component. Figure 7 gives the proton energy spectrum. Figure 8 gives the heavy ion LET spectrum. It is the heavy ion component that is responsible for the continuous low level single event effects in susceptible electronic parts in interplanetary space. GCR is impossible to shield against as Figure 8 will show. Error correction techniques must be used to deal with GCR induced SEE. Solid state recorders are particularly susceptible to single event upsets because the number of memory bits runs in the billions. Good test data for the solid state recorder memory devices are required to get a prediction for the SEU rate.

Single Event Effects during Solar Flares

Both energetic protons and heavy ions can cause single event upsets (SEU) in memory chips, processor registers, FPGAs, etc. Heavy ions can cause latch up and burnout as well. If a part has an upset LET threshold less than ~15 MeV-cm^2/mg, proton induced SEUs can occur. Parts with upset LET thresholds greater than ~20 MeV-cm^2/mg do not experience proton induced upsets. Figure 10 gives the peak integral proton flux associated with the large October 1989 flare. This spectrum can be used to estimate the peak SEU rate due to protons in radiation soft parts.

The heavy ion composition of solar flares varies from flare to flare. The LET spectrum of heavy ions associated with a solar flare covers a wide range of LET values. The JPL heavy ion model based on the work of H.H. Breneman and E.C. Stone is an average flare composition model. The heavy ion spectra derived from the JPL model are given in Figure 9 for aluminum shielding value of 60, 120 and 250 mils. The set of curves on Figure 9 identified as "Heavy Ion Let Spectra (Environment Alone)" is the flux of all heavy

ions in a 99% confidence level solar flare environment, from the JPL model, sorted according to the LET of the particle. The set of curves identified as "Effective LET Spectra (Device Dependent)" takes into account the path length distribution of heavy ions in the sensitive volume of a 2x20x20 micron rectangular parallelepiped. It is the effective LET spectrum that must be used to calculate the estimated SEU rate due to heavy ions. Unfortunately, the effective LET spectrum depends on the sensitive volume of the device. The device upset cross-section must be known also. The SEU rate during a large solar flare event is an enhancement over the background rate due to Galactic Cosmic Rays.

Dose Model for the Antenna

The antenna was modeled as a laminar sandwich of 650 angstroms aluminum, 0.5 mils kapton, 650 angstroms gold and 0.5 mils kapton. The structure was a planar circular disk with a 1200 cm radius. This very thin structure was input into the transport code NOVICE to calculate the dose at points through the structure using the particle data from the most severe orbit: 30° inclination, 0° argument of perigee. Table 1 gives the results of that calculation. There is no shielding to attenuate the radiation dose. The dose in the various layers is in the 10's Megarads. The surface dose on the kapton is 128.7 Mrad. These calculations were performed a point at the center of the circular disk. This is comparable to a simpler 1-D calculation which gives 191 Mrad. Special attention should be given to the consequences of potential material property changes due to these high dosages: Thermal, structural strength, delamination, electrical conductivity.

Dose (Mrad/year)				
Layer Thickness	**Depth(cm)**	**Al**	**Kapton**	**Au**
650 Angstrom	0.	**90.6**		
	3.25E-6	88.0		
	6.5E-6	83.5	**121.1**	
0.5 mil	6.415E-4		42.6	
	1.2765E-3		41.6	18.3
650 Angstrom	1.27975E-3			18.0
	1.283E-3		40.8	17.8
0.5 mil	1.918E-3		41.5	
	2.453E-3		67.8	
	2.553E-3		**128.7**	

Table 1. Particle data from 1-year in orbit 5000 x 40000 km 30° inclination 0° Argument of Perigee were used in a transport code. The antenna was modeled as two 1200cm radius circular 0.5 mil sheets of *kapton* with 650 angstroms *gold* between them and 650 angstroms of *aluminum* on one face and bare kapton on the other face. The surface doses are shown in bold type.

cc: J.Clawson
L.Compton
R. Freeland
H. Garrett
R. Helms
G.Spitale

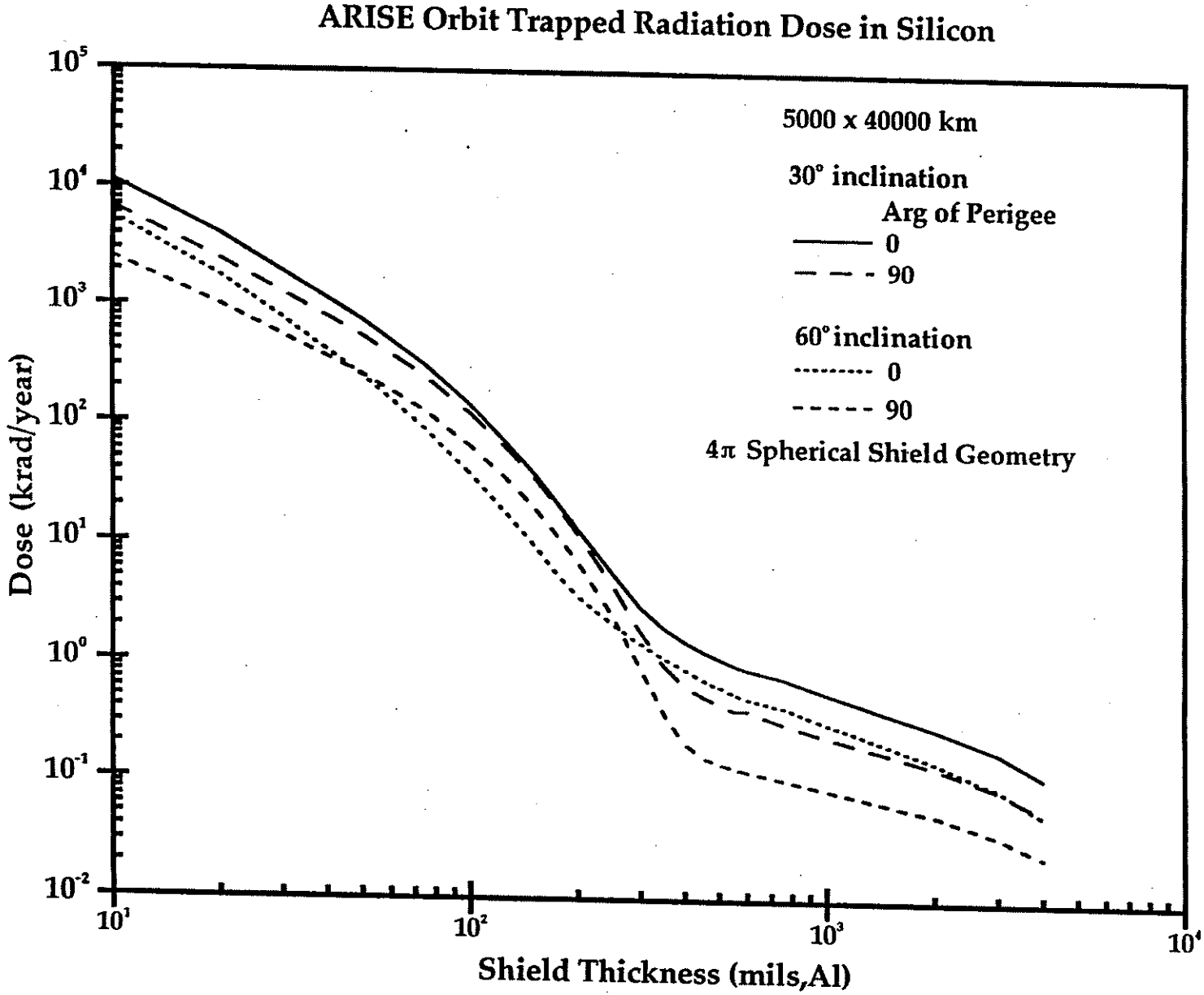
ARISE Orbit Trapped Radiation Dose in Silicon
5000 x 40000 km
30° inclination
Arg of Perigee
0
90
60° inclination
0
90
4π Spherical Shield Geometry
Dose (krad/year)
Shield Thickness (mils,Al)

Figure 1

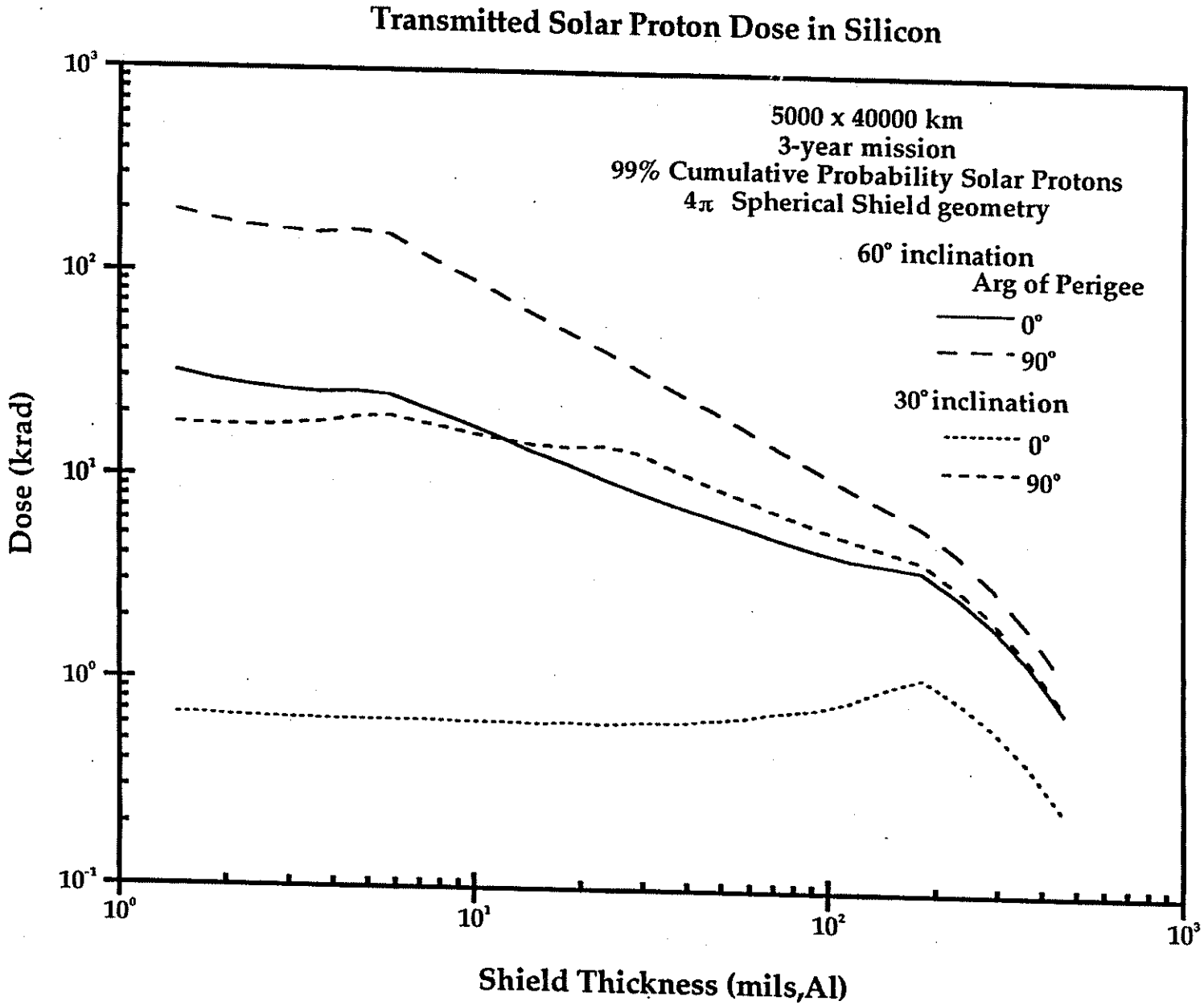
Transmitted Solar Proton Dose in Silicon
5000 x 40000 km
3-year mission
99% Cumulative Probability Solar Protons
4π Spherical Shield geometry
60° inclination
Arg of Perigee
0°
90°
30° inclination
0°
90°
Dose (krad)
10³
10²
10¹
10⁰
10⁻¹
10⁰
10¹
10²
10³
Shield Thickness (mils,Al)

Figure 2

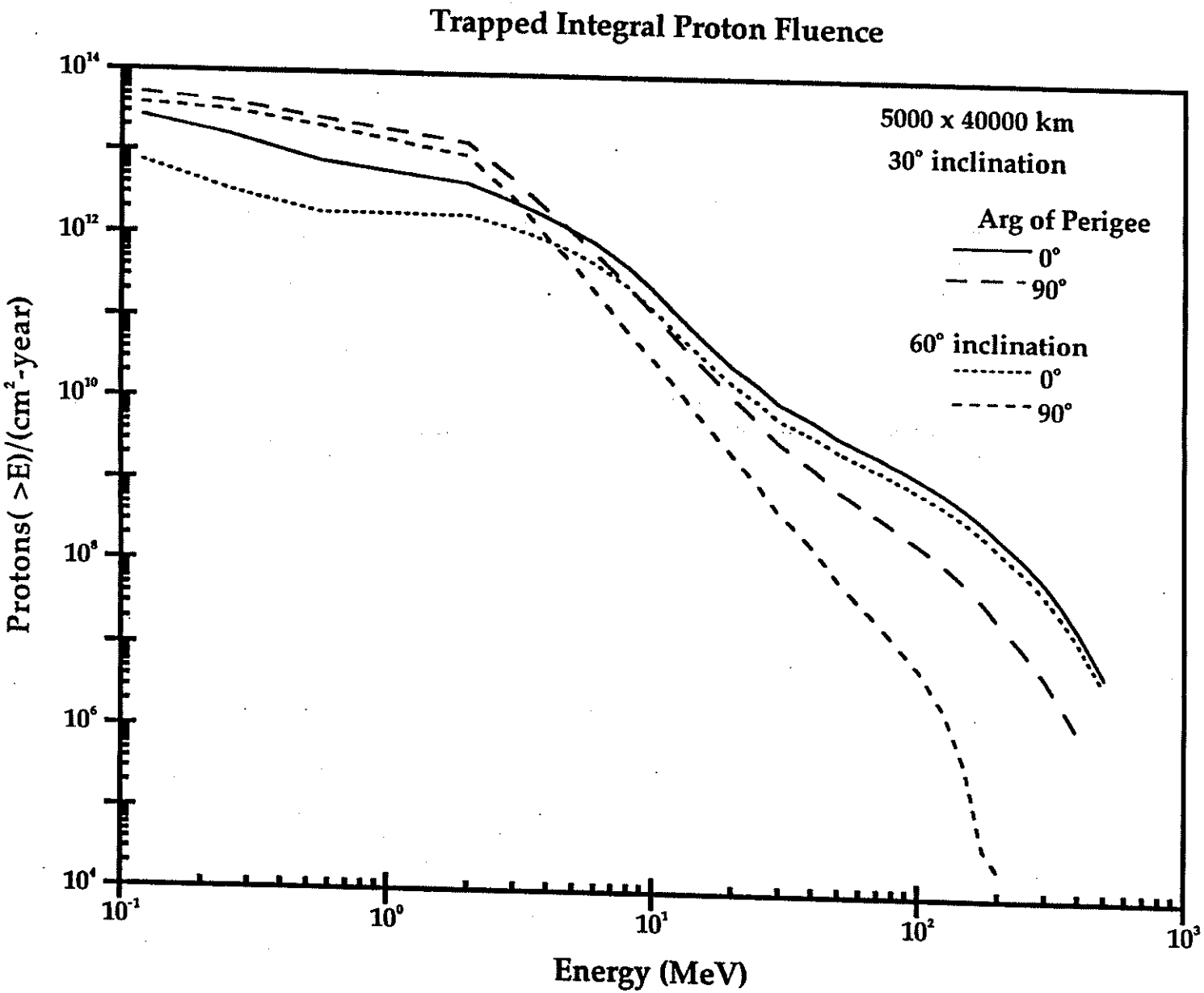
Trapped Integral Proton Fluence
5000 x 40000 km
30° inclination
Arg of Perigee
0°
90°
60° inclination
0°
90°
Protons(>E)/(cm²-year)
10¹⁴
10¹²
10¹⁰
10⁸
10⁶
10⁴
10⁻¹
10⁰
10¹
10²
10³
Energy (MeV)

Figure 3

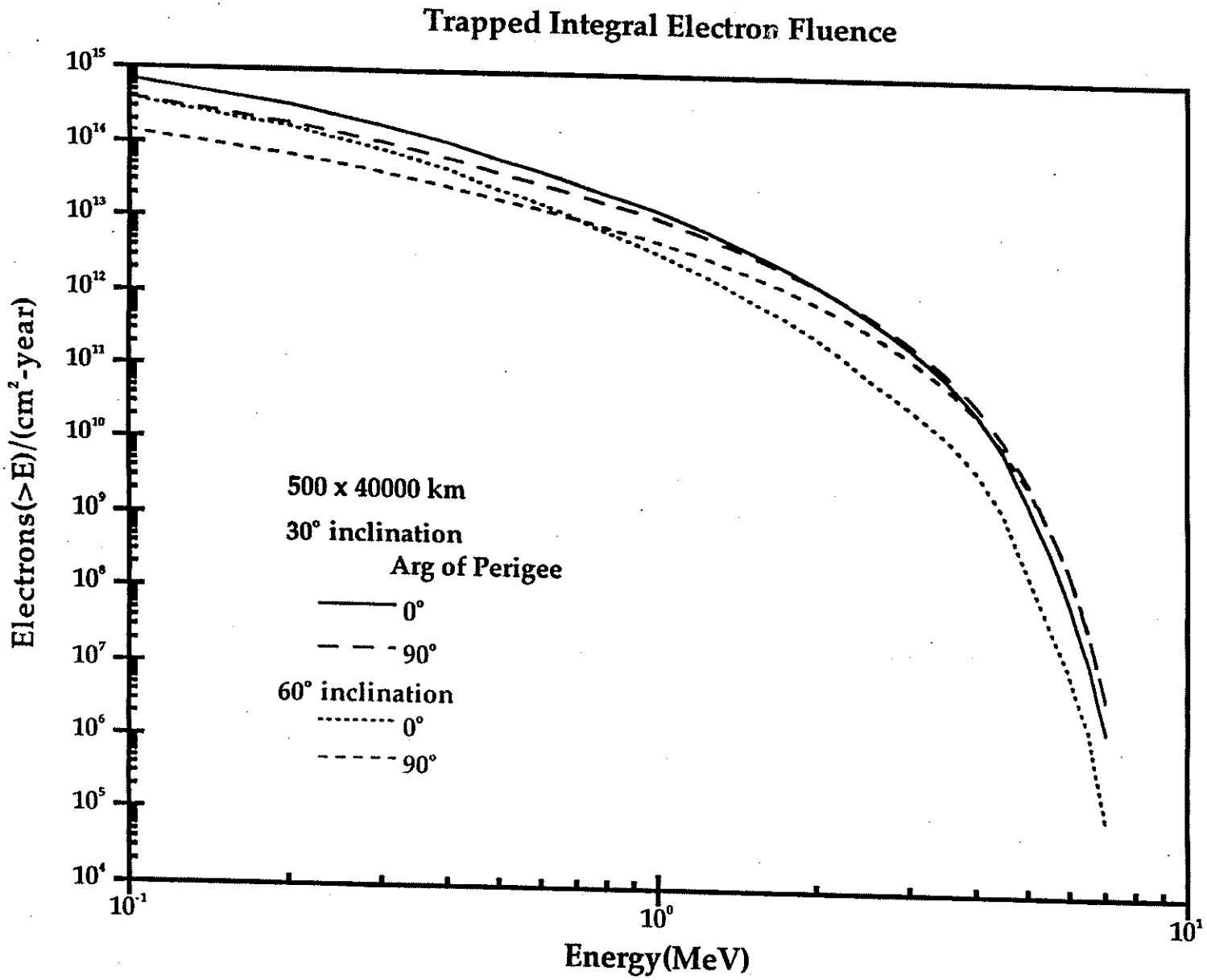
Trapped Integral Electron Fluence
Electrons(>E)/(cm²-year)
10¹⁵
10¹⁴
10¹³
10¹²
10¹¹
10¹⁰
10⁹
10⁸
10⁷
10⁶
10⁵
10⁴
10⁻¹
10⁰
10¹
Energy(MeV)
500 x 40000 km
30° inclination
Arg of Perigee
0°
90°
60° inclination
0°
90°

Figure 4

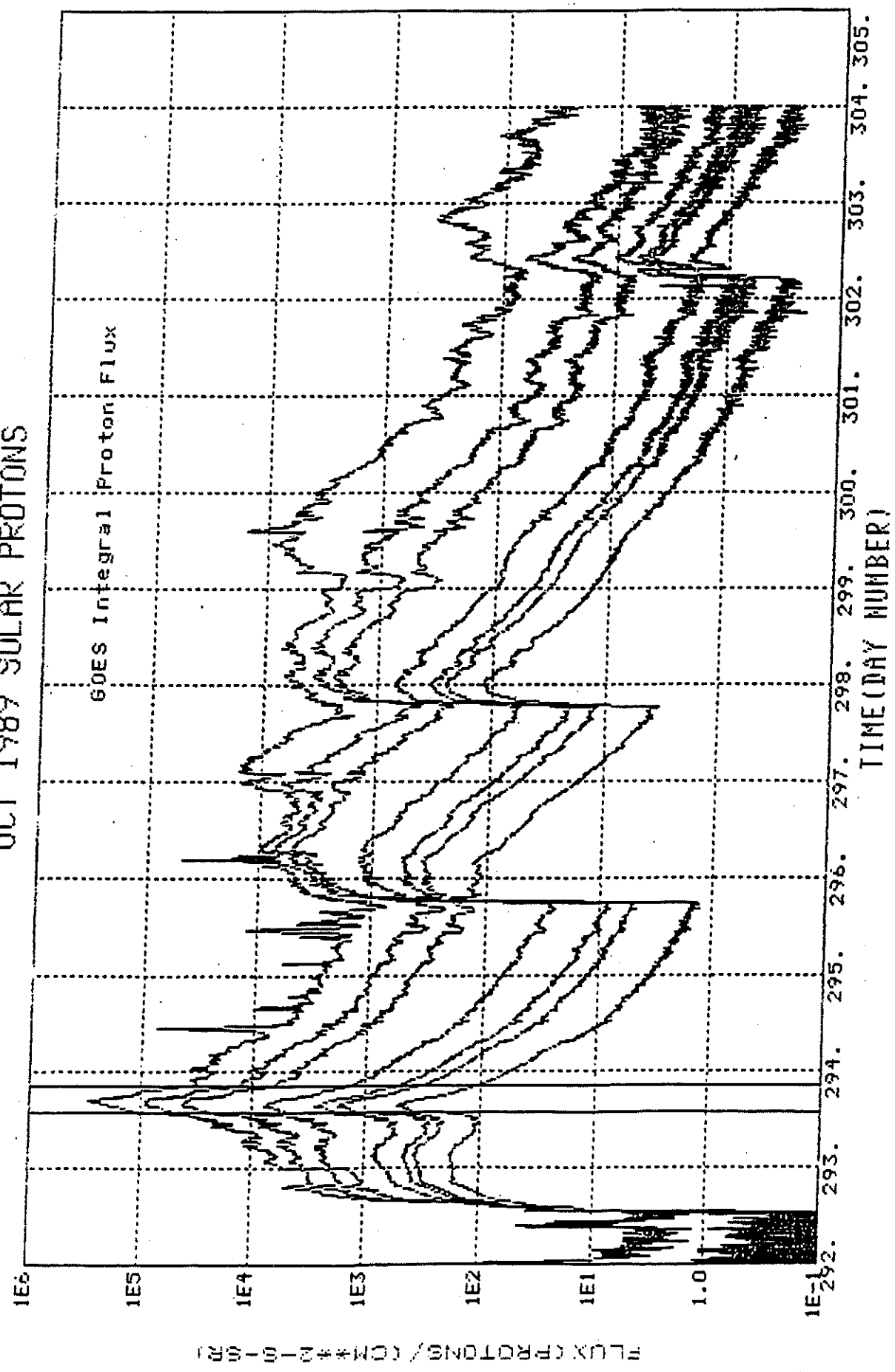
OCT 1989 SOLAR PROTONS
GOES Integral Proton Flux
FLUX (PROTONS/(CM**2-S-SR)
1E6
1E5
1E4
1E3
1E2
1E1
1.0
1E-1
292.
293.
294.
295.
296.
297.
298.
299.
300.
301.
302.
303.
304.
305.
TIME(DAY NUMBER)

Figure 5

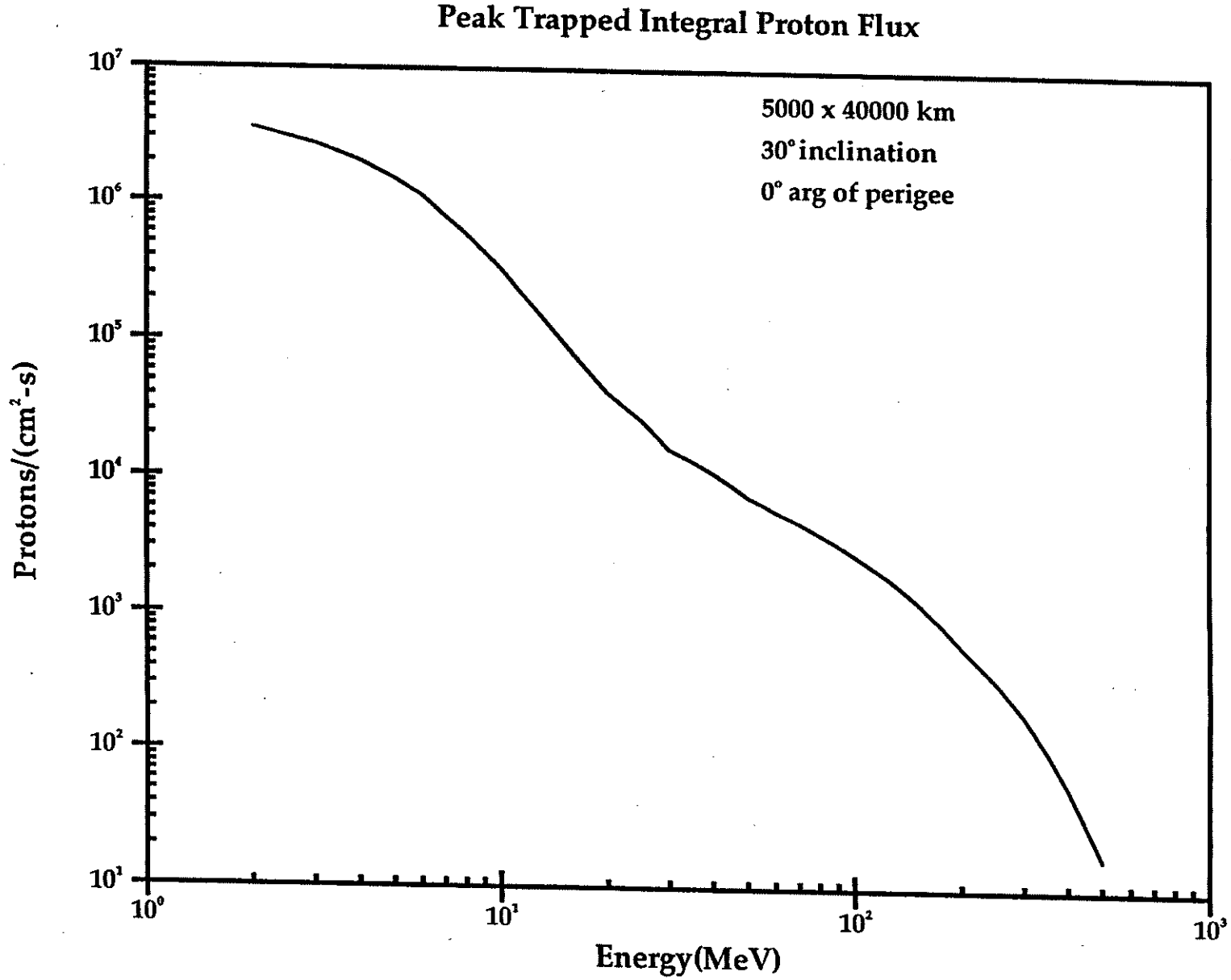
Peak Trapped Integral Proton Flux
5000 x 40000 km
30° inclination
0° arg of perigee
Protons/(cm²-s)
10⁷
10⁶
10⁵
10⁴
10³
10²
10¹
10⁰
10¹
10²
10³
Energy(MeV)

Figure 6

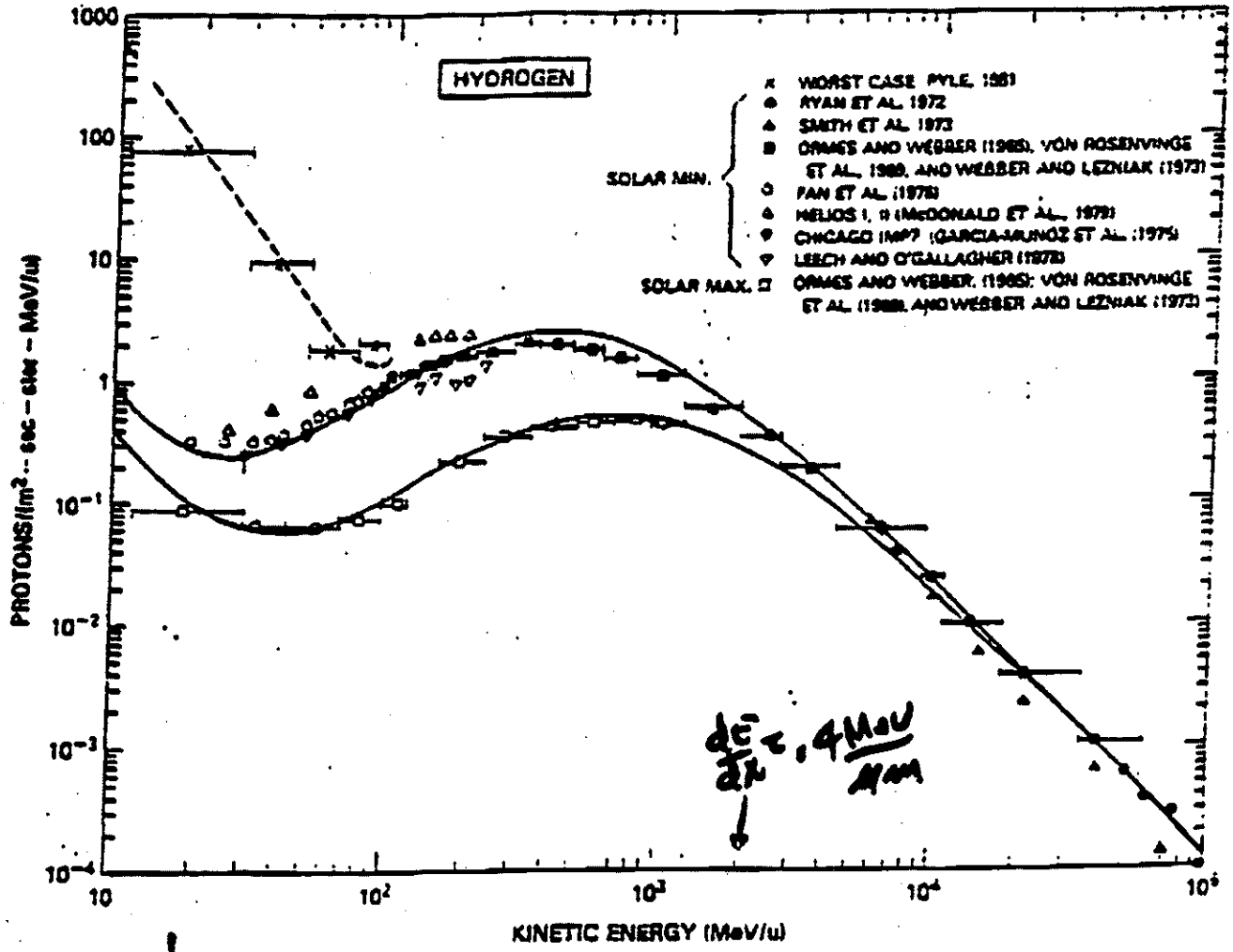

Fig. 2.2 — The differential energy spectrum of hydrogen (mostly protons). The data are selected to show the solar maximum and solar minimum forks. The smooth curve is an analytic function contrived to fit the data. The dashed curve is a worst-case spectrum.

Adams et al. (1981)

Figure 7

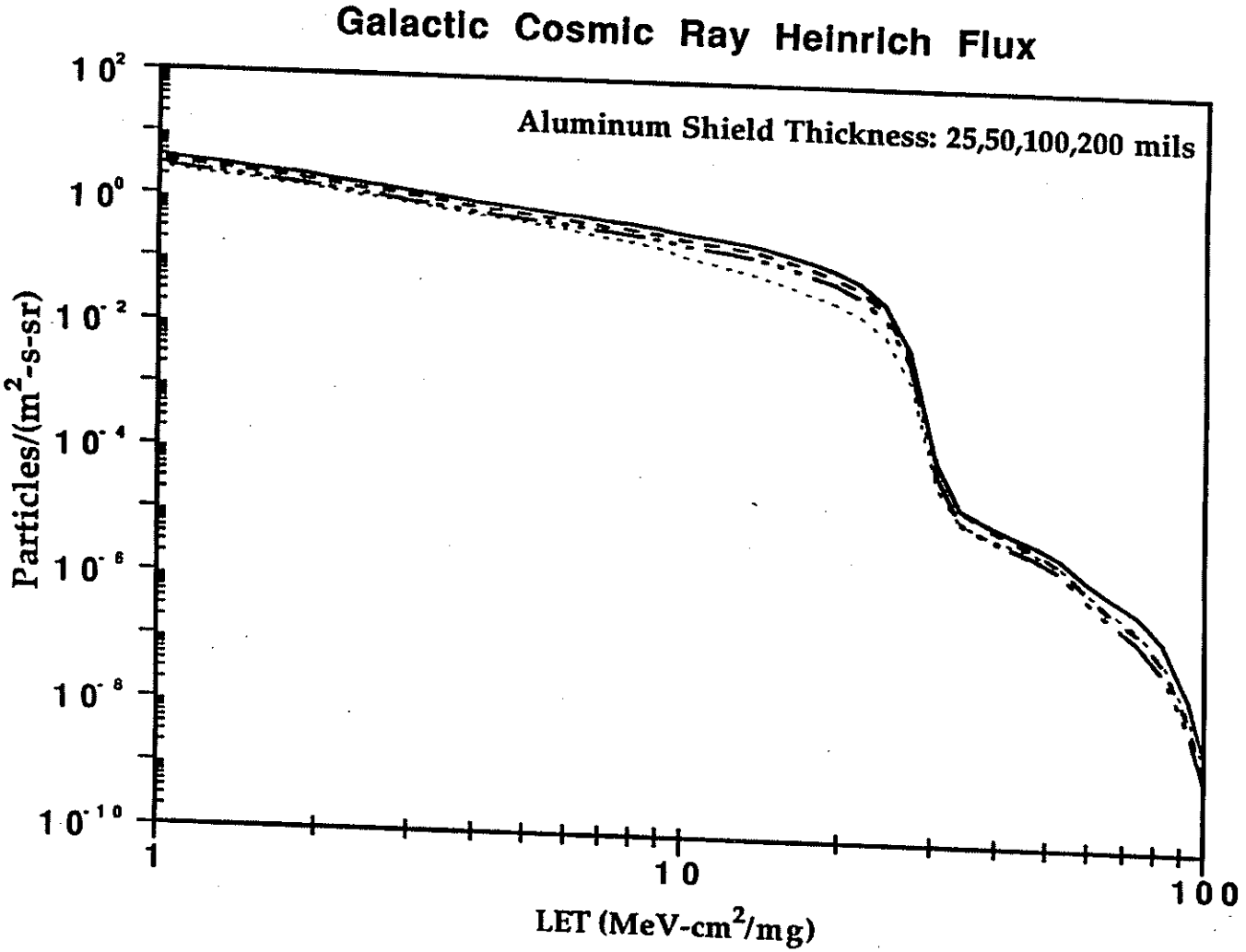
Galactic Cosmic Ray Heinrich Flux
Aluminum Shield Thickness: 25,50,100,200 mils
Particles/(m²-s-sr)
10²
10⁰
10⁻²
10⁻⁴
10⁻⁶
10⁻⁸
10⁻¹⁰
1
10
100
LET (MeV-cm²/mg)

Figure 8

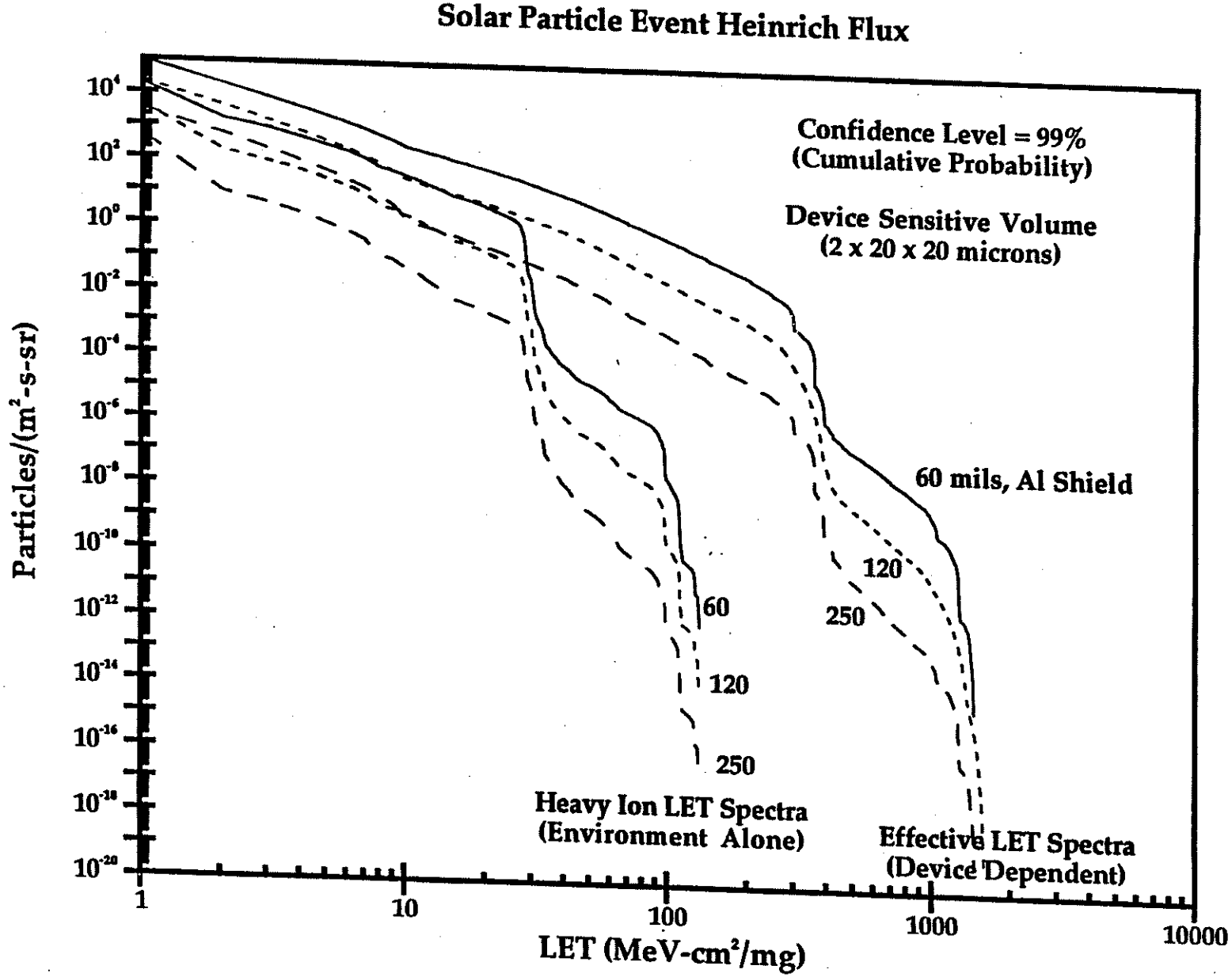
Solar Particle Event Heinrich Flux
Confidence Level = 99%
(Cumulative Probability)
Device Sensitive Volume
(2 x 20 x 20 microns)
60 mils, Al Shield
120
250
60
120
250
Heavy Ion LET Spectra
(Environment Alone)
Effective LET Spectra
(Device Dependent)
Particles/(m²-s-sr)
LET (MeV-cm²/mg)
1
10
100
1000
10000

Figure 9

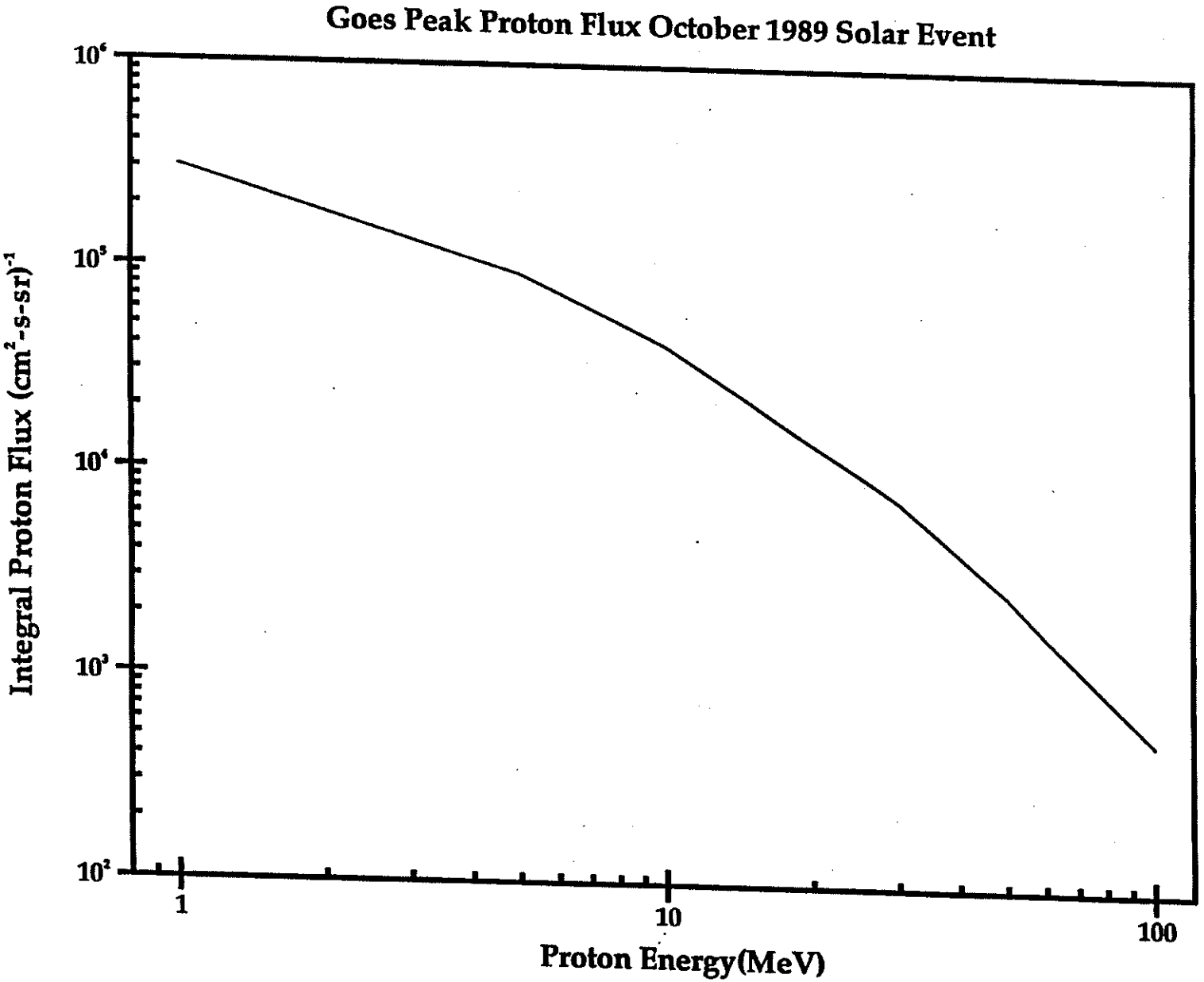
Goes Peak Proton Flux October 1989 Solar Event
Integral Proton Flux (cm²-s-sr)⁻¹
10⁶
10⁵
10⁴
10³
10²
1
10
100
Proton Energy(MeV)

Figure 10

APPENDIX F

ARISE ESD environment

SURFACE CHARGING OF THE ARISE MAIN ANTENNA

Henry Garrett
01/29/98

SUMMARY

Objects immersed in a space plasma will charge relative to the plasma. Indeed, the potential on a space structure has been observed to reach -20 kV in a few seconds. Such high absolute potentials are not in and of themselves dangerous. Unfortunately, they can lead to high differential potentials and these are dangerous as arc discharges may occur. The large size of the Arise antenna structure and its intrinsic design--virtually a large capacitor--may make the problem worse. Here, the range of charging expected and the possible effects that the charging may cause will be briefly reviewed. As will be discussed, the actual situation may not be as serious as these statements imply. Even so, the unique design and mission profile of the Arise mission will need to be periodically reviewed to verify that they avoid the more severe effects of charging.

SURFACE CHARGING

Spacecraft charging is now known to come in two "flavors"--surface charging (considered here) where the surface currents associated with the ambient plasma, photoelectron emission, or artificial beam sources can produce a varying surface potential, and "internal" or "buried" charging (considered separately) where ~100 keV electrons or higher can penetrate the surface of a spacecraft and deposit in or on surfaces internal to the spacecraft faraday shield. In the case of surface charging, the various currents to the surface must balance or a charge imbalance occurs. The charge imbalance adjusts itself to bring about current balance. In sunlight, a surface will typically charge to a few volts positive relative to the plasma. In the absence of sunlight (in the shadow of the Earth or in the spacecraft shadow) and, assuming the spacecraft is a uniform aluminum sphere, the resulting potential between the sphere and space has been plotted for the Earth's magnetosphere in Fig. 1. The plasma conditions assumed were for a moderate to severe magnetospheric environment such as would occur during a geomagnetic storm. The potential values shown represent the range of values that Arise will experience as it orbits the Earth.

The Arise antenna is not a conducting aluminum sphere. Its lenticular shape is characterized by two thin (~.5 mil) sheets--one metalized (aluminum or gold) and the other kapton or similar transparent plastic. The conducting metal surface will likely charge to a uniform potential like the sphere varying in magnitude from ~2 V positive in sunlight to values similar to those in Fig. 1. The kapton surface, being a dielectric, will have a variable potential across its surface (see below, however) depending on the angle of the sunlight and the anisotropies in the plasma fluxes. For quantitative comparison, a simple charge balance calculation for an actual observed worst case charging event gave potentials of -30 kV for aluminum versus -20 kV for a kapton surface (this ratio can be applied to Fig. 1 as well). Therefore, under worse case conditions (the aluminum surface in complete sunlight at ~0 V, the kapton in shadow at -20 kV), a differential potential between the two surfaces of 20 kV might be observed. An actual charging case for a kapton surface on the SCATHA spacecraft is shown in Fig. 2 for moderate charging conditions (the kapton surface is rotating in and out of sunlight at 1 rpm) of -1.5 kV.

CONSEQUENCES OF HIGH DIFFERENTIAL CHARGING

Given the 5,000 x 40,000 km altitude range of the Arise orbit, and depending on the exact inclination and argument of perigee, the Arise antenna will clearly be exposed on occasion to high differential potentials. The following is a list of possible consequences of such differential charging (note: these reality of these effects will be evaluated later):

1) Arc discharges at the edges of the antenna where the potential gradients (i.e., electric fields) are greatest. Given the large size of the conducting metalized area, a large, sustained arc may be possible causing severe mechanical damage.

2) Electrostatic noise from the arc can be picked up by the spacecraft/antenna receiver causing electronic damage.

3) The large electrostatic field may deform the shape of the antenna.

4) The charge on the kapton surface could effect the propagation of the rf signal through the kapton.

5) The charged surface could oscillate in response to plasma waves (plasma waves have been observed to produce potentials of 100 V at periods of seconds on spacecraft surfaces).

6) Paschen breakdown of the gas between the two surfaces.

In reviewing these effects, it will be assumed that the spacecraft/antenna receiver will be designed to the standards in NASA TP 2361 (1984) and therefore relative immune from spacecraft charging itself. Secondly, it will be assumed that the support ring for the antenna plays little or no role in the charging process. The main source of concern is thus the antenna proper.

Consider first Issue 1, a sustained arc discharge. This type of behavior has been postulated in the past and some laboratory evidence exists that in the presence of a light source and sufficient charging plasma, a sustained arc can exist. Several issues may mitigate this behavior, however. First, the kapton may, because of its thinness, be sufficiently conducting due to the radiation local radiation environment to allow charge to bleed off. This would be very dependent on the exact characteristics of the material and the environment, however. Secondly, the gradient near the edge of the antenna may be limited by space charge--secondary plasma generated near the edge by various processes. Finally, the metalized surface may consist of electrically isolated gores so that the surface contributing to the arcing is relatively small (this may happen naturally as the material ages and cracks). In any case, arcing, if steps to mitigate it are not taken, will likely occur near the edge of the array when the plasma environment is sufficient to cause potential differences of 200 V or more.

The noise from an arc discharge has been characterized in ground tests. For nearby circuits, coupling can be quite damaging. However, as most of the circuitry will be on the spacecraft/antenna receiver, the fall with distance should be sufficient to limit any such coupling (note: structures mechanically coupling the antenna and the spacecraft must provide electrical isolation). As to pick-up by the antenna receiver, the arc spectrum in the range of concern is believed to be sufficiently low to not be of concern but this should be evaluated in detail.

Deformation of the antenna will depend on its pressurization, surface tension, and on the details of the spacing. The antenna to first order resembles a large parallel plate capacitor--the field between two parallel plates is constant. The project may need to estimate the effects of a 20 kV field on the shape of the antenna. Surface tension and pressurization may be sufficient to stabilize the surface shape but rapid variations in the potential with orbit could make it worse. JPL has codes capable of accurately estimating the charge buildup/surface potential for various orientations and plasma environments.

This study has not attempted to estimate the charge density on the kapton surface and may need to be evaluated (I suspect they are quite low). However, the ambient plasma and secondary plasma produced by the surface typically have densities of at most a few 1000's of particles per cubic centimeter with a few particles per cubic centimeter being more likely. Such densities are not likely to have any effect on signal propagation.

Plasma waves and plasma interactions have been proposed as a possible source of "luffing" in solar sails. Such effects may need to be evaluated for the Arise but given the level of these effects (typically 100 V or less), the far larger effects of the overall surface charging (10's of kV) would be expected to dominate any such interactions.

As the antenna pressurization should be well below the Paschen breakdown level, the last issue is not likely though it should be kept in mind when selecting the final pressure.

CONCLUSIONS/RECOMMENDATIONS

The Arise antenna will charge to large levels in the space environment. Provided that the spacecraft/receiver antenna is properly designed to avoid ESD, the main concern suggested here is differential charging which could lead to self-sustaining arcs. This process can be controlled by making the surface of the antenna entirely conducting, using plasma sources to limit the differential charge, or limiting the conducting areas from which charge can be drawn. Before any decision is made, it is recommended that laboratory tests be carried out to determine the charging characteristics of whatever materials are picked--a moderately conducting material sufficiently transparent to the radio waves of concern might be the simplest answer. Plasma source would work but given the large area of the area, would be prohibitive in size or number.

The detailed charging of the Arise antenna can be computed for various orientations, configurations, and environments if the project so desires. While moderately expensive, such models would allow a determination of the effects of charge on the shape of the antenna. It is recommended that the project support such efforts to better understand how the antenna will charge.

In closing, it should be remembered that many spacecraft have survived in the environment that Arise will fly without any serious problems. Charging has been observed, however, and has been postulated as the cause of serious damage on a few spacecraft. Arise represents a new, unique type of design that may be susceptible to the effects of charging if careful consideration of mitigation techniques is not a part of the overall design. In general, whenever charging has been taken into account, systems have proven robust--only when completely ignored has it been a problem.

FIGURES

Figure 1. For "worst-case" environments near Earth, the following chart has been prepared to indicate whether space charging should be considered in the design of the spacecraft. For example, at geostationary equatorial orbits, spacecraft can charge to in excess of 25000 volts. If one part of the spacecraft is at 25000 V and another is near zero, as can occur if one dielectric region is in dark, and the spacecraft frame is in sunlight, electrostatic discharges can occur. (The threshold of breakdown is considered to be about 400 volts in space, or lower.) The asymmetry in the picture is due to the offset of Earth's magnet pole.

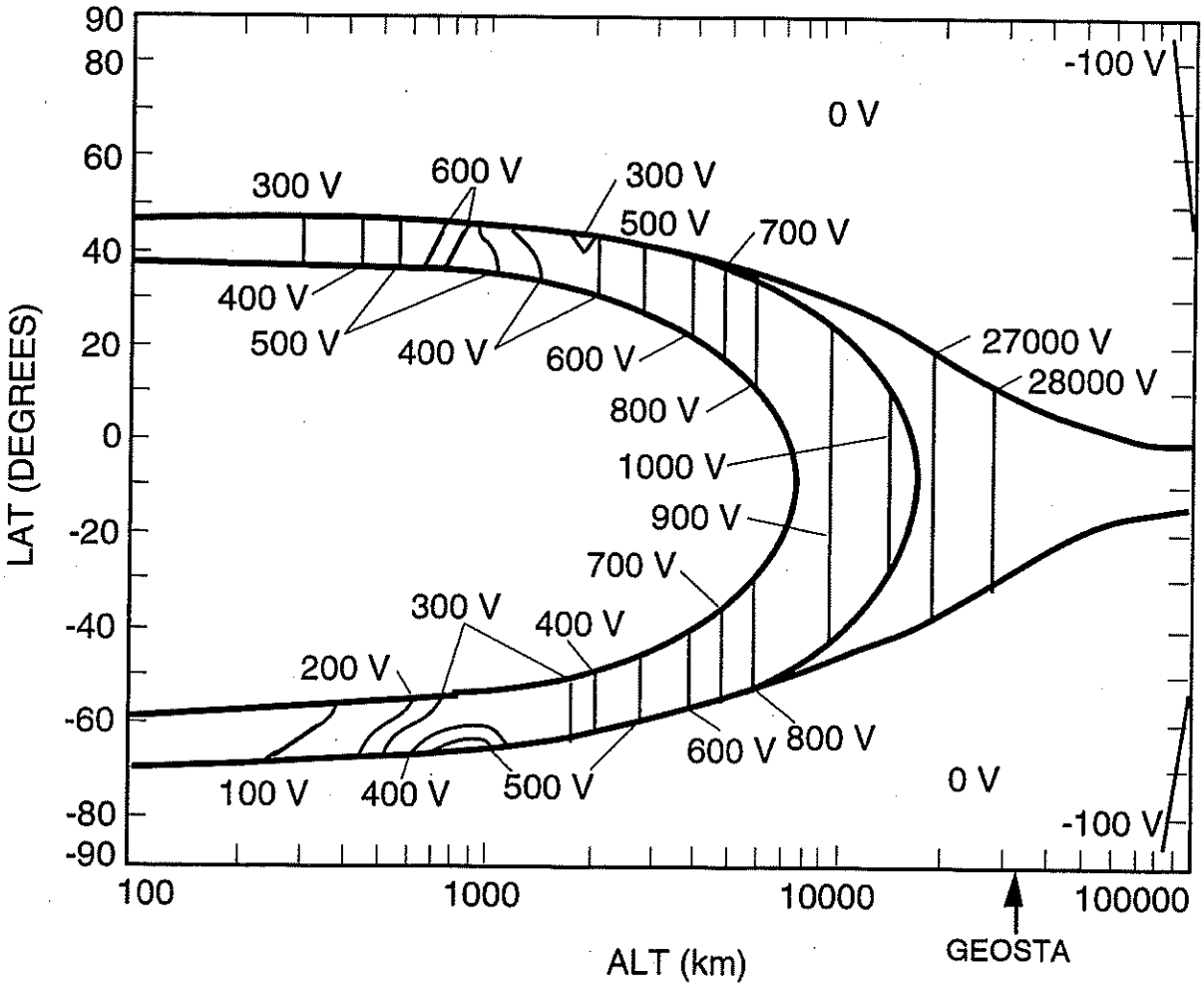

Figure 2. Potential on an electrically isolated Kapton sample near geosynchronous orbit on the SCATHA spacecraft.

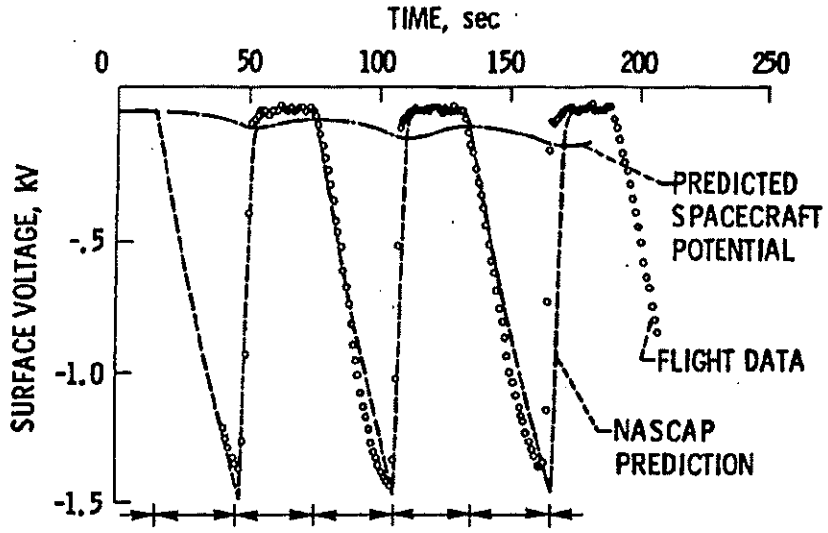

APPENDIX G

Power Subsystem

ARISE Power System Appendix : Backup and Supporting Data
Carol Lewis, Sal DiStefano, Gene Wester
Prepared 3/23/98; Data as of 1/30/98

Table A. Solar Array Assumptions

	Cell effic (BOL)	W/m^2 (BOL)	W/kg (BOL)
GaAs	19%	199	68
GaInP/GaAs	21.5%	225	77
GaInP/GaAs/Ge	24.3 %	255	87
CIS (LMA est.)	10%	93	100
CIS (L'Garde est.)	10%	93	136
High effic. Si (2005 proj.)	19%	199	86

- BOL numbers for 1-sun AM0, 28^{o}C (baseline)
- Assume actual array operating temperature of 85^{o}C
- 10% CIS cells avail est. 1999
  - LMA est. originally provided 2/97
  - L'Garde est. w/Al rigidization originally provided 3/97

Table B. Assumptions for the Solar Array Recharging the Battery

- Portion of solar array power is needed to recharge battery
- Assume battery charge efficiency = 0.79
- Assume battery discharge (energy) efficiency = 0.95
- Assume 3.5 hr available to recharge battery per orbit

- Battery prefers charge rate of at least 0.1 C
- 200 W of solar array required to do this
- If recharge time is shorter, more array area/mass required

Table C. Estimated Degradation Factors for Solar Array

- For 3 - 5 yr mission (BOL vs. EOL) -Assumptions
  - Temperature coefficient factor
    0.873 for GaAs, 0.868 for III-V multijunctions, 0.715 for Si or CIS
  - Cell packing factor 0.85 (15% of array area not covered with cells)
  - Radiation degradation 0.85
  - Temperature cycling 0.98
  - Fabrication losses 0.98
  - Micrometeorites 0.98
  - Wiring/diode 0.96
  - IR losses 0.98
  - UV degradation 0.98
  - Offpointing 1.00

Table D. Possible Radiation Environment

- Assume ARISE orbit 5,000 - 40,000 km altitude
- Radiation data from GaAs Solar Cell Radiation Handbook (B. Anspaugh)
- AP8 proton model
  - high energy peak at L = 1.5 R_e (0.5 R_e from surface = 3186 km altitude)
  - intermediate energies peak at L = 2 R_e (1.0 R_e from surface = 6371 km altitude)
- AE8 electron model
  - inner zone L = 1.2 - 2.8 R_e (0.2 - 1.8 R_e from surface = 1274 - 11468 km altitude)
    - peak at L = 1.4 R_e (0.4 R_e from surface = 2548 km altitude)
  - outer zone L = 3-11 R_e (2-10 R_e from surface = 19113 - 63711 km altitude)
    - peak at L = 4-5 R_e (3-4 R_e from surface = 19113 - 25484 km altitude)
  - L = distance from center of Earth; R = 6371 km

Table E: Battery Assumptions

- Assume 30 min eclipse/orbit but during only 3 consecutive months of year
  - 3 yr mission = 2417 eclipses (battery cycles)
  - 5 yr mission = 4028 eclipses (battery cycles)
- 3 yr probably OK for Li-ion (nominally up to 2000 cycles at 50% DOD)
- 5 yr calculated for both Li-ion and Ni-based batteries
- Looked at 3 types of Ni-based batteries which can withstand many cycles at 35% DOD
  - Common pressure vessel (CPV) NiH_2 - available now
  - Single pressure vessel (SPV) NiH_2 - should be available near-term
  - NiCd - available now

Table F: Assumed Battery Baselines at BOL

	Whr/kg	Whr/liter	Max DOD for max cycles
Li-ion	100	120	50%
CPV NiH_2	35	25	35%
SPV NiH_2	53	68	35%
NiCd	25	35	35%

Table G: Power Electronics Assumptions

- In general power electronics (PMAD) includes peak power tracker, and distribution/regulation/control electronics
  - More specifically includes DC/DC converters for each load, bus limiter, power control, power distribution network, bench test equipment (BTE), ground support equipment (GSE) and pyro.
- Flight hardware does not include BTE and GSE.

APPENDIX H

ARISE Cost Estimates

RunSim100 RunSim1000 | RunSim500 | Arise

Monte Carlo Follows:

DNP Estimate

LoadData

			Model	Total
Phase A/B/C/D				
1.0	**Project Management**			12.3
	1.1	Project Manager & Staff		7.7
	1.2	Administration & Control		Incl in 1.1
	1.3	Launch Approval		0.0
	1.4	Mission Assurance		Incl in 1.1
	1.5	Outreach	4.6	4.6
2.0	**Science**		2.8	2.8
3.0	**Project & Mission Engineering**		5.4	5.4
	3.1	Project Engineering		
	3.2	Mission Analysis		
4.0	**Payload**			27.4
	4.1	Payload Management		1.2
	4.2	Payload Engineering		0.5
	4.3	Instruments		23.0
		4.3.1 Instrument 1	27.5	23.0
		4.3.2 Instrument 2	0.0	0.0
		4.3.3 Instrument 3	0.0	0.0
		4.3.4 Instrument 4	0.0	0.0
		4.3.5 Instrument 5	0.0	0.0
		4.3.6 Instrument 6	0.0	0.0
		4.3.7 Instrument 7	0.0	0.0
		4.3.8 Instrument 8	0.0	0.0
		4.3.9 Instrument 9	0.0	0.0
		4.3.10 Instrument 10	0.0	0.0
		4.3.11 Other Instruments	0.0	0.0
	4.4	Instrument I&T Support	2.7	2.7
	4.5	Instrument Contract Management		
	4.6	Instrument Contract Fee		
5.0	**Spacecraft**			144.1
	5.1	Spacecraft System Management		1.7
	5.2	Spacecraft System Engineering		2.5
	5.3	Subsystems		139.9
		5.3.1 Attitude Control	27.5	32.0
		5.3.2 Command & Data	14.5	6.0
		5.3.3 Telecommunications	29.1	25.3
		Inflatable		6.0
		5.3.4 Power	7.5	11.0
		5.3.5 Propulsion	10.3	12.0
		5.3.6 Structures, Mechanisms, Cabling	9.2	21.8
		5.3.6.5 S/C Mechanical Buildup	2.9	2.9
		5.3.7 Thermal Control	2.9	2.9
		Cryo Coolers		11.0
		5.3.8 Software	Incl. in 5.3.2	7.0
		5.3.9 Launch Vehicle Adapter	Incl. in 5.3.6	2.0
		5.3.10 Other		0.0
		5.3.11 Other		0.0
	5.4	Spacecraft Contract Management		
	5.5	Spacecraft Contract Fee		
6.0	**ATLO**		10.1	20.1
	6.1	Integration & Test Management & Planning		
	6.2	System Integration & Test		
	6.3	Environmental Test		
	6.4	Data System		
	6.5	Launch Operations		
	6.6	Post-Launch Operations		
7.0	**Mission Operations**		12.6	35.0
	7.1	Ops Management & Infrastructure		
	7.2	Mission Operations Plan		
	7.3	Ground Software Development		
	7.4	Data Processing		
	7.5	Launch + 30 Days		
8.0	**Launch Vehicle**			60.0
9.0	**Other**			0.0
		Phase A/B/C/D Total (without LV)		247.1
		Launch Vehicle		60.0
R-ABCD		Reserves	@ 20%	49.4
		Total Phase A/B/C/D		356.6
Phase E				
E1.0	**Project Management**			0.7
	E1.1	Project Manager & Staff		0.5
	E1.5	Outreach (move to 7.1.1)	0.3	0.3
E2.0	**Science**		1.3	1.3
E7.0	**Mission Operations**		27.9	17.6
	E7.3	Ops Management & Infrastructure		
	E7.4	Data Processing		
	E7.6	Flight System Operations		
	E7.7	Tracking, Data Acq. & Institutional Support		
E9.0	**Other**			0.0
		Phase E Total		19.0
R-E		Reserves	@ 10%	2.0
		Total Phase E		21.0
		Probable Total Project Cost		378
		+20% (excl of reserves & LV)		431
		-20% (excl of reserves & LV)		324

Mission: LoadData Functions

Point Distribution

Technical Parameters	Mean	StdDev	Min	Max	PDB Update Time	ValidValues	Units
Power Type	AdvSi	0	0	0	01 Apr 1998 17:14	AMTEC, ARPS, AdvSi, AdvGaAs, GaAs	None
ISP (sec)	325	0	0	0	01 Apr 1998 17:14		sec
Total Power (w)	1200	0	0	0	01 Apr 1998 17:14		W
DL Data Rate (kbps)	600	0	0	0	01 Apr 1998 17:14		kbps
Data Storage (Gb)	0.1	0	0	0	01 Apr 1998 17:14		Gbits
Pointing Knowledge (arcsec)	30	0	0	0	01 Apr 1998 17:14		arcsec
Band Type S/UHF	X	0	0	0	01 Apr 1998 17:14	UHF, S, X, Ka, Optical	None
Band Type X/Ka	X	0	0	0	01 Apr 1998 17:14	UHF, S, X, Ka, Optical	None
Redundancy 1-3	Single	0	0	0	01 Apr 1998 17:14	Single, Selected, High	None
Redundancy 0-1	Single	0	0	0	01 Apr 1998 17:14	Single, Selected, High	None
Radiation Total Dose (krad)	100	0	0	0	01 Apr 1998 17:14		krad
ACS Mass (kg)	174	0	0	0	01 Apr 1998 17:14		kg
Telecomm Mass (kg)	94	0	0	0	01 Apr 1998 17:14		kg
Propulsion Mass (kg) (dry)	82.5	0	0	0	01 Apr 1998 17:14		kg
Structures Mass (kg)	110	0	0	0	01 Apr 1998 17:14		kg
Phase A Length (mos)	18				01 Apr 1998 17:14		Months
Phase B Length (mos)	18	0	0	0	01 Apr 1998 17:14		Months
Phase C/D Length (mos)	48	0	0	0	01 Apr 1998 17:14		Months
Phase E Length (mos)	60	0	0	0	01 Apr 1998 17:14		Months
Cruise Length (mos) (total)	36	0	0	0	01 Apr 1998 17:14		Months
Encounter Length (mos) (total)	0	0	0	0	01 Apr 1998 17:14		Months
Scientists ABCD	2	0	0	0	01 Apr 1998 17:14		None
Scientists E Cruise	2	0	0	0	01 Apr 1998 17:14		None
Scientists E Encounter	2	0	0	0	01 Apr 1998 17:14		None
Outreach Level	[illegible]	0	0	0	01 Apr 1998 17:14	High, Typical, Low	None
Tracking Time at Encounter (8hr tracks per week)	14	0	0	0	01 Apr 1998 17:14		None
Thermal Control	Passive	0	0	0	01 Apr 1998 17:14	Active, Passive	None
Maneuvers	Low	0	0	0	01 Apr 1998 17:14	High, Typical, Low	None
Tracking Time during Cruise (8hr tracks per week)	14	0	0	0	01 Apr 1998 17:14		None
Number of Integratable Elements	7	0	0	0	01 Apr 1998 17:14		None
Launch Vehicle Cost	80	0	0	0	01 Apr 1998 17:14		FY98 $M
Instrument Mass (kg) 1	70	0	0	0	01 Apr 1998 17:14		kg
Instrument Design Life (years) 1	12	0	0	0	01 Apr 1998 17:14		Years
Instrument Type 1	Other	0	0	0	01 Apr 1998 17:14	EF&MF, X-Ray, Other	None
Instrument Copy 1	N	0	0	0	01 Apr 1998 17:14	Yes, No	None
Instrument University-Built 1	Y	0	0	0	01 Apr 1998 17:14	Yes, No	None
Instrument Mass (kg) 2		0	0	0	01 Apr 1998 17:14		kg
Instrument Design Life (years) 2		0	0	0	01 Apr 1998 17:14		Years
Instrument Type 2		0	0	0	01 Apr 1998 17:14	EF&MF, X-Ray, Other	None
Instrument Copy 2		0	0	0	01 Apr 1998 17:14	Yes, No	None
Instrument University-Built 2		0	0	0	01 Apr 1998 17:14	Yes, No	None
Instrument Mass (kg) 3		0	0	0	01 Apr 1998 17:14		kg
Instrument Design Life (years) 3		0	0	0	01 Apr 1998 17:14		Years
Instrument Type 3		0	0	0	01 Apr 1998 17:14	EF&MF, X-Ray, Other	None
Instrument Copy 3		0	0	0	01 Apr 1998 17:14	Yes, No	None
Instrument University-Built 3		0	0	0	01 Apr 1998 17:14	Yes, No	None
Instrument Mass (kg) 4		0	0	0	01 Apr 1998 17:14		kg
Instrument Design Life (years) 4		0	0	0	01 Apr 1998 17:14		Years
Instrument Type 4		0	0	0	01 Apr 1998 17:14	EF&MF, X-Ray, Other	None
Instrument Copy 4		0	0	0	01 Apr 1998 17:14	Yes, No	None
Instrument University-Built 4		0	0	0	01 Apr 1998 17:14	Yes, No	None
Instrument Mass (kg) 5		0	0	0	01 Apr 1998 17:14		kg
Instrument Design Life (years) 5		0	0	0	01 Apr 1998 17:14		Years
Instrument Type 5		0	0	0	01 Apr 1998 17:14	EF&MF, X-Ray, Other	None
Instrument Copy 5		0	0	0	01 Apr 1998 17:14	Yes, No	None
Instrument University-Built 5		0	0	0	01 Apr 1998 17:14	Yes, No	None
Instrument Mass (kg) 6		0	0	0	01 Apr 1998 17:14		kg
Instrument Design Life (years) 6		0	0	0	01 Apr 1998 17:14		Years
Instrument Type 6		0	0	0	01 Apr 1998 17:14	EF&MF, X-Ray, Other	None
Instrument Copy 6		0	0	0	01 Apr 1998 17:14	Yes, No	None
Instrument University-Built 6		0	0	0	01 Apr 1998 17:14	Yes, No	None
Instrument Mass (kg) 7		0	0	0	01 Apr 1998 17:14		kg
Instrument Design Life (years) 7		0	0	0	01 Apr 1998 17:14		Years
Instrument Type 7		0	0	0	01 Apr 1998 17:14	EF&MF, X-Ray, Other	None
Instrument Copy 7		0	0	0	01 Apr 1998 17:14	Yes, No	None
Instrument University-Built 7		0	0	0	01 Apr 1998 17:14	Yes, No	None
Instrument Mass (kg) 8		0	0	0	01 Apr 1998 17:14		kg
Instrument Design Life (years) 8		0	0	0	01 Apr 1998 17:14		Years
Instrument Type 8		0	0	0	01 Apr 1998 17:14	EF&MF, X-Ray, Other	None
Instrument Copy 8		0	0	0	01 Apr 1998 17:14	Yes, No	None
Instrument University-Built 8		0	0	0	01 Apr 1998 17:14	Yes, No	None
Instrument Mass (kg) 9		0	0	0	01 Apr 1998 17:14		kg
Instrument Design Life (years) 9		0	0	0	01 Apr 1998 17:14		Years
Instrument Type 9		0	0	0	01 Apr 1998 17:14	EF&MF, X-Ray, Other	None
Instrument Copy 9		0	0	0	01 Apr 1998 17:14	Yes, No	None
Instrument University-Built 9		0	0	0	01 Apr 1998 17:14	Yes, No	None
Instrument Mass (kg) 10		0	0	0	01 Apr 1998 17:14		kg
Instrument Design Life (years) 10		0	0	0	01 Apr 1998 17:14		Years
Instrument Type 10		0	0	0	01 Apr 1998 17:14	EF&MF, X-Ray, Other	None
Instrument Copy 10		0	0	0	01 Apr 1998 17:14	Yes, No	None
Instrument University-Built 10		0	0	0	01 Apr 1998 17:14	Yes, No	None
						Spin, 3-Axis	None
	0	0	0	0	01 Apr 1998 17:13		None
	85	0	0	0	01 Apr 1998 17:14		Years
							None
							W
							kbps

Mission: LoadData Functions

Point Distribution

Technical Parameters	Mean	StdDev	Min	Max	PDB Update Time	ValidValues	Units
Power Type	AMTEC	0	0	0	02 Apr 1998 00:36	AMTEC, ARPS, AdvSi, AdvGaAs, GaAs	None
ISP (sec)	220	1	5	10	02 Apr 1998 00:36		sec
Total Power (w)	150	0	0	0	02 Apr 1998 00:36		W
DL Data Rate (kbps)	25	2	10	20	02 Apr 1998 00:37		kbps
Data Storage (Gb)	8	80	240	400	02 Apr 1998 00:36		Gbits
Pointing Knowledge (arcsec)	205	3	3	20	02 Apr 1998 00:36		arcsec
Band Type S/UHF	X	100	100	500	02 Apr 1998 00:37	UHF, S, X, Ka, Optical	None
Band Type X/Ka	X	100	100	500	02 Apr 1998 00:37	UHF, S, X, Ka, Optical	None
Redundancy 1-3	High	20	10	100	02 Apr 1998 00:36	Single, Selected, High	None
Redundancy 0-1	High	20	10	100	02 Apr 1998 00:36	Single, Selected, High	None
Radiation Total Dose (krad)	4000	0	0	0	02 Apr 1998 00:36		krad
ACS Mass (kg)	21.4	10	60	100	02 Apr 1998 00:36		kg
Telecomm Mass (kg)	19.45	4	10	25	02 Apr 1998 00:37		kg
Propulsion Mass (kg) (dry)	82.5	0	1	5	02 Apr 1998 00:36		kg
Structures Mass (kg)	47.1	4	15	30	02 Apr 1998 00:37		kg
Phase A Length (mos)	31	0	0	0	02 Apr 1998 00:36		Months
Phase B Length (mos)	22	0	0	0	02 Apr 1998 00:36		Months
Phase C/D Length (mos)	37	0	0	0	02 Apr 1998 00:36		Months
Phase E Length (mos)	36	0	0	0	02 Apr 1998 00:36		Months
Cruise Length (mos) (total)	1	0	0	0	02 Apr 1998 00:36		Months
Encounter Length (mos) (total)	4	0	0	0	02 Apr 1998 00:36		None
Scientists ABCD	2	0	0	0	02 Apr 1998 00:36		None
Scientists E Cruise	8	0	0	0	02 Apr 1998 00:36		None
Scientists E Encounter	High	0	0	0	02 Apr 1998 00:36		None
Outreach Level	14	0	0	0	02 Apr 1998 00:36	High, Typical, Low	None
Tracking Time at Encounter (8hr tracks per week)	Passive	1	1.5	5	02 Apr 1998 00:37	Active, Passive	None
Thermal Control	Low	0	0	0	02 Apr 1998 00:36	High, Typical, Low	None
Maneuvers	14	0	0	0	02 Apr 1998 00:36		None
Tracking Time during Cruise (8hr tracks per week)	7	0	0	0	02 Apr 1998 00:36		None
Number of Integratable Elements	70	0	0	0	02 Apr 1998 00:36		FY98 $M
Launch Vehicle Cost	10	0	0	0	02 Apr 1998 00:36		kg
Instrument Mass (kg) 1	12	0.2	0.8	2	02 Apr 1998 00:36		Years
Instrument Design Life (years) 1	EM Field	0	0	0	02 Apr 1998 00:36	EF&MF, X-Ray, Other	None
Instrument Type 1	N	0	0	0	02 Apr 1998 00:36	Yes, No	None
Instrument Copy 1	N	0	0	0	02 Apr 1998 00:36	Yes, No	None
Instrument University-Built 1		2	0	0	02 Apr 1998 00:37		kg
Instrument Mass (kg) 2		12	0	0	02 Apr 1998 00:37		Years
Instrument Design Life (years) 2	EM Field	0	0	0	02 Apr 1998 00:37	EF&MF, X-Ray, Other	None
Instrument Type 2	N	0	0	0	02 Apr 1998 00:37	Yes, No	None
Instrument Copy 2	N	0	0	0	02 Apr 1998 00:37	Yes, No	None
Instrument University-Built 2		5	0	0	02 Apr 1998 00:36		kg
Instrument Mass (kg) 3		12	0	0	02 Apr 1998 00:36		Years
Instrument Design Life (years) 3	EM Field	0	0	0	02 Apr 1998 00:36	EF&MF, X-Ray, Other	None
Instrument Type 3	N	0	0	0	02 Apr 1998 00:36	Yes, No	None
Instrument Copy 3	N	0	0	0	02 Apr 1998 00:36	Yes, No	None
Instrument University-Built 3		1.5	0	0	02 Apr 1998 00:36		kg
Instrument Mass (kg) 4		12	0	0	02 Apr 1998 00:36		Years
Instrument Design Life (years) 4	EM Field	0	0	0	02 Apr 1998 00:36	EF&MF, X-Ray, Other	None
Instrument Type 4	N	0	0	0	02 Apr 1998 00:36	Yes, No	None
Instrument Copy 4	N	0	0	0	02 Apr 1998 00:36	Yes, No	None
Instrument University-Built 4							kg
Instrument Mass (kg) 5							Years
Instrument Design Life (years) 5						EF&MF, X-Ray, Other	None
Instrument Type 5						Yes, No	None
Instrument Copy 5						Yes, No	None
Instrument University-Built 5							kg
Instrument Mass (kg) 6							Years
Instrument Design Life (years) 6						EF&MF, X-Ray, Other	None
Instrument Type 6						Yes, No	None
Instrument Copy 6						Yes, No	None
Instrument University-Built 6							kg
Instrument Mass (kg) 7							Years
Instrument Design Life (years) 7						EF&MF, X-Ray, Other	None
Instrument Type 7						Yes, No	None
Instrument Copy 7						Yes, No	None
Instrument University-Built 7							kg
Instrument Mass (kg) 8							Years
Instrument Design Life (years) 8						EF&MF, X-Ray, Other	None
Instrument Type 8						Yes, No	None
Instrument Copy 8						Yes, No	None
Instrument University-Built 8							kg
Instrument Mass (kg) 9							Years
Instrument Design Life (years) 9						EF&MF, X-Ray, Other	None
Instrument Type 9						Yes, No	None
Instrument Copy 9						Yes, No	None
Instrument University-Built 9							kg
Instrument Mass (kg) 10							Years
Instrument Design Life (years) 10						EF&MF, X-Ray, Other	None
Instrument Type 10						Yes, No	None
Instrument Copy 10						Yes, No	None
Instrument University-Built 10							
						Spin, 3-Axis	None
	0	6	15	30	02 Apr 1998 00:36		None
	8.5	10	60	120	02 Apr 1998 00:36		Years
							None
							W
							kbps

Shrb Type

Prop type

PL Power (w)

PL Data Rate (kbps)

OFF-AXIS GREGORIAN
Mass and Inertia
f = 11.55 m, D = 25 m, f#p = 0.23

UNIT	MASS (kg)	CENTER OF MASS (m)			MASS INERTIA at Local CG (Global C/S) (kg*m^2)		
		X	Y	Z	Ixn	Iyn	Izn
S/C Buss - Cylindrical 2.5m dia. X3.5m, Al 3/16" Misc S/C Equip. & Instr. - (Coolers, ACS, Strar Tracker/Sensors, Buss modules, Power, Telecom Elect., CDH,CCS, etc.)	1442.3	0.00	-2.25	8.00	2614.7	1415.2	2614.7
Feed Array	35.0	0.00	-0.50	9.25	0.0	0.0	0.0
Deployment Canister	57.3	0.00	-0.50	8.00	0.0	0.0	0.0
Telecom - Optical Com	15.0	0.00	-4.00	8.00	0.0	0.0	0.0
Primary - Reflector Surface Al - Kp (0.5 mil) - Au (300 psi membrane stress)	11.5	0.00	13.13	5.49	581.5	591.0	888.7
Primary - Canopy Surface CP-1 (0.5 mil)	10.5	0.00	11.77	7.99	532.7	530.4	825.2
Primary - Torus Inflatable Rigidized Al (10.5" dia, 12 mil thick)	18.3	0.00	12.50	6.77	1909.0	2341.6	3385.8
Primary - Spring Tensioners F = 0.5 lb	1.3	0.00	12.52	6.78	83.7	182.6	228.3
SubReflector - Eliptical Gl/Cyanate 1.2 x 1.65m, e = 0.555	11.0	0.00	-0.83	13.01	1.8	1.8	3.6
Truss - SubReflector Spt. 3.9m Gr/Ep Deployable	4.6	0.00	-1.08	11.12	5.8	5.3	0.5
Bottom Strut - Primary Spt. 8.2m Gr/Ep Deployable	8.4	0.00	-0.38	3.92	45.9	45.9	0.0
Strut - Primary Side Spt. Inflatable Rigidized Al (2 ea. - 16" dia, 14 mil thick) 23.1 m	15.0	0.00	9.07	9.04	464.1	819.2	1272.4
Solar Array	18.9	0.00	-2.69	8.00	11.0	589.5	600.5
TOTAL Global C/S at Reflector Vertex	*1793.3*	*0.00*	*-1.55*	*8.04*	*18791.7*	*7307.3*	*21857.4*

R. Helms
9/13/98

APPENDIX I

ARISE Team

The following personnel have contributed their expertise to the design of the ARISE spacecraft and mission.

ARISE Study Team

James S. Ulvestad
Preproject Scientist
for ARISE
NRAO

Carol Lewis
Power

Vincent Randolph
Avionics

Art B. Chmielewski
Arise Preproject Mgr.

Leo Lichodziejewski
Inflatable Structures
L'Garde

Larry Roe
Inflation Design
University of Arkansas

Pradeep Bhandari
Cryocoolers

Roger Linfield
VLBI Science

Joel Smith
VLBI Consultant

Robert Chave
Mech. adaptive shaping

Bob Miyake
Thermal Design

Dan Thunnissen
Propulsion

Sal DiStefano
Power

David Murphy
Orbits and Coverage

Charles Wang
Telecon

Robert Freeland
Antenna Materials

Muriel Noca
Systems

Rick Wietfeldt
VLBI & VLBI Processing

Todd Gaier
Science Instruments

Marco Quadrelli
Altitude Control Sys.

Paul B. Willis
Antenna Materials

Rick Helms
Sructures

Yahya Rahmat-Samii
Antenna Design
U.C.L.A.

Also:
Henry Garrett - Space environments
Mike Jones - Ground systems
Gene Wester- Power
Robert Hoferer - Antenna Design & RF compensation (UCLA)
Sam Sirlin - Antenna dynamics, altitude control

ARISE Science Advisory Group

Moshe Elitzur
Maser theory,
Star-forming regions
University of Kentucky

Dr. Lincoln Greenhill
Megamasers, masers,star formation
Harvard-Smithsonian
Astrophysical Obs

Roger Linfield
VLBI Science

Prof. Alan Marscher
Gamma-ray blazars,
jet formation
Boston University

Dr. Robert Mutel
Radio stars, blazars
University of Iowa

Dr. Susan Neff
Active & merging
galaxies
NASA/GSFC

Dr. Robert Preston
Active galactic nuclei,
radio stars

Dr. Denise Gabuzda
Polarization of blazar jets
Lebedev Physical Institute, Russia

Dr. Leonid Gurvits
Distant Radio Sources in Cosmology
Joint Inst for VLBI in Europe (JIVE)

Prof. Hisashi Hirabayashi
Star formation, AGN,
Space VLBI techniques
Inst for Space & Astronautical Science
(ISAS), Japan

Not pictured:
Prof. Jacqueline Hewitt
Gravitational lenses
Massachusetts Institute of Technology

Dr. Arieh Konigl
Radio jet, disk formation & Interactions
University of Chicago

Dr. Julian Krolik
Small-scale disks in active galactic nuclei
Johns Hopkins University

Dr. Jonathan Romney
Active galactic nuclei
National Radio Astronomy Observatory

Dr. Ann Wehrle
Multi-frequency monitoring of blazars
California Institute of Technology

Dr. Michael Garrett
Gravitational lenses
Joint Institute for VLBI in Europe (JIVE)

Prof. Russell Taylor
Radio stars
University of Calgary

Prof. Esko Valtaoja
Blazars, high-frequency variable sources
Tuorla Observatory